



2018

## ASSESSING THE APPLICATION OF THE UNMANNED AERIAL SYSTEMS (UAS) IN EARTHWORK VOLUME MEASUREMENT

Xi Wang

University of Kentucky, xi.wang@uky.edu

Digital Object Identifier: <https://doi.org/10.13023/etd.2018.259>

[Right click to open a feedback form in a new tab to let us know how this document benefits you.](#)

### Recommended Citation

Wang, Xi, "ASSESSING THE APPLICATION OF THE UNMANNED AERIAL SYSTEMS (UAS) IN EARTHWORK VOLUME MEASUREMENT" (2018). *Theses and Dissertations--Civil Engineering*. 68.  
[https://uknowledge.uky.edu/ce\\_etds/68](https://uknowledge.uky.edu/ce_etds/68)

This Doctoral Dissertation is brought to you for free and open access by the Civil Engineering at UKnowledge. It has been accepted for inclusion in Theses and Dissertations--Civil Engineering by an authorized administrator of UKnowledge. For more information, please contact [UKnowledge@lsv.uky.edu](mailto:UKnowledge@lsv.uky.edu).

## **STUDENT AGREEMENT:**

I represent that my thesis or dissertation and abstract are my original work. Proper attribution has been given to all outside sources. I understand that I am solely responsible for obtaining any needed copyright permissions. I have obtained needed written permission statement(s) from the owner(s) of each third-party copyrighted matter to be included in my work, allowing electronic distribution (if such use is not permitted by the fair use doctrine) which will be submitted to UKnowledge as Additional File.

I hereby grant to The University of Kentucky and its agents the irrevocable, non-exclusive, and royalty-free license to archive and make accessible my work in whole or in part in all forms of media, now or hereafter known. I agree that the document mentioned above may be made available immediately for worldwide access unless an embargo applies.

I retain all other ownership rights to the copyright of my work. I also retain the right to use in future works (such as articles or books) all or part of my work. I understand that I am free to register the copyright to my work.

## **REVIEW, APPROVAL AND ACCEPTANCE**

The document mentioned above has been reviewed and accepted by the student's advisor, on behalf of the advisory committee, and by the Director of Graduate Studies (DGS), on behalf of the program; we verify that this is the final, approved version of the student's thesis including all changes required by the advisory committee. The undersigned agree to abide by the statements above.

Xi Wang, Student

Dr. Gabriel B. Dadi, Major Professor

Dr. Timothy R. B. Taylor, Director of Graduate Studies

ASSESSING THE APPLICATION OF THE UNMANNED AERIAL SYSTEMS (UAS)  
IN EARTHWORK VOLUME MEASUREMENT

---

DISSERTATION

---

A dissertation submitted in partial fulfillment of the requirements for the degree of  
Doctor of Philosophy in the College of Engineering  
at the University of Kentucky

By

Xi Wang

Lexington, Kentucky

Director: Gabriel B. Dadi, Assistant Professor of Civil Engineering  
Lexington, Kentucky 2018

Copyright© Xi Wang 2018

## ABSTRACT OF DISSERTATION

### ASSESSING THE APPLICATION OF THE UNMANNED AERIAL SYSTEMS (UAS) IN EARTHWORK VOLUME MEASUREMENT

Earthwork operations are often one of the major cost items on infrastructure construction projects. Because earthwork is largely influenced by unstable construction conditions and organization plans, it becomes the emphasis and difficulties of the cost control in the construction process. Therefore, precise estimates of actual earthwork volumes are important for both owners and contractors alike to ensure appropriate payments are made. However, measuring work on site requires lots of time and labors because of various and irregular site conditions. Conventional measurement methods, such as planned quantities from the drawings or estimates from equipment activity, are rough estimates with significant opportunities for errors and safety concerns.

Recently, unmanned aerial systems (UAS) have become popular for numerous surveying applications in civil engineering. They require less cost and time consumptions compared with traditionally manual methods. Also, they are able to perform photogrammetric data acquisition with equipped digital cameras in hazardous, complex or other conditions that may present high safety risks. However, UAS photogrammetry for research applications is still in its infancy, especially in construction management, and research conducted on UAS photogrammetry for earthwork volume estimation are very limited.

Therefore, this research intends to investigate and validate the feasibility and efficiency of utilizing the UAS photogrammetry surveying technique to estimate earthwork volume. The research is conducted into three steps based on distinct case studies: firstly, adapting a basic analysis through a case study to preliminarily prove the effectiveness of the UAS photogrammetry method in earthwork volume measurement; also providing an analytical foundation for further utilizations; secondly, Quantitatively assessing the impact of flight parameters and environmental factors on the accuracy of UAS photogrammetry in earthwork volume measurement and identifying the most influential individual or combinations through observations and a statistical multiple regression analysis; at last, comparing volumes calculated by using the UAS platform and other two conventional methods which are Average-End-Area method and grid method in AutoCAD to further

validate the feasibility of using the UAS technology in the process of earthwork volumes estimation.

The results indicate that the UAS is an effective method for earthwork volume measurement. According to published standards, practice experience, and literature, the measurement errors are in an acceptable range when parameters are under control. In addition, the UAS demonstrates its advantages in balancing between the accuracy and efficiency compared with conventional earthwork volume measurement methods.

**KEYWORDS:** Construction, Earthwork Volumes, UAS, Photogrammetry, Point Cloud, Productivity

Xi Wang  
\_\_\_\_\_  
Student's Signature

07/05/2018  
\_\_\_\_\_  
Date

ASSESSING THE APPLICATION OF THE UNMANNED AERIAL SYSTEMS (UAS)  
IN EARTHWORK VOLUME MEASUREMENT

By

Xi Wang

Dr. Gabriel B. Dadi

---

Director of Dissertation

Dr. Timothy R.B. Taylor

---

Director of Graduate Studies

07/05/2018

---

Date

*To my father.*

## ACKNOWLEDGEMENTS

This work cannot be completed without the people who have helped me in this journey.

There are so many thank you-s to say, but no amount of words can express my gratitude:

To my advisor, Dr. Gabriel Dadi, for his continuous support of my Ph.D. study and research over the years, for his patience, motivation, and knowledge. He guided me during all the time of research and writing of this dissertation. I could not have imagined having a better advisor and mentor for my Ph.D. study. He sets an example of excellence as a mentor, instructor, and researcher.

To the rest of my committee, Dr. Timothy Taylor, Dr. Sean Bemis, Dr. Timothy Stombaugh and Dr. Nelson Akafuah. I am thankful for their participations to advise and discuss my research topic. In addition, I would like to thank Mr. Roy Sturgill and Mr. Todd Saladin for their help in data collections.

To my parents, Dai and Kou, for their both emotional and financial supports in my every dream over these years, even though I am ten thousand miles away from them. There's no way I could make it without them.

To my best friend, Minhao Dai, for believing in me, for being with me in difficult times, and for enduring my endless talks about this work, and for loving me at my best and at my worst.

If the success is a shining star up high in the sky, all of them are the ladder or the spaceship of mine.



TABLE OF CONTENTS

ACKNOWLEDGEMENTS.....iii

LIST OF TABLES.....vii

LIST OF FIGURES.....viii

1. INTRODUCTION

1.1 Background and Motivation..... 10

1.2 Research Purpose ..... 17

1.3 Research Scope ..... 17

1.4 Research Methodology..... 19

1.5 Dissertation Outline..... 19

2. ESTIMATING EARTHWORK VOLUMES THROUGH THE USE OF UNMANNED AERIAL SYSTEMS

2.1 Introduction ..... 21

2.2 Methodology ..... 23

2.2.1 Capture Geo-referenced Images of the Facility ..... 23

2.2.2 Process the Images into an Accurate 3D Point Cloud ..... 27

2.2.3 3D Point Cloud Model Generation ..... 28

2.2.4 Accuracy Test for 3D Model ..... 33

2.3 Result..... 34

2.4 Conclusion..... 39

3. THE INFLUENCE OF POTENTIAL FACTORS ON MEASUREMENT ACCURACY OF APPLYING THE UNMANNED AERIAL SYSTEMS (UAS) AND PHOTOGRAMMETRY IN CONSTRUCTION EARTHWORK

3.1 Introduction ..... 41

3.2 Influential Factors ..... 43

    3.2.1 Flight Altitude..... 43

    3.2.2 Image Overlapping Rate ..... 45

    3.2.3 Ground Control Points (GCPs)..... 46

    3.2.4 Soil Types ..... 47

3.3 Methodology ..... 48

    3.3.1 Photogrammetric Process..... 48

    3.3.2 The UAS Device and Flight Plans ..... 50

    3.3.3 Assessment of Accuracy ..... 55

3.4 Results and Discussion..... 56

    3.4.1 Flight Duration and Number of Images ..... 56

    3.4.2 Analysis of Positional Accuracy ..... 57

    3.4.3 Soil Types ..... 68

3.5 Conclusion..... 70

4. COMPARISONS BETWEEN APPLICATIONS OF THE UAS AND CONVENTIONAL METHODS IN EARTHWORK VOLUME MEASUREMENT

4.1 Introduction ..... 72

4.2 Average-End-Area (AEA) Method and Grid Method..... 75

4.3 The UAS and Photogrammetry ..... 79

4.4	Case Study.....	82
4.4.1	Project Description.....	82
4.4.2	Methodology.....	83
4.4.3	Results.....	89
4.5	Conclusion.....	91
5.	CONCLUSION .....	93
APPENDICES		
	Appendix A. Positional Errors Analysis Results of Flight Plans.....	97
	Appendix B. Earthwork Volumes Calculated by Average-End-Area Method and Grid Method. ....	100
	BIBLIOGRAPHY .....	120
	VITA.....	128

## LIST OF TABLES

Table 1.1 Earthwork Volume Measurement Method used by DOTs .....	11
Table 2.1 Coordinates of GCPs .....	35
Table 2.2 Distances Measurements of 3D Point Cloud Model in Stage 1 (ft).....	35
Table 2.3 Distances Measurements of 3D Point Cloud Model in Stage 2 (ft).....	35
Table 2.4 Volume Calculation Results (ft <sup>3</sup> ).....	38
Table 3.1 Flight Duration and numbers of Images taken at Different Flight Altitudes....	57
Table 3.2 RMSE (ft) of Flights Processed by Different Number of GCPs.....	60
Table 3.3 Summary of RMSE Distribution .....	61
Table 3.4 Comparisons between RMSE and Log (RMSE) on the Distribution and Summary Statistic .....	65
Table 3.5 Summary of Fit in Multiple Regression Analysis .....	66
Table 3.6 ANOVA of Multiple Regression Analysis .....	66
Table 3.7 Impact of Soil Types on the Accuracy of Volumetric Measurements.....	69
Table 4.1 Comparisons of Earthwork Volumes Computed by Different Methods .....	89
Table 4.2 Comparisons of Labor Hours between UAS and Conventional Survey Methods .....	90
Table 4.3 Comparisons of Cost between UAS and Conventional Survey Methods.....	91
Table 6.1 Coordinates of GCPs (ft) .....	97
Table 6.2 Residue Values of Each Flight Plan When Applying Different Number of GCPs (ft) .....	98
Table 6.3 Results of Average-End-Area Method .....	100
Table 6.4 Elevations of Grid Intersections (ft) .....	105

## LIST OF FIGURES

Figure 2.1 Grid Mission Image Acquisition Plan (Pix4D, 2016) .....	25
Figure 2.2 Enough Overlaps and Not Enough Overlaps between 2 Flights (Pix4D, 2016) .....	25
Figure 2.3 Grid Mission Plan for Stage 1. ....	26
Figure 2.4 Grid Mission Plan for Stage 2. ....	26
Figure 2.5 Processing Options for Point Cloud Generation .....	30
Figure 2.6 Marking a GCP.....	30
Figure 2.7 Point Cloud Model of the Site at Stage 1 .....	31
Figure 2.8 Point Cloud Model of the Site at Stage 2 .....	32
Figure 2.9 Locations of GCP 1 and GCP 2.....	34
Figure 2.10 Locations of GCP 3 and GCP 4.....	34
Figure 2.11 Locations of GCP 5 and GCP 6.....	35
Figure 2.12 Stockpile Volume Drawn in Point Cloud Model .....	36
Figure 2.13 Trench Volume Drawn in Point Cloud Model (front).....	37
Figure 2.14 Trench Volume Drawn in Point Cloud Model (Below ground).....	37
Figure 2.15 Grid on the Base of the Volume (Not the Real Dimensions) .....	38
Figure 3.1 Relation between Flight Altitude and Image Area (Pix4d, 2018).....	44
Figure 3.2 Bundle of Rays from Multiple Images .....	46
Figure 3.3 Structure from Motion (SfM) .....	49
Figure 3.4 UAS used in the study, DJI Inspire 1 .....	51
Figure 3.5 Overview of the Study Area.....	52
Figure 3.6 Strategy of the UAS Flights and Processing .....	53
Figure 3.7 Pix4D Mobile Application Interface .....	53
Figure 3.8 Grid Flight Pattern over the Study Area.....	54
Figure 3.9 GPS Rover .....	55
Figure 3.10 Relationship between Flight Altitude and Overlapping Rate on Flight Duration and Number of Images.....	57
Figure 3.11 Distribution of GCPs on the Study Area .....	58
Figure 3.12 Relationship of Overlapping Rates against Flight Altitudes and RMSE .....	61
Figure 3.13 Relationship between Number of GCPs and Average Positional Error on (1) Flight Altitude and (2) Image Overlapping Rate .....	62
Figure 3.14 Estimations of the Independent Variables Significance.....	66
Figure 3.15 Distribution of Residuals.....	67
Figure 3.16 Sample Piles of Different Soil Type.....	68
Figure 3.17 Circle Pattern of Images Collections for Each Soil Type.....	69
Figure 4.1 Earthwork Volume Measurement Methods Applied by DOTs.....	73
Figure 4.2 Stations and Cross-Sections of a Highway Project .....	76
Figure 4.3 Grid Method Calculation.....	77
Figure 4.4 Project Location (VDOT, 2018).....	83
Figure 4.5 3D Contour Map and Properties of the Site after 1st Visit.....	84
Figure 4.6 3D Contour Map of the Site after 2nd Visit .....	85
Figure 4.7 Map of Survey Points .....	85
Figure 4.8 Information of Survey Points .....	86
Figure 4.9 Overlay of Multiple 3D Contour Map and Cross-sections Intervals.....	87

Figure 4.10 Grid Pattern (10ft) of the Earthwork Area .....	88
Figure 4.11 Elevations of each Grid Intersection .....	88

## **1. INTRODUCTION**

### **1.1 Background and Motivation**

Earthwork operations are engineering works created through the moving or processing of massive quantities of soil or unformed rock. The purpose is to reconfigure the topography of a site to achieve the design levels (Nunnally, 2004). Earthwork is an important part of all greenfield construction projects. It is mainly executed during the early stages of construction, which means completion of earthwork within the prescribed time can control the overall project schedule. In addition, earthwork operations are often one of the major cost items on infrastructure construction projects. Because earthwork is largely influenced by unstable geographical conditions and construction organization plans, it can create cost uncertainties during the construction process. It is important, therefore, to make the best possible measurement of the quantity of soil and rock materials that has been excavated and placed. Without an accurate estimation, contractors are not able to present an accurate bid, properly assign construction assets or formulate a project schedule, and owners are not able to ensure appropriate payments are made.

Normally, in the design stage of a project, the design team determines the estimated quantity of the earthwork volume based on the collected data of the existing ground profile. This procedure is completed before and after construction for verifications. For example, according to the 2012 Kentucky state standard specification, when the contract provides for payment based on field measurements of the material excavated, the owner will measure the excavation in its original position by taking cross sections before the work starts and after it is entirely completed. However, the measuring work on site requires a

large amount of time and labor due to various site conditions and safety concerns. For owners, especially some state agencies, it is difficult to measure the earthwork volume on site for verification due to the shortage of staff (Dadi, et al. 2016). Also, most states still depend on drawing or equipment activity to calculate the volume of earthwork. Both approaches are rough estimates with significant opportunities for errors. Mistakes could come from math errors, incorrect formula, neglect of transition areas, or mixing cut and fill quantities. Therefore, appropriate and correct payments cannot be guaranteed, whether is because of manual operations or objective limitations. The Table 1.1 shows the different methods the DOT from each state currently uses for earthwork volume measurement, specifically for excavation volume, according to the latest version of standard specifications published by the Department of Transportation of each state.

**Table 1.1 Earthwork Volume Measurement Method used by DOTs**

State	Earthwork Volume Measurement Method				
	Cross-section method	Digital Surface Model	Equipment Activity	Photogrammetric procedures	Others
Alabama	✓		✓		
Alaska	✓		✓		
Arizona	✓				
Arkansas	✓			✓	
California	✓				
Colorado	✓				
Connecticut	✓				
Delaware	✓				
Florida					
Georgia	✓			✓	✓
Hawaii	✓				
Idaho	✓				



**Table 1.1 (Continued). Earthwork Volume Measurement Method used by DOTs**

Illinois	✓				
Indiana	✓				
Iowa	✓				
Kansas	✓				
Kentucky	✓				
Louisiana	✓				
Maine	✓				
Maryland	✓				
Massachusetts	✓				
Michigan	✓				
Minnesota	✓	✓			
Mississippi	✓				
Missouri	✓				
Montana	✓				✓
Nebraska	✓				
Nevada	✓				
New Hampshire	✓				
New Jersey	✓				
New Mexico					✓
New York	✓				
North Carolina	✓	✓			✓
North Dakota	✓				
Ohio	✓				
Oklahoma	✓	✓			✓
Oregon	✓	✓	✓		
Pennsylvania	✓			✓	✓
Rhode Island	✓				✓
South Carolina	✓				
South Dakota	✓				✓
Tennessee	✓				
Texas	✓				

**Table 1.1 (Continued). Earthwork Volume Measurement Method used by DOTs**

Utah	✓	✓			
Vermont					✓
Virginia	✓				
Washington	✓	✓			
West Virginia	✓				
Wisconsin	✓				
Wyoming	✓				✓

In recent years, the surveying industry has seen significant changes because of modern technological developments creating innovations such as a Robotic Total Station (RTS) and LiDAR for measuring and computing elements of the earth surface. Unmanned Aerial System (UAS) are another innovation that has become attractive for many surveying applications in civil engineering. The UAS, or colloquially drones, was originally developed and used for military implementations. They are remotely controlled aircrafts or helicopters equipped with various sensors, such as cameras, Global Positioning System (GPS), or other communication devices. The developed GPS technology enable the UAS to provide accurate geo-referenced visual assets. With cooperation of photogrammetry, a technology that encompasses methods of image measurement and interpretation to collect the shape and location information of an object from single or multiple photographs, a geo-referenced three-dimensional (3D) model is generated for survey applications. In principle, the main purpose of a photogrammetric measurement is the 3D reconstruction of an object in digital form (coordinated and derived geometric elements) or graphic form (images, drawings, maps) (Luhmann, 2014). To be more specific, the 3D reconstruction is based on automatically finding thousands of common points between images. Each characteristic point in an image is called a key-point. When two key-points on two different images are

found to be the same, they are matched and referred to as a tie point. Each group of correctly matched key-points will generate one 3D point. The developed 3D model can be computed and exported as a point cloud, ray cloud, or Digital Elevation Model (DEM) after processing. The 3D outputs are adopted for various applications.

As introduced earlier, the UAS were initially developed and used for military applications, but it attracts many researchers and experts to apply it for diverse non-military purposes. So far, much research has been conducted on 3D mapping and modeling by UAS and photogrammetry in some typical domains:

- Archaeology and cultural heritage. Bendea, H., et al. evaluated the 3D mapping accuracy of UAS photogrammetry to state the suitability for archaeological purposes (Bendea, et al. 2007). Hernandez, J., et al. presents a novel, low-cost, user-friendly photogrammetric tool for generating high-resolution and scaled 3D models of complex sites, and the results obtained with unmanned aerial vehicle (UAV) photogrammetry of an archaeological site indicate that this approach is semi-automatic, inexpensive and effective. Francisco-Javier (2015) described the configuration and technical specifications of an UAS for the acquisition of images needed for the production of orthomosaics to be used in archaeological application and investigated the combined effect of flight parameters on mapping quality.
- Environmental surveying. Ezequiel et al. (2014) discussed the use of a low-cost unmanned aerial vehicle (UAV)-based remote sensing system for different applications, namely post-disaster assessment, environmental management and monitoring of infrastructure development through multiple user cases. They also

presented the methodological and experimental aspects of correctly implementing a UAS-photogrammetry system. Also, they evaluated the accuracy of the results under various mapping conditions, including direct and indirect geo-referencing with different numbers, distributions and types of ground control points (Shahbazi, et al 2015).

- Transportation. Puri et al. (2007) applied UAS to collect spatial-temporal visual data that are used to generate traffic-related statistical profiles, serving as inputs to traffic simulation models; Benjamin et al. (2006) investigated the use of UAS to monitor roadway traffic and develop and demonstrate several applications using data collected from a UAS flying in an urban environment. There is also much research focusing on the application of UAS photogrammetry in civil engineering. Metini and Hamel (2007) described the dynamics of the UAS for monitoring of structures and maintenance of bridges. They presented a novel control law based on computer vision for quasi-stationary flights above a planar target; Morgenthal and Hallermann (2014) discussed the use of the UAS for inspection of critical structural components and hot spots that are hard to reach. They presented possible applications of Unmanned Aerial Vehicles in bridge inspection and the first steps in developing a semi-autonomous inspection method for automatic damage detection in post flight analysis. Rathinam et al (2008) addressed the problem of monitoring civil systems such as oil-gas pipelines using an autonomous UAS based on visual feedback. A single structure detection algorithm was developed to identify and localize various structures including highways, roads, and canals. Javier et al. (2012) performed an expert analysis (heuristic evaluation) as well as a

user participation analysis on a quadricopter to determine the features of an ideal safety inspection drone. The results of these two evaluations led to recommendations for the required features of an Ideal Safety Inspection Drone.

- In the aspect of earthwork volume measurement, Sibert and Teizer (2014) evaluated the performance of the application of the UAS in surveying earthwork projects. They developed a performance model for estimating the position error and conducted tests in several realistic construction environments. Hugenholtz et al. (2014) quantified the accuracies of an in-house developed UAS through a stockpile volumetric survey. They compared the UAV photogrammetric results with conventional GNSS survey results and tested the repeatability of the UAV system. Lee and Yosoon (2013) used unmanned aerial vehicles (UAV) to overcome the limits of ground photographic shooting angles to conduct low-elevation photography of sediment disaster areas. They conducted real-time positioning by reference to ground control targets to assess disaster situations and disaster relief horizontal accuracy.

However, UAS and photogrammetry for research applications is still in its infancy, and research conducted on UAS and photogrammetry for earthwork volume estimation are still limited. For example, the accuracy analysis in most publications only depends on measuring point positional error. There is not a quantitative analysis with respect to the influence from multiple factors on the mapping quality. Also, notably absent from most articles discussed above is a comprehensive analysis with respect to the impact of UAS photogrammetry application on cost and safety. Therefore, this research intends to investigate and validate the feasibility and efficiency of utilizing the UAS and

photogrammetry surveying technique to estimate earthwork volume and then improve the practice of earthwork volume measurement. The detailed objectives are stated as following:

## **1.2 Research Purpose**

The primary objective of this research is to investigate and validate the effectiveness and efficiency of using the UAS and photogrammetry to measure earthwork volumes. The result can be used as a practical reference regarding the use of the UAS for construction managers or engineers when measuring earthwork volumes.

To achieve the goal of comprehensively assessing the application of the UAS and photogrammetry in earthwork volume measurement, this research needs to figure out:

- The procedures of using the UAS to capture images on site and processing the collected images in photogrammetry software;
- How to determine the measurement accuracy of the post-processed output;
- The important factors for UAS performance and how these factors impact on the measurement accuracy;
- The advantages and disadvantages of the UAS and photogrammetry technology compared with conventional methods when measuring earthwork volumes.

All of the questions should be answered through quantitative analysis and observations based on the data collected from field experiments on site.

## **1.3 Research Scope**

This research discusses the applications of UAS and digital photogrammetry. According to the object and camera position, photogrammetry can be classified into five categories:

satellite, aerial, close-range, terrestrial, and macro (Luhmann et al., 2013). This research focus on the category of aerial photogrammetry due to the images are captured by the UAS. Also, although the quality of the UAS could affect the measurement results, especially the quality of equipped cameras, this research does not consider the use of expensive, high-end devices but employs the popular, economic, and stable equipment, with which construction professionals are able to operate easily and conveniently on site.

The images are processed in a photogrammetry software. The software generates the measurement through complex mathematic computations. Because the focus of this study is on the investigation of the practical performance of the UAS and photogrammetry in earthwork volumes estimations, this dissertation does not consider the impact of processing factors in software on the measurement accuracy. The selections of values of processing parameters follow the optimal recommendations from technical professionals.

The selection of earthwork volume measurement methods and the estimation process could be different from construction projects regarding the size of areas, topographical conditions, or the budget. The earthwork job sites selected in this research are from highway projects. The earthwork of a highway project usually requires a large amount of cost and labor because it usually produces a large quantity of earthwork and its length make the surveying process more difficult. Therefore, the highway project is an application that could benefit from improving the current practices of earthwork volume measurements.

Last but not least, this research aims to validate the effectiveness of this emerging technology. The effectiveness is embodied and realized by the measurement accuracy in

this research, and the measurement accuracy can be quantified and used to perform verifications and comparisons.

#### **1.4 Research Methodology**

This research intends to investigate and validate the feasibility and efficiency of utilizing the UAS and photogrammetry surveying technology to estimate earthwork volume through three distinct projects, the details are described as follows:

- Adapting a basic accuracy to prove the effectiveness of the UAS photogrammetry method in earthwork volume measurement; also providing an analytical foundation for further utilizations.
- Quantitatively assessing the impact from potential factors on the accuracy of UAS photogrammetry in earthwork volume measurement and identifying the most influential individual or combinations through statistical multiple regression analysis.
- Comparing volumes calculated by using the UAS platform and two other conventional methods which are Average-End-Area method and grid method in AutoCAD to further validate the feasibility of using the UAS technology in the process of earthwork volumes estimation.

#### **1.5 Dissertation Outline**

This dissertation is composed of five chapters. The process to investigate the effectiveness and efficiency of using the UAS and photogrammetry technology in earthwork volume estimations are presented in a structured manner.



The first chapter introduces the background, motivations, literature review and an overview of the research including purposes, scope and methodology.

The second chapter presents the basic procedures of making UAS flight strategy and measurement results after image processing in digital photogrammetry software based on a highway extension project.

The third chapter analyzes important flight and environmental factors that affect the photogrammetric measurement results through multiple test flights over a study area.

The fourth chapter introduces conventional earthwork measurement methods and compares the earthwork volumes of a highway project calculated by these methods with the volume computed by the UAS platform.

The fifth chapter summaries the contribution of the research to the practice and the body of knowledge. As well as, the limitations of this research and potential topics for future study.

## **2. ESTIMATING EARTHWORK VOLUMES THROUGH THE USE OF UNMANNED AERIAL SYSTEMS**

### **2.1 Introduction**

On a construction project, an accurate and reliable estimate of earthwork quantities can be key to survival for earthwork contractors. Earthwork volumes are usually used in determining the economic distribution of earthwork (Oglesby and Hicks, 1988). The contractor will not be able to present an accurate bid, correctly assign construction assets, or plan a project schedule without an accurate estimate. Also, disagreements on the estimated volumes can result in the owner and contractor going to the courts for settlement (Gates and Scarpa, 2004). However, the measurement of actual work on site is much more difficult to estimate. It is extremely time consuming because of irregularly shaped areas, different slopes, and variable sub-surface conditions (Cope, 1993). A frequent practice would be to estimate based on the size of the bucket of the equipment used and the number of cycles completed. Other practices involve conventionally volumetric estimations based on survey points such as average-end-area or cross-sections methods. However, researchers have realized the imprecision and limitations of traditionally survey methods. For instance, the cross-section method can only be applied at survey stations, and an assumption about the homogeneity of ground slopes between consecutive cross-sections has to be made (Contreras et al., 2012). Also, there are more safety concerns regarding unexpected landslide and ground movement.

Due to the importance and high demands of earthwork volumes estimation, three-dimensional (3D) measurement methods become more popular to facilitate the volumetric analysis. A 3D intelligent model of the target object or area is created to reflect the

elevation and surface. The accuracy of volume calculation using 3D methods mainly depends on the correct reconstruction of the earth surface that is usually represented by specific 3D coordinate points with various distributions (Yakar, 2008). Laser scanning and photogrammetry are two of the most common approaches for making non-contact and rapid spatial measurements due to their flexibilities to execute volume calculations regardless of time, weather and site conditions (Ragheba and Ragabb, 2011). However, laser scanners are high cost techniques with an intensive and complex post-processing (Cardenal et al., 2008). Also, laser scanners are unable to generate sufficient information on particular objects or object features directly in exact global orientation. Therefore, the usage of unmanned aerial system/vehicle (UAS/UAV) is increasing in popularity.

The UAV, or also colloquially drones, was originally developed and used for military implementations. They are remotely controlled aircrafts or helicopters equipped with precision sensors. Inertial motion units (IMU) and gyroscopes are used to recognize the alignment and position of the aircraft so that a pilot can control the navigation without much manual operation. Also, highly accurate and low-cost Global Positioning Systems (GPS) (Siebert and Teizer, 2014) can maintain the position of a UAV system in a global reference system everywhere in real time. The application and performance of the UAV are further improved when digital photos and video cameras are capable of converting UAV systems to highly mobile sensor platform. Unmanned aerial systems (UAS) typically consist of unmanned aerial vehicles (UAVs) and ground equipment for planning and transferring flight routes to the UAV as well as for monitoring the UAV telemetry data. In recent years, UAV systems are being utilized for diverse non-military purposes such as photogrammetry for 3D modeling (Colomina and Molina, 2014), remote sensing and

mapping (Nex and Remondino, 2014), forest and agricultural applications (Saari et al., 2011 and Rango et al., 2006), and many other fields. Specifically, Siebert and Teizer (2014) performed an evaluation of an UAV system that was built to rapidly and autonomously acquire mobile 3D mapping data. They also developed a performance model for estimating the position errors in several realistic construction environments. Hudzietz and Saripalli (2011) presented a method for UAV based structure-from-motion mapping and showed it to be a viable option for large scale, high resolution terrain modeling. Subsequently, aerial images taken of the landscape can be reconstructed into 3D models of the terrain, which means a UAV-based platform for photo collection in large-scale terrain modeling is economic, efficient, and accurate. All of successful applications are mainly due to the fact that UAS/UAV are economic, efficient, safer, and easy to operate when collecting images. However, only few researches are found in the literature are about the application of UAV/UAS in civil engineering applications, especially construction management. In this pilot project, the UAS/UAV and digital photogrammetry technology, which have the capacity to acquire high-resolution imagery from any angle and identify different object characteristics in a cost effective and efficient way, is introduced to estimate earthwork volume of a highway extension project in Lexington, KY.

## **2.2 Methodology**

### **2.2.1 Capture Geo-referenced Images of the Facility**

As introduced previously, UAV platforms are an innovative and reliable source of data capture for 3D modeling. An UAV, or drone, is capable of performing the photogrammetric data acquisition with equipped digital cameras. It can fly in manual, semi-automated and autonomous modes. With cooperation of image processing/ photogrammetry software, 3D

results like Digital Surface Model (DSM) / Digital Terrain Model (DTM), contour lines, textured 3D models, etc. can be produced in an automated way. In this project, the 3D model of the construction site was built by Pix4Dmapper which is a professional UAV processing software with images to be captured by the dual-controlled DJI Inspire 1 drone. Pix4Dmapper automatically converts images taken by hand or drone, and delivers highly precise, geo-referenced 3D models, maps and mosaics. To be more specific, Pix4Dmapper is based on automatically finding thousands of common points between images. Each characteristic point in an image is called a key-point. When two key-points on two different images are found to be the same, they are matched and referred to as a tie point. Each group of correctly matched key-points will generate one 3D point. When there is high overlap between two images, the common area captured is larger and more key-points can match together. More key-points could improve the computation accuracy for the 3D location of each point. Thus, the key rule is to maintain high overlap between the images. The recommended overlap for most cases is at least 75% frontal overlap (with respect to the flight direction) and at least 60% side overlap (between flying tracks). In this project, no large vertical objects such as buildings and power towers will be modeled and calculated, so the grid pattern flight plan can be applied to capture images (Figure 2.1).

The large area of interest may have negative influence on modeling. To avoid this, multiple flight plans can merge into one single project. Pix4Dmapper is able to process images taken from multiple flights. In order to obtain accurate results, each plan should capture the images with enough overlaps. Also, there should be enough overlap between two image acquisition plans (see the Figure 2.2). The data should be collected under the same conditions, e.g. same flight heights, sun direction, weather conditions. Especially the flight

height, it is always recommended to keep the same flight height for each image collection because all images could have the same level of detail which helps facilitate key-points matching between images.

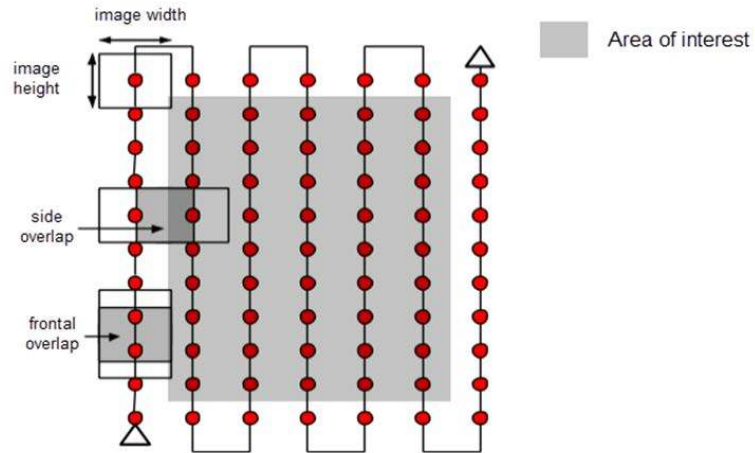


**Figure 2.1 Grid Mission Image Acquisition Plan (Pix4D, 2016)**

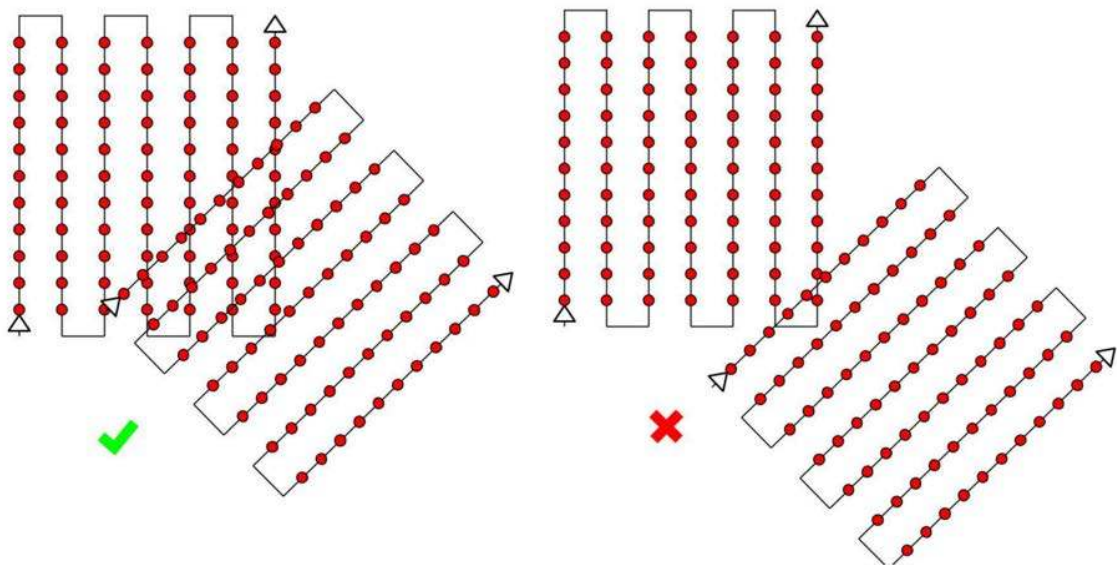


**Figure 2.2 Enough Overlaps and Not Enough Overlaps between 2 Flights (Pix4D, 2018).**

In this project, the authors visited the site two times and flew the drone twice for each visit considering the size of the target area. The purpose of the survey was to identify the volume change of earthwork between two stages during the construction. There were 74 days between the two visits. The grid mission flight plan was adopted in this survey because it covered the main earthwork area and surrounding environment, (Figure 2.3 and Figure 2.4).



**Figure 2.3 Grid Mission Plan for Stage 1.**



**Figure 2.4 Grid Mission Plan for Stage 2.**

Generally, the images captured by the drone are geo-located. The default Coordinate system is WGS84, which is not only the standard U.S. Department of Defense definition of a global reference system for geospatial information, but also is the reference system for the Global Positioning System (GPS). Although Pix4Dmapper can process images and build the model without geo-locations, lower precision results are expected if less than 3 images are geo-located. Without the actual coordinates measured by GPS, the scales and measurements of the model may be imprecise. Even though the original images have no geo tags, the quality and accuracy still can be controlled by Ground Control Points (GCP) that are manually added into model after initial processing.

The selection of an optimal image acquisition plan is the first step to build an accurate 3D model of the facility. After capturing the image/data, the image processing and manual modification are the most important procedures for accuracy improvement and quality control. The detailed image processing will be introduced in the next step.

### **2.2.2 Process the Images into an Accurate 3D Point Cloud**

There are three steps of image processing by Pix4Dmapper. They are initial processing, point cloud densification, and DSM, Orthomosaic creation. When initial processing starts, Pix4Dmapper computes key-points on images. It will use key-points to find matches between images. Based on initial matches, the software runs an Automatic Aerial Triangulation (AAT) and Bundle Block Adjustment (BBA). These two methods allow the software to automatically process with or without known camera positions and exterior orientations. By initial processing, the software produces a 3D model made of 3D points called Automatic Tie Points. Each tie point's corresponding 2D key-points are automatically detected in images and used to compute 3D position. Each image is



processed based on the estimation of camera position when the image is acquired, which is calibration process.

However, there is a probability that the calibration is not precise enough. The calibration process introduces error and noises in the 3D model. Reconstruction errors might appear in areas having very few Automatic Tie Points or somewhere the points seem to form double layers. Inadequate overlap is always the main reason of inaccurate calibration. One method to improve calibration is taking more pictures to ensure enough overlaps. Another way is the introduction of manual tie points, especially for the missing areas of the model. A Manual Tie Point is a point without 3D coordinates marked in images by users. At least two images should be marked for estimation. Then the estimated 3D point is re-projected in all the images where it might be visible. In many situations, a poor re-projection is resulted from the material of surface and invisibility of vertical facades. In this project, the construction is undergoing the earthwork stage, and no buildings block the area of interest. The site does not have reflective surface such as water or sand. The terrains with water, snow or sands are difficult to be mapped due to surfaces that have almost no visual features. Sun reflection on the water and waves cannot be used for visual matching because of large uniform areas.

### **2.2.3 3D Point Cloud Model Generation**

The initial process generates a model that is only composed of tie points. It not suitable for visualization and accurate measurements but the processing time is short. For further usage and modifications, a point cloud model should be created. A point cloud is a set of data points in a three-dimensional coordinate system, and each point is defined by X, Y, and Z coordinates. The point cloud is normally used to represent the external surface of an object.

It is also applied in quality inspection, multitude of visualization, and animation, etc. Basically, a 3D point cloud model generation follows this procedure built by the photogrammetry software (Pix4D 2018):

1. Key-points extraction: Identifying specific features as key-points in the photos.
2. Key-points matching: Find which images have the same key-points and match them.
3. Optimization and orientation of camera model: Calibrate the internal and external parameters of the camera.
4. Adding GCPs for precise orientation: Locate the model if geolocation information is provided.
5. Point Densification: Additional Key-points are created based on the Automatic Tie Points that generate a Densified Point Cloud.

During this process, selecting appropriate processing options and correctly locating the GCPs are crucial steps for creating dense point cloud model. Image scale and point density are two important parameters for the 3D point cloud model creation. Image scale defines the scale of the images at which additional 3D points are calculated, and point density defines the density of the point cloud model. For example,  $\frac{1}{2}$  image scale means only half size images will be used to compute additional 3D points. Low point density means a 3D point is computed for every  $(16/\text{image scale})$  pixel. These two parameters are interactive with each other and decide the point cloud densification and processing time. As shown in Figure 2.5, this case used  $\frac{1}{2}$  image scale and optimal point density for processing.

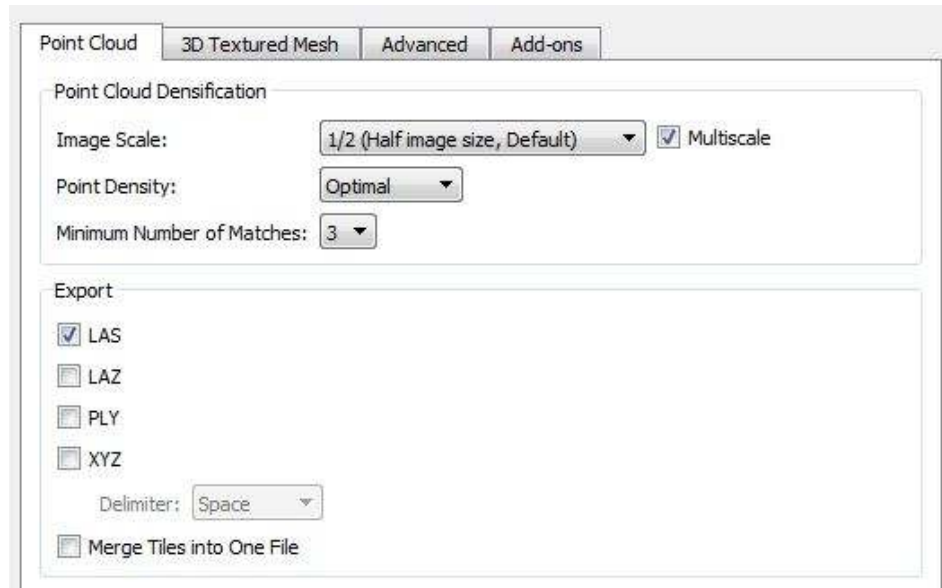


**Figure 2.5 Processing Options for Point Cloud Generation**

Another crucial step is to add the GCPs in the model. After collecting and measuring GCPs in field, GCPs should be marked in the rayCloud generated during the initial processing. When selecting a GCP in the model, the software will display its properties and the list of images in which it is visible. Next is to mark the exact position of the GCP on at least 2 images. When the green cross is at the correct position in most images, it means the GCP is added successfully (Figure 2.6). The closer to the exact position when marking, the more precise the GCPs locations can be.



**Figure 2.6 Marking a GCP**

For more realistic visual operations, the triangle mesh should be generated. Although triangle mesh model is best for visualization, it is not clear enough for detailed modification on a small scale. Therefore, most operations are performed on the point cloud level. After initial processing and point cloud densification, two 3D point cloud models of the site at different stage are created based on 310 and 425 images captured by the UAV (Figure 2.7 and Figure 2.8).



**Figure 2.7 Point Cloud Model of the Site at Stage 1**

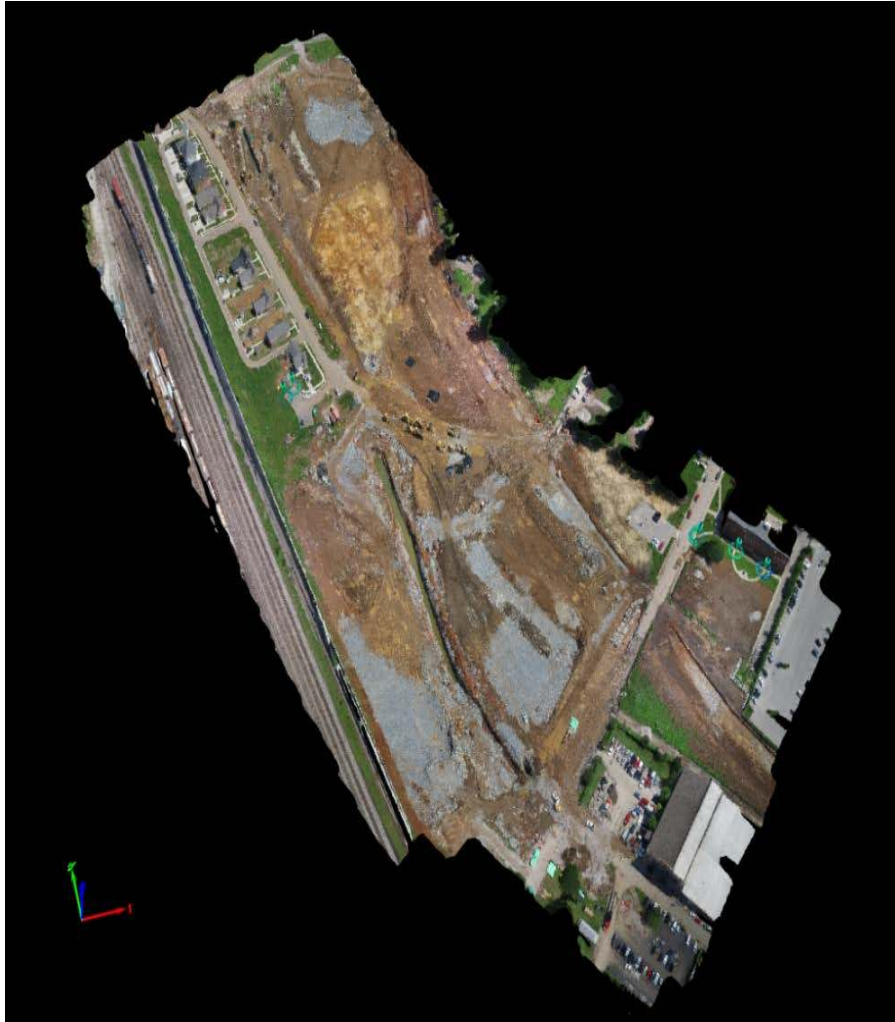


**Figure 2.8 Point Cloud Model of the Site at Stage 2**

The parameters of each process can be adjusted to optimize the accuracy and visualization of models. For example, the key-points image scale allows users to define the image size used to extract the key-points in the initial processing. The full image scale is set precise results. Our goal is to obtain an accurate result of measurements, so the rapid image scale is not optimal choice. Also, point density and minimum number of matches can be defined based on the expectation of users. In this project, default values were selected for most parameters. The grid flight mission ensures images are taken with optimal overlaps to get an accurate 3D model based on the flat terrain surface of this project. There are no major

impacts on the measurement accuracy when selecting different values within a reasonable range. For example, the main difference between ½ image scale and ¼ image scale are computing speed in this project. A detailed illustration about the selection of parameters will not be discussed here.

#### **2.2.4 Accuracy Test for 3D Model**

For the use in surveying application, an absolute accuracy test is mandatory. The quality of the 3D model depends on the number of images and manual tie points. The use of Ground Control Points (GCPs) is an effective method to improve accuracy. GCPs are points with known coordinates measured by highly accurate GPS units or hands in the area of interest. As illustrated above, Pix4Dmapper can process projects with or without geolocations, but accurate GCPs make the global accuracy of the project higher. GCPs will give the scales, orientations and positions to the final results. The geo-tags of images may be inaccurate, and thus the 3D model is relatively correct in position. The linear measurements should be applied to fit the entire project to the correct scales. The GCPs can be measured in the field with topographic methods, taken from existing geospatial data or Web Map Service (WMS) such as Google Map. After obtaining GCPs measurements, the project team imported the GCPs with the GCP / Manual Tie Point Manager and re-optimized the model. When the optimization is finished, the GCPs need to be marked. As same as adding a manual tie point, when marking the GCPs on the images, each mark is used to compute a new 3D point. At least 2 images need to be marked in order to compute the estimated 3D positions. In this project, 6 GCPs were added in the 3D point cloud model for both stages. Three photogrammetric measurements were conducted and compared to the conventional surveying method. A GPS rover was used to obtain the real coordinate of

each GCP so that the lengths between two points could be calculated. The difference between real and computed position indicated the errors in measurements. The performance of UAV/UAS and photogrammetry techniques will be evaluated.

### 2.3 Result

In this project, 6 GCPs were collected on site for both stages (Figure 2.9, Figure 2.10, and Figure 2.11). Table 2.1 displays the coordinates of every GCP measured by the GPS. Two comparisons were conducted for the accuracy analysis. The positional errors are shown in Table 2.2 and Table 2.3.

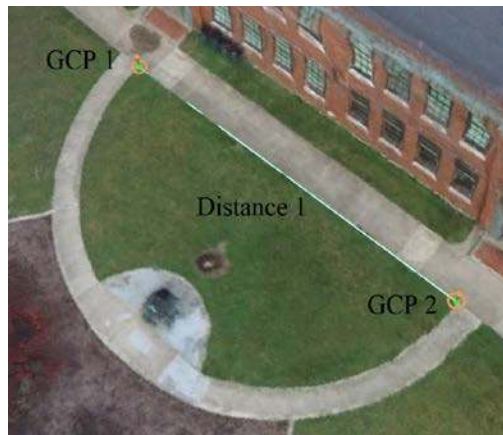


**Figure 2.9 Locations of GCP 1 and GCP 2**



**Figure 2.10 Locations of GCP 3 and GCP 4**



**Figure 2.11 Locations of GCP 5 and GCP 6**

**Table 2.1 Coordinates of GCPs**

Name	Coordinates (X, Y, Z)
GCP 1	(3906793.513, 5278893.381, 952.222)
GCP 2	(3906737.437, 5278945.076, 952.437)
GCP 3	(3906853.023, 5278816.615, 947.889)
GCP 4	(3906847.645, 5278810.920, 947.806)
GCP 5	(3907452.225, 5277871.866, 935.115)
GCP 6	(3907432.788, 5277846.469, 935.629)

**Table 2.2 Distances Measurements of 3D Point Cloud Model in Stage 1 (ft)**

Name	Photogrammetric Measurement	GPS Measurement	Error (%)
Distance 1	74.2467	76.2795	0.043
Distance 2	7.8083	7.8083	0
Distance 3	31.9882	31.9554	0.1025

**Table 2.3 Distances Measurements of 3D Point Cloud Model in Stage 2 (ft)**

Name	Photogrammetric Measurement	GPS Measurement	Error (%)
Distance 1	75.5249	76.2795	0.98
Distance 2	7.8412	7.8084	0.4
Distance 3	31.9226	31.9554	0.1026



The reason for creating two models at different times was to identify the progress of earthwork. The difference of earthwork volumes between two stages is not convincing if the accuracy of two models are not in the same level. One can assume the images of two models captured in same conditions if the error is within a reasonable range. According to the results obtained by Pix4D and conventional GPS surveying method, the average error of measurements is 1.77 inches. The errors between the measurements of two stages are within a range of 0.1% to 0.9%. The main changes of earthwork between two stages are a stockpile and a trench based on the observations. In Pix4D, the volume is computed using the point cloud model. When creating a volume object, we draw the base surface of the volume by making the vertices of the base. A manual tie point is associated to each vertex of the volume (Figure 2.12, Figure 2.13 and Figure 2.14). The position of each vertex can be moderated for accuracy improvement. Then, the software will generate the total volumes, including cut and fill volumes, and the measurement errors.

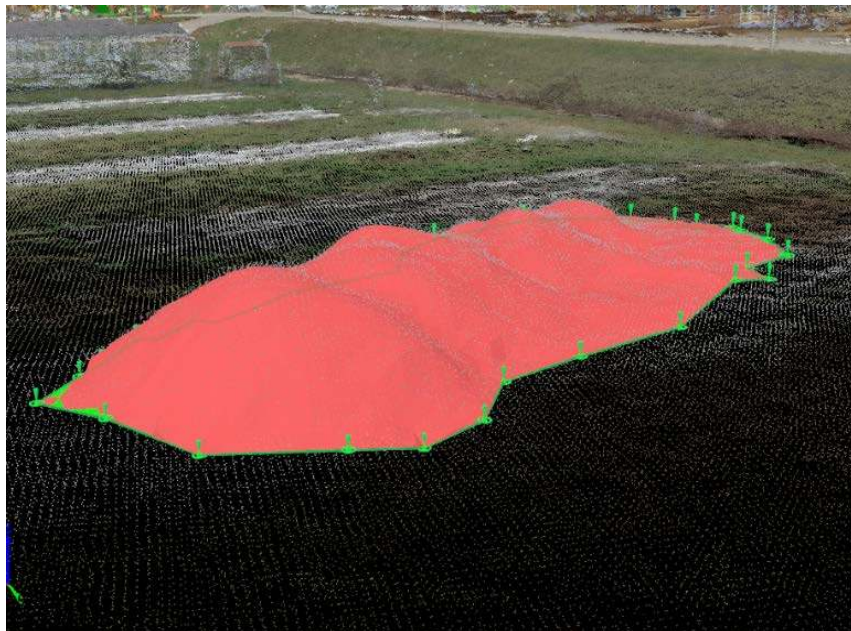


**Figure 2.12 Stockpile Volume Drawn in Point Cloud Model**

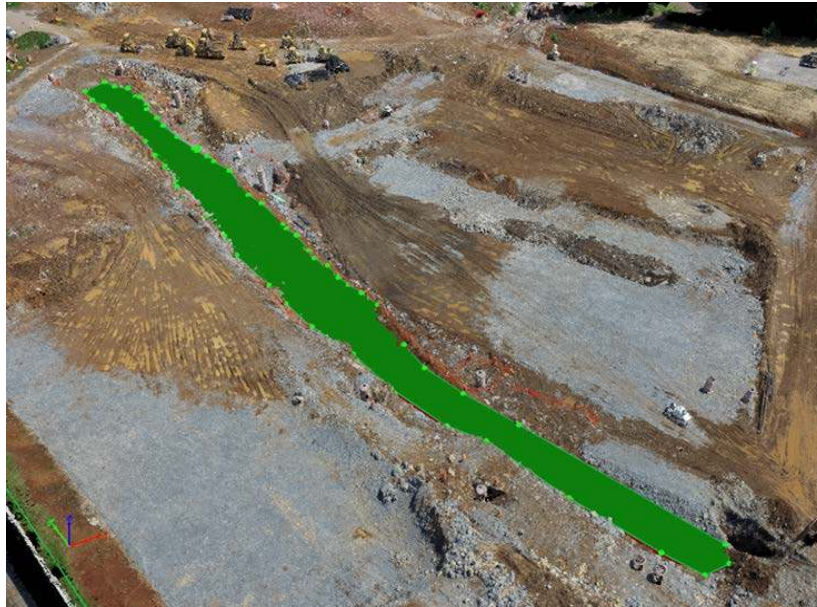


**Figure 2.13 Trench Volume Drawn in Point Cloud Model (front)**

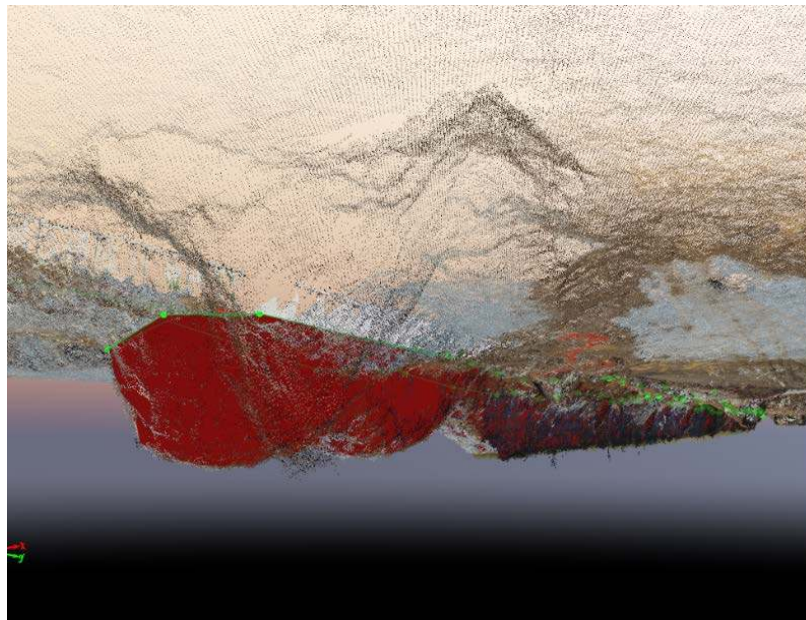


**Figure 2.14 Trench Volume Drawn in Point Cloud Model (Below ground)**

The computation result is shown in Table 2.4. The Pix4Dmapper estimates the error of volume calculation based on spatial resolution and the coordinate of each point. The spatial resolution depends on Ground Sampling Distance (GSD), which is the distance between

two consecutive pixel centers measured on the ground. The Pix4Dmapper projects a grid with GSD spacing on the base of the volume (Figure 2.15).

**Table 2.4 Volume Calculation Results (ft<sup>3</sup>)**

Object	Total Volume	Estimated Error
Stockpile	2850.2468	±206.94 (7%)
Trench	-385558.82148	±3311.4563 (0.9%)



**Figure 2.15 Grid on the Base of the Volume (Not the Real Dimensions)**

For each cell of the grid, its volume is given by Equation 1:

$$V = L \times W \times (H_1 - H_2) \quad (1)$$

Where,

$L$  = GSD = the length of the cell.

$W$  = GSD = the width of the cell.

$H_1$  = the terrain altitude of each cell at the center of the cell

$H_2$  = the base altitude of each cell at the center of the cell.

The altitude of a 3D point is calculated with an accuracy of 1 to 3 times the GSD. The average error for the altitude of each point is 1.5 times the GSD (Pix4D 2018). The volume error for each cell is estimated by:

$$E_i = L_i \times W_i \times Z_{ei} = GSD \times GSD \times 1.5 GSD = 1.5 \times GSD^3 \text{ (Pix4D 2018)}$$

Where:

$E_i$  = the volume error of one cell.

$L_i$  = the length of the cell.

$W_i$  = the width of the cell.

$Z_{ei}$  = the error in Z direction of the cell.

In this project, the error of the stockpile is much larger than the trench; one of possible reason is that the contour of the stockpile is not distinct as the trench. The more vertices of the volume base that are marked, the more accurate of the calculation result will be. Since the experiment in this project is unique, so there is no reference to compare. Siebert and Teizer (2014) conducted a performance analysis of the developed UAV system for excavation work on a highway construction site. They compared the volumes of three earth piles computed by the automated UAV-direct geo-referenced mapping approach with the result obtained by Robotic Total Station (RTS) method. The average survey error of their experiment was around 11%. Although the case study is different, it still can be a valuable reference. In addition, the study shows that 4.5% overestimated error when using cross-section measurement methods (100ft cross-section distance) according to the standard specification published by the Kentucky transportation cabinet, which also prove the effectiveness of the UAS and photogrammetry method.

## **2.4 Conclusion**

According to the comparisons between measurements by UAS/UAV photogrammetry and traditional manual methods, the average error is in allowable range according to latest

literature. The results support the accuracy and mapping suitability of UAV photogrammetry applications in earthwork construction. Also, the UAV aerial photogrammetric approach was more efficient, taking around 5.5 hours to complete the on and off-site work.

This paper presents an application of UAS/UAV in construction earthwork that may help with time and accuracy improvements over the conventional means of estimating actual earthwork quantities. However, there still needs more accuracy tests through comparison with other more surveying methods such as laser scanning; factors and errors influencing UAV/UAS photogrammetric measurements need more definitions and discussions. Some technical and operational limitations of current UAV systems may need resolution, such as compatibility issues between different devices, and limited flight durations. Also, there are a lot of potential applications of UAS/UAV in various aspects of construction management. For instance, the soil density could be estimated by tracking the weight of the excavated soil from truck measurement and the volume calculated from this work. Also, could help the manager monitor construction activities from site preparation through project completion in expensively. This accurate cost and time saving process allows the team to review multiple aspects of the construction process and to make correct decisions or actions.

### **3. THE INFLUENCE OF POTENTIAL FACTORS ON MEASUREMENT ACCURACY OF APPLYING THE UNMANNED AERIAL SYSTEMS (UAS) AND PHOTOGRAMMETRY IN CONSTRUCTION EARTHWORK**

#### **3.1 Introduction**

Unmanned aerial systems (UAS) is an all-encompassing description that encapsulates the aircraft component, sensor payloads, and a ground control station. The unmanned aerial vehicle (UAV) platform is equipped with various sensors including cameras, Global Positioning Systems (GPS) and other specialized communication devices. The UAVs are capable of operating at different levels of autonomy controlled by a ground control station that is the activity hub during UAV missions and provides necessary capability to plan and execute UAV missions (Natarajan, 2001). The UAS can transfer visual assets collected by UAVs platform to its ground control station in near real-time (Irizarry and Costa, 2016). Photogrammetry, a technology using visual assets to derive measurements and three-dimensional (3D) models of real-world objects or scenes, uses the mathematics of light rays to build up information about the geometry of objects and the location of the camera when the images are taken. The photogrammetry technology aims to process or convert images captured by the UAS into various outputs such as point cloud models according to different needs. As more accurate GPS and camera technologies have developed, the use of UAS is becoming increasingly popular in various domains such as archaeology and cultural heritage (Bendea et al., 2007 and Gómez-Candón et al., 2014), forest and agricultural (Grenzdörffer et al., 2008), environment surveying (Ezequiel et al., 2014), emergency management (Chou et al., 2010 and Molina et al., 2012), and transportation (Puri et al. 2007). In the civil engineering domain, UAS have been adopted to solve various

problems such as bridge inspection (Metni et al., 2007 and Hallermann et al., 2014), soil erosion (d'Oleire-Oltmanns et al., 2012), earthwork monitoring (Siebert and Jochen, 2014) and measurement (Wang, X et al., 2017), and 3D model creation (Feifei, X et al., 2012).

To be more specific, in civil engineering, especially in construction engineering, the application of the UAS and photogrammetry has been preliminarily proved. Waugh (2006) generated a panorama view of the site situation through linking a series of site photos. Abeid et al. (2003) developed a construction control system by combining the construction progress chart with a database of site pictures; Memon et al. (2005) prototyped a digitized construction monitoring system, which is used to monitor and evaluate actual construction progress. Kim and Kano (2008) developed photo images in 3D computer graphics showing the as-built site conditions at a particular time. Zhu and Brilakis (2009) reconstructed a house and a wheel loader as two example cases validating photogrammetry as an optical sensor-based spatial data collection method for infrastructure modelling; Metni and Hamel (2007) described the dynamics of a UAS for monitoring of structures and maintenance of bridges; Morgenthal and Hallermann (2014) discussed the use of a UAS for inspection of critical structural components and hot spots that are hard to reach. Rathinam et al (2008) addressed the problem of monitoring some such civil systems such as oil-gas pipelines using an autonomous UAS based on visual feedback. In construction, Siebert and Teizer (2014) evaluated the performance of the application of the UAS in surveying earthwork projects. They developed a performance model for estimating the position error and conducted tests in several realistic construction environments. Hugenholtz et al. (2014) quantified the accuracies of an in-house developed UAS through a stockpile volumetric survey. These applications proved the feasibility and use of UAS and photogrammetry

technology in recording and tracking the construction progress for helping engineers and managers perform the quality control of construction projects.

However, the utilization of the UAS and photogrammetry technologies in construction is still at an early stage. The application range is still limited. For instance, only few studies discussed the application of UAS in earthwork measurement, even though it is one of the major components of a construction project. Due to some realistic issues such as local regulations, limited resource of test fields, or strict flight conditions, few research was conducted from a practical perspective to evaluate the effectiveness of this emerging technology. Therefore, this paper aims to conduct a quantitative analysis to analyze the influence of important UAS flight parameters and site conditions on the measurement accuracy. According to practical experience and literature, flight altitude, image overlapping rate, GCPs and soil type are key factors during the operation of UAS and modeling quality control (Sibert and Teizer, 2014; Mesas-Carrascosa et al., 2016; Nassar and Jung, 2012). The goal of this project is to compare the positional accuracy of points when applying different parameters in order to identify the effectiveness of each factor and interactions between them, thereby providing a practical reference for managers and engineers to allow for efficient application of UAVs and photogrammetry in construction projects.

## **3.2 Influential Factors**

### **3.2.1 Flight Altitude**

One of the most important flight parameters during the UAS operations is the flight altitude. It not only determines the size of pixel on an image, but also the flight durations and the



area to be covered (Christiansen et al., 2017). To be more specific, the flight altitude is related to the Ground Sampling Distance (GSD). GSD is the distance between two consecutive pixel centers measured on the ground. The larger the value of GSD, the lower the spatial resolution of the image and the less visible details. For example, a GSD of 2 inches means that one pixel in the image represents linearly 2 inch on the ground which is  $2*2 = 4$  square inch area. The GSD is positively correlated with flight altitude. At a defined focal length, decreasing the altitude results in lower GSD values. Lower GSD value indicates one pixel will capture a smaller area and therefore the image will have a higher spatial resolution, as shown in Figure 3.1

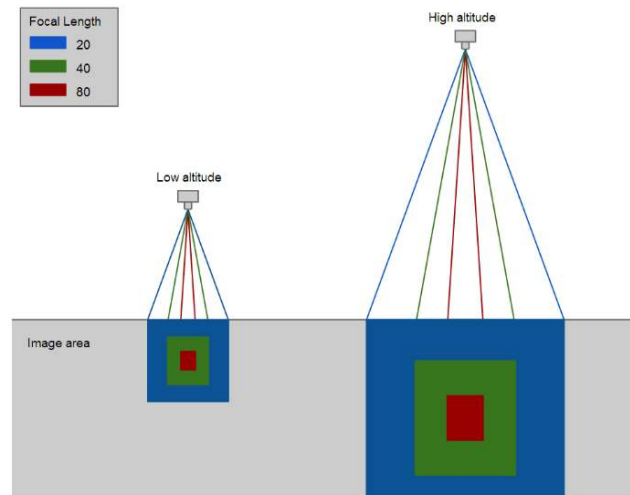


**Figure 3.1 Relation between Flight Altitude and Image Area (Pix4d, 2018)**

In selecting flight altitude, it is essential to consider the balance between the spatial resolution and area covered. Higher spatial resolution will contribute to image quality but may result in overlong flight duration. Due to the battery life limitation of the UAS, the operation has to be fragmented into multiple flights. Under different flight conditions, the image quality cannot be guaranteed because of issues such as variation in illumination,

saturated images, or appearance of shadows. Therefore, flight altitude is one of the most influential factors involving UAS performance.

### **3.2.2 Image Overlapping Rate**

Another crucial factor is the overlapping rate between images. Photogrammetry is a technology of image processing to interpret the shape and location of an object from one or more photographs of that object. It aims to reconstruct an object from graphic form to three-dimensional (3D) form. The shape and position of an object are determined by reconstruction bundles of rays which define the spatial direction of the ray to the corresponding object point. From the intersection of at least two corresponding and separated rays, an object point would be located in 3D space. Every image generates a spatial bundle of rays. A dense network, which is used to orient and calculate the associated 3D object point locations, is generated when all the bundles of rays from multiple images are intersected (Figure 3.2). During this process, Automatic Aerial Triangulation and Bundle Block Adjustment are key procedures to process the images. Automatic Aerial Triangulation is performed to determine the position and the orientation of the camera at the moment of each image being captured. The Bundle Adjustment is the program that processes the photographic measurements to produce the final XYZ coordinates of all the measured points (Michelitti, et al. 2015). Therefore, image processing is based on automatically finding thousands of common points between images. Each characteristic point in an image is called a key-point. When two key-points on two different images captured at different locations are found to be the same, they will match together. Each group of correctly matched key-points will generate one 3D point (Luhmann, T et al., 2014). When there is high overlap between each images, the camera on the UAS is able to capture

a larger common area to generate more matched key-points and thus improve the computation accuracy. In addition, the image overlap rate is related to the flight altitude regarding both accuracy and efficiency. For example, for a given focal length, increasing the altitude will increase the overlap between images. Also, although higher overlap will improve the quality of modelling, it requires longer UAS operation time. Therefore, image overlapping rate is another influential factor on the balance between the spatial quality and efficiency.

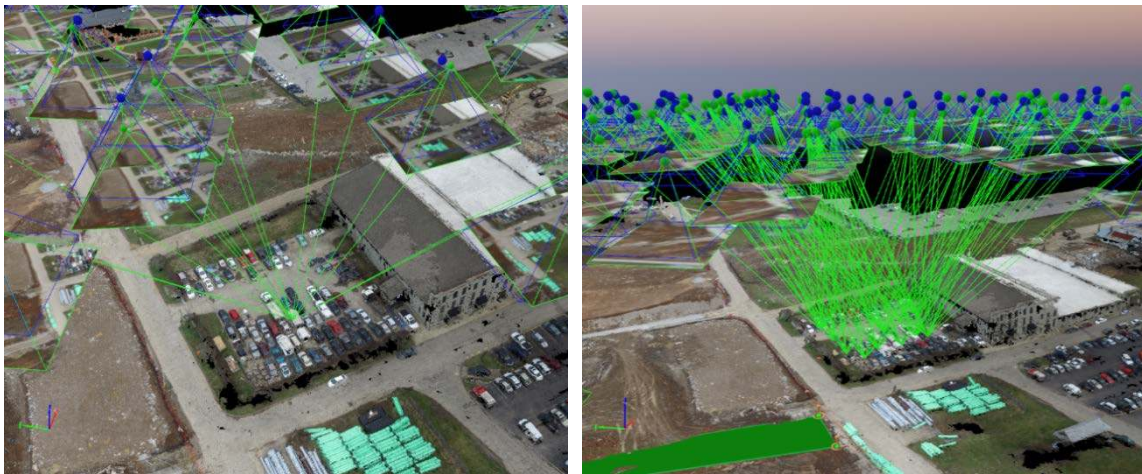


**Figure 3.2 Bundle of Rays from Multiple Images**

### **3.2.3 Ground Control Points (GCPs)**

For the use in surveying application, an absolute accuracy test is mandatory. The quality of the 3D model depends on the number of images and manual tie points. The use of Ground Control Points (GCPs) is an effective method to improve accuracy. GCPs are points with known coordinates measured by highly accurate GPS units in the area of interest. The photogrammetry software is able to process projects with or without geolocations, but accurate GCPs improve the global accuracy of the project. GCPs will give the scales, orientations, and positions to the final results (Wang et al., 2012). The geo-tags

of images may be inaccurate, and thus the 3D model is relatively correct in position. The linear measurements should be applied to fit the entire project to the correct scales (Agüera-Vega, et al., 2016). The GCPs can be measured in the field with topographic methods or taken from existing geospatial data or Web Map Service (WMS) such as Google Map. After obtaining GCPs measurements, the GCPs should be imported and used to re-optimize the model. However, unlimited number of GCPs does not lead to significant improvements in the global accuracy of models. Instead, it reduces the efficiency due to more GCPs requiring more time and labor to do measurements on site. Therefore, the number of GCPs and its distribution are important to control the modelling quality and accuracy of measurements.

#### **3.2.4 Soil Types**

The material of the mapping surface also has great impacts on the quality of models during the image processing. A 3D image is a non-contact measurement method applied to produce a 3D representation of a physical object (Furukawa and Ponce 2010). The point cloud model is the major output of image processing through photogrammetry. A point cloud is composed of a set of vertices used to represent the external surface of objects in a 3D coordinate system. The photogrammetry software generates a point cloud model through measuring a large number of points on the surface of an object (Nassar and Jung 2012). Therefore, the different surface material of an object may affect the modelling quality at various levels. In many situations, a poor re-projection is resulted from the material of surface and invisibility of vertical facades. Reflective surfaces such as water or sand are difficult to be mapped due to a lack of visual features. Sun reflection on the water and waves cannot be used for visual matching because of large uniform areas. In a

construction project, sand, gravel, clay, and rock are the four most common and fundamental materials encountered during earthwork operations (Nunnally, 2010). Each of them has different texture and colors; therefore, each soil type should be tested to identify their reflection capability and influence on the surface reconstruction.

### **3.3 Methodology**

#### **3.3.1 Photogrammetric Process**

Photogrammetry is a technology of image processing to interpret the shape and location of an object from one or more photographs of that object. This study uses a UAS to capture images of the site. Generally, the process begins with the flight mission planning. Once all the requirement and parameters are defined for the flight mission, a flight plan or an image acquisition plan is developed and aerial imagery is collected based on the project specifications. At the same time, a ground control survey needs to be conducted to improve the positional accuracy of the 3D outputs. After the image acquisition and the ground control survey, methods of image interpretation and measurement are required to complete the transformation between images and object.

To be more specific, the photogrammetry software first identifies and measures conjugate points in the overlapping photographs (Schenk, 1997). During this process, Automatic Aerial Triangulation (AAT) is the basic method used to analyze and perform exterior orientation of aerial images to calculate the 3D coordinate of object points (Yuan et al, 2015). In other words, the AAT represents the mathematical process of establishing accurate relationships between the individual image coordinate systems and a defined datum and projection on the ground (Tang et al., 1997). The main objective is to ensure

that each model can be oriented accurately as required. At the same time, the Bundle Block Adjustment (BBA), another basic method cooperating with the AAT to produce the final three-dimensional coordinates of all the measured points, is performed by a Structure from Motion (SfM) algorithm. Using UAS platforms, the SfM is operated using highly redundant information extracted from a group of high percentage overlaps that register the 3D structure of an object (Snavely et al., 2006). SfM extract features in each image of the photogrammetric block, which is matched to their corresponding features in another image. These matched features are used to compute the relative position of the camera sensor during the flight operations thus the orientation of each sensor can be calculated (Westoby et al 2012), as shown in Figure 3.3.

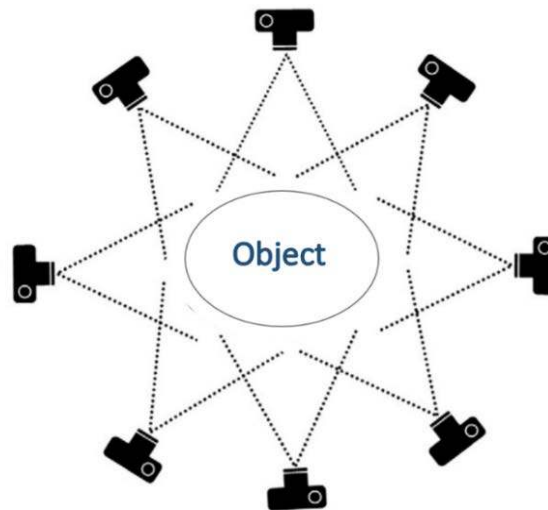


**Figure 3.3 Structure from Motion (SfM)**

The first output of the photogrammetric process is a point cloud model. A point cloud is a set of data points in a three-dimensional coordinate system, and each point is defined by X, Y, and Z coordinates. The point cloud is normally used to represent the external surface of an object. It is also applied in quality inspection, a multitude of visualization, and animation, etc. For more realistic visual operations, the triangle mesh should be generated. Although

triangle mesh model is optimal for visualization, it is infeasible for detailed modifications on a small scale. Therefore, most operations are performed on the point cloud model. However, in general, the geolocational accuracy of images on the UAS platform is not high (Mesas-Carrascosa, et al., 2016), which is the reason why the GCPs measured in the field with a greater accuracy is essential to improve the spatial quality of the model.

Although linear measurements are feasible in the point cloud model, when calculating the volume of an object, a Digital Surface Model (DSM) needs to be derived to orthorectify each image. Then, the orthorectified images are mosaicked to obtain an orthomosaic of the site area (Chiabrande et al., 2011). The DSM represents the elevations of the reflective surfaces of features elevated above the bare earth (Hirt et al, 2010). Especially in earthwork construction, at the time of UAS capturing images, the contractors may still make height adjustments on site, thus, the construction manager or engineers need to see the locations and heights of areas where completed earthwork differs from the plans (Sebastien and Teizer, 2014). Therefore, the DSM allows generating various views and reports that are useful for practitioners.

### **3.3.2 The UAS Device and Flight Plans**

The UAS used for image acquisition in this study was the DJI Inspire 1. This UAS is a vertical takeoff and landing aircraft powered by a 22.2V battery (Figure 3.4). Its system has a maximum takeoff weight of 7.71lbs and maximum wind resistance up to 10m/s. The maximum flight duration is approximately 18 minutes. The UAS is equipped with a 1/2.3 inch CMOS sensor with a 20mm lens, and the stock camera has 4096 × 2160 resolution for still images (DJI 2018). During operation, the autopilot flight setting will activate the image trigger. The UAS autopilot sends a signal to the equipped sensor to register a photos and

at the same time records the geo-referencing information such as location and navigation angles which can be used for post-processing on an SD card.



**Figure 3.4 UAS used in the study, DJI Inspire 1**

The study area was 163×247 ft in size and located at Coldstream Dairy Research Farm Complex of University of Kentucky (Figure 3.5). The complex includes a free-stall barn with 108 stalls for the milking herd, a tie-stall barn with 36 stalls used primarily for cows on research trials, a small free-stall barn with 18 stalls and Calan individual feeders, milking parlor that holds 8 cows (essentially 2 "double 2" parlors), replacement, heifer, dry cow, and maternity facilities, and a management building that serves as an office, teaching facilities, and laboratory space. The reasons of selecting this area as the test field were (1) having legal access, (2) it is located outside the city where it is broad and spacious.





**Figure 3.5 Overview of the Study Area**

Multiple flights were conducted following the scheme presented in Figure 3.6. This flight plan cooperates with different flight altitudes, image overlapping rates and the use of GCPs. A set of flight missions were performed at altitudes of 60, 90, 120 and 150ft. Due to the height of wire poles on the farm, it is dangerous to fly the UAS lower than 60ft. For each altitude, the UAS captured photos based on two different forward and side overlapping rates respectively: 40%-70% and 60%-90%. All the flight missions were performed under the same weather conditions, especially wind speed. In this study, Pix4Dmapper photogrammetry software was selected to process images and generate 3D point cloud and DSM models of the study area.

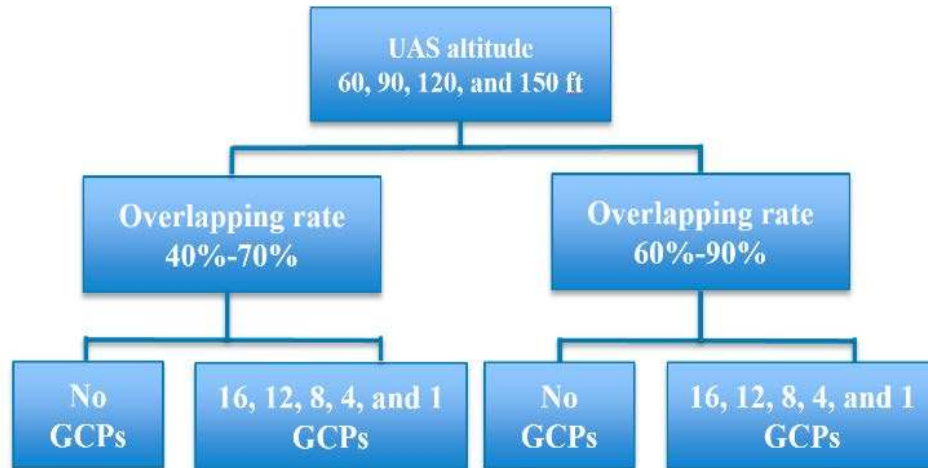


**Figure 3.6 Strategy of the UAS Flights and Processing**

To avoid the uncertainty of manual operation, the UAS was operated automatically based on the designed parameters and flight paths under the control of Pix4D mobile applications (Figure 3.7). In addition, all the flight missions followed the grid pattern because this study aimed to perform mapping over an area with large size rather than modeling a vertical object (Figure 3.8). In most cases, a grid pattern provides an effective platform to keep the same flight heights and to observe the variety of different image overlap rates.

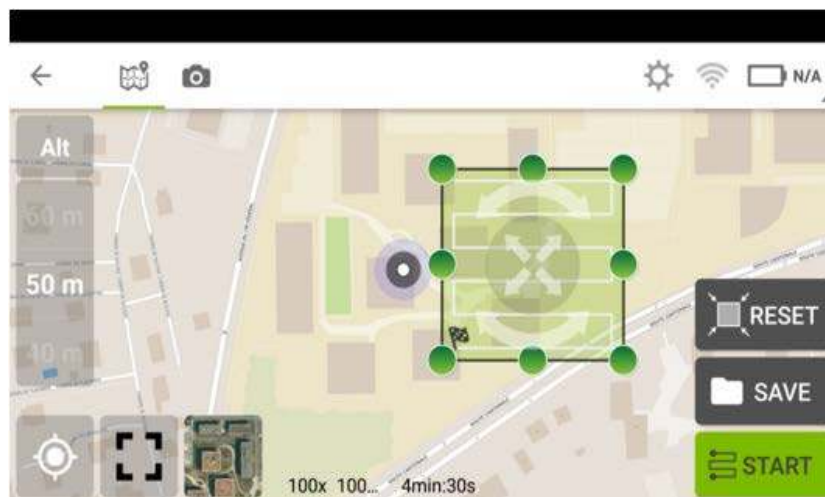


**Figure 3.7 Pix4D Mobile Application Interface**

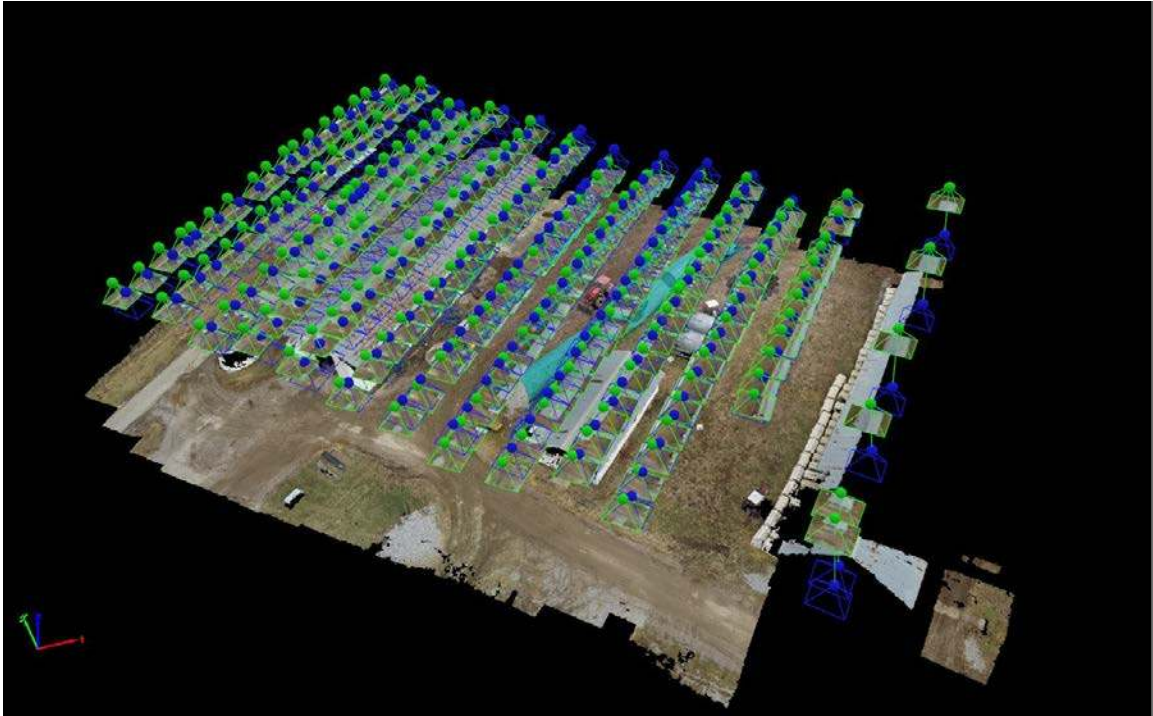


**Figure 3.8 Grid Flight Pattern over the Study Area**

Afterward, images captured by each flight were processed with and without GCPs. The coordinates of GCPs were measured by a EPOCH 50 GNSS Rover which is (Figure 3.9). Total 16 GCPs were measured located evenly across the area of interest to minimize the errors in scale and orientation. If GCPs are gathered at the same location, one side or the very edge of the area, the geo-reference would lose balance, which would make the GCPs unreliable or dysfunctional. Additionally, it is also recommended to place one GCP in the center of the area to further improve the quality of the reconstruction. Images were processed using a different number of GCPs in order to find the optimal strategy to add GCPs regarding both accuracy and efficiency. More details about GCPs will be introduced in the next section.



**Figure 3.9 GPS Rover**

### **3.3.3 Assessment of Accuracy**

The major output of image processing is a point cloud model. The accuracy of the position of each point directly contributes to the linear or volumetric measurements. To be more specific, the positional absolute accuracy is the indicator or measure of how a spatial object is accurately positioned on the map with respect to its true position on the ground, within an absolute reference frame such as UTM coordinate system (Küng et al., 2011). The 16 GCPs are performed as checkpoints to be used for measurement of positional accuracy no matter how many GCPs are used for processing. In this study, the position accuracy of points is evaluated by Root Mean Square Error (RMSE). (Luhmann, Thomas, et al. 2014, Siebert and Teizer, 2014). RMSE is a frequently used measure of the variances between values predicted by a model and the values observed (Armstrong and Collopy, 1992). The RMSE represents the sample standard deviation of the differences between predicted values and observed values. The RMSE is applied to aggregate the magnitudes of the errors in predictions for different times into a single measure of predictive power (Pontius et al, 2008). RMSE is an indicator of accuracy to compare errors of different models for a specific set of data as it is scale-dependent (Hyndman and Koehler 2006). Thus, the

comparisons between different flights will be indicated through RMSE. The RMSE is carried out by using the equation (1) as follows;

$$RMSE = \pm \sqrt{\frac{\sum(n_1 - n_2)^2}{N-1}} \quad (1)$$

where,

$n_1$  = difference between two parameters

$n_2$  = mean differentiation

$N$  = total number of points

### **3.4 Results and Discussion**

#### **3.4.1 Flight Duration and Number of Images**

This study conducted a total of 8 flights. The initial altitude was 60ft, and then the UAS ascended 30ft to fly the same area again. This operation repeated until all designed flight altitudes were tested. Table 3.1 illustrates the flight duration and number of images when selecting different values of flight altitude and image overlapping rate. Flight duration, collected in seconds, indicates the flight time needed for an individual altitude excluding the landing and taking off time. Number of Images indicates the total number of photos captured during an individual flight. The R2 is used to verify the linear regression model fits the collected data and to present the exponential correlation between the flight parameters. It was observed that the number of images and flight duration decrease as the flight altitudes increase for both images overlapping rates because more area can be covered by a single image (Table 3.1 and Figure 3.10). Between two different overlapping rates, higher overlapping rates require longer flight duration and significantly increases the number of captured images.

**Table 3.1 Flight Duration and numbers of Images taken at Different Flight Altitudes**

Flight Altitude (ft)	70%-40% Overlapping Rate		90%-60% Overlapping Rate	
	Flight Duration (s)	Number of Images	Flight Duration (s)	Number of Images
60	186	24	1149	185
90	156	15	863	93
120	151	9	326	58
150	115	8	288	43

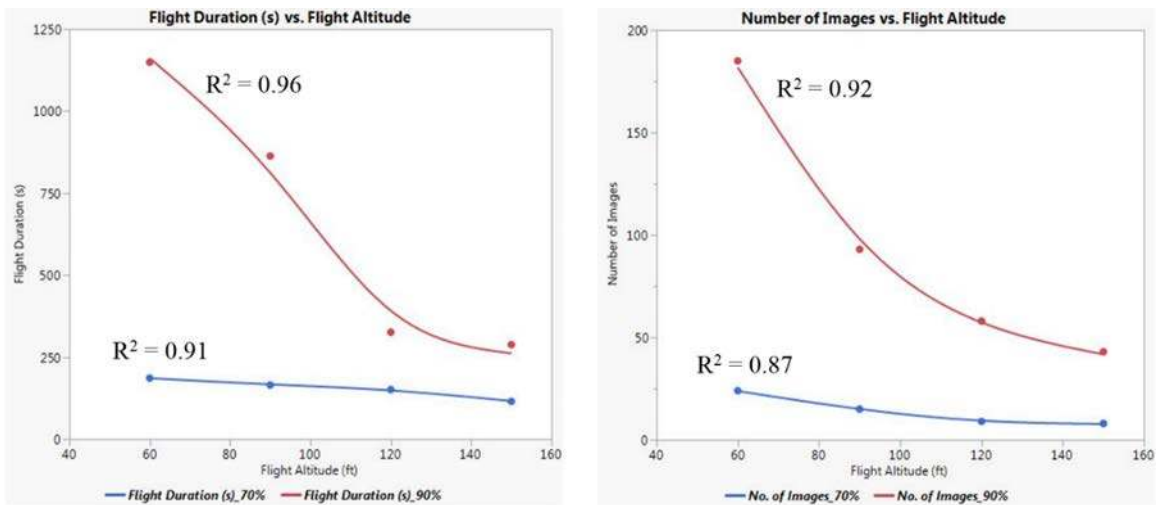


**Figure 3.10 Relationship between Flight Altitude and Overlapping Rate on Flight Duration and Number of Images**

### 3.4.2 Analysis of Positional Accuracy

An absolute accuracy analysis is mandatory in the surveying applications. As discussed earlier, the absolute accuracy is defined by the difference between the position of features on a processed model and their true position on the Earth. Because the calculation of earthwork volume is based on the point cloud model, the precision of point location is crucial to the result of volume computations. In this study, the computed coordinates of

GCPs were compared with their actual coordinates measured by the GPS rover. The positional accuracy was evaluated by RMSE, and the RMSE for each flight plan was calculated based on the average error of check points in X, Y, and Z dimensions. 16 GCPs were collected as the check points (Figure 3.11) shows. The coordinates are recorded in Appendix A.

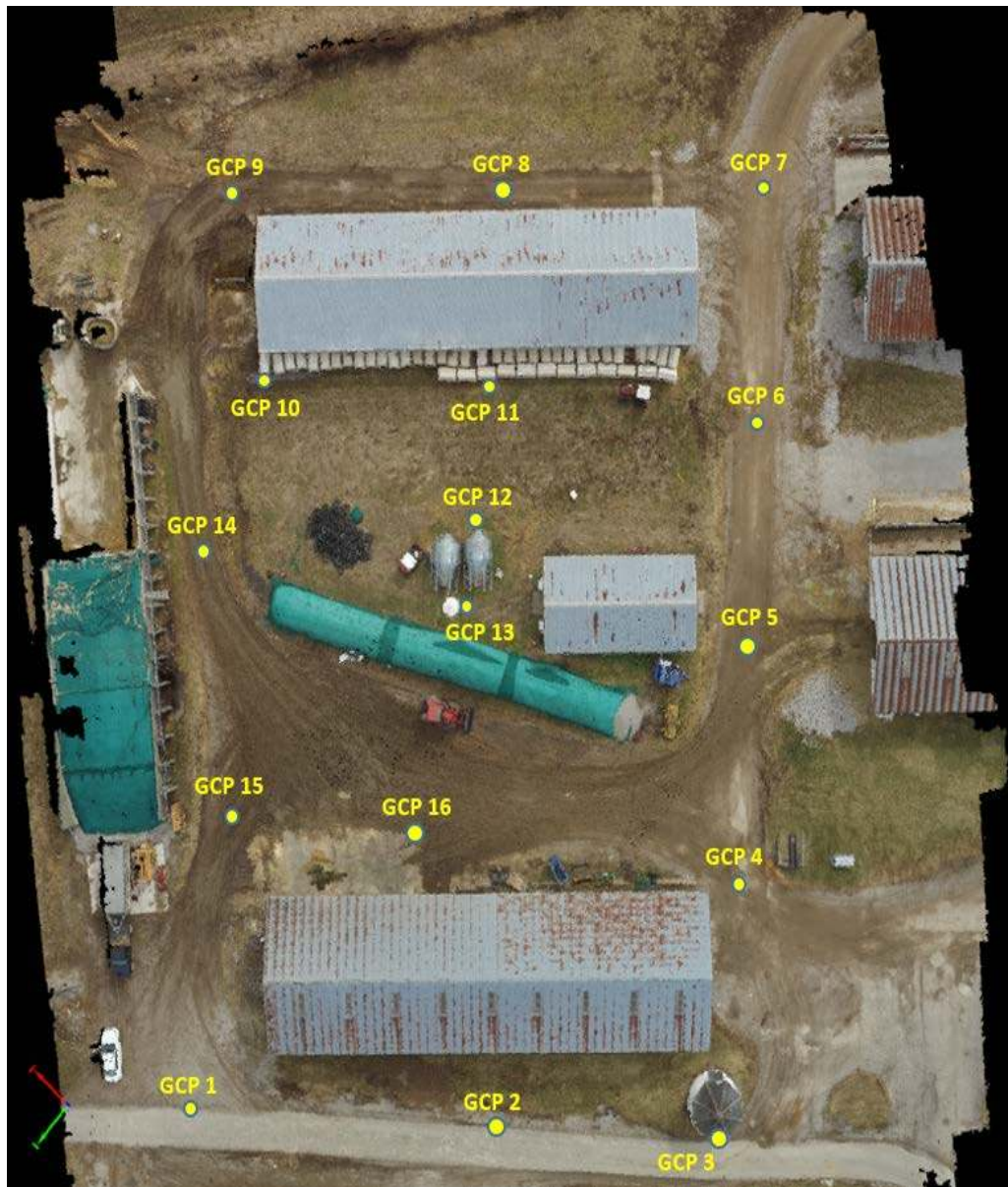


**Figure 3.11 Distribution of GCPs on the Study Area**

Besides the flight altitudes and image overlapping rate, the positional accuracy also largely depends on the number and distribution of GCPs because the navigation systems of most commercial UAS are not accurate enough for direct geo-referencing (Turner, D et al, 2014). However, in practice, especially on a construction site, the process of collecting GCPs may require a large amount of labor and time depending on the site conditions. In addition, GCPs should always be located evenly in the area of interest to minimize the errors in scale and orientation. If GCPs are gathered at the same location, all on one side, or at the very edge of the area, the geo-reference will lose balances, which makes the GCPs unreliable or dysfunctional. Therefore, the influence of the number and distribution of GCPs on the positional accuracy needs to be investigated to avoid unnecessary laboring and cost. In this study, images of each flight plan were processed with and without GCPs. To evaluate the effectiveness of different numbers of GCPs. Each flight was processed with 16, 12, 8, 4, and 1 GCPs.

The CPU specifications of the desktop used for analysis were Intel(R) Core(TM) i7-4790 CPU @ 3.60GHz, with RAM is 32GB. The operating system was Windows 7 Professional, 64-bit, and the photogrammetry platform was Pix4Dmapper Pro. Table 3.2 shows the RMSE of each points when applying different number of GCPs at multiple flight altitudes and image overlapping rates. Table 3.3 shows mean and standard deviation of data in each column to prove the validity. Without standard deviation, it is difficult to identify the data are close to the average or whether the data are spread out over a wide range. If the standard deviation is much larger than the average, the set data is lack of uniformity for further analysis. In this case study, the standard deviation for each population are much smaller than mean values, which means that most of the numbers are close to the average to build



a more asymmetric distribution. Therefore, the RMSE for each population is valid for further analysis.

From Table 3.2, it can be observed that the errors significantly decrease when all GCPs were used for processing because the GCPs provide an accurate orientation of the coordinates reference system. Also, the results showed random RMSE behavior when no GCPs were used due to the lack of geometric constraints of aerial-triangulation computation. This behavior is independent of flight heights and image overlapping rates. With the image overlapping settings, the results indicate higher overlapping rates results in smaller errors when applying all GCPs regardless of flight altitudes. However, as the flight altitude increases, the errors decrease if selecting the lower overlapping rate.

**Table 3.2 RMSE (ft) of Flights Processed by Different Number of GCPs**

Flight Altitude (ft)	Image Overlapping Rate (%)	Number of GCPs					
		No GCPs	1 GCPs	4 GCPs	8 GCPs	12 GCPs	16 GCPs
60	70%-40%	4.09	4.08	0.92	0.78	0.55	0.52
	90%-60%	5.35	4.25	0.29	0.28	0.28	0.28
90	70%-40%	4.99	4.55	0.81	0.70	0.64	0.50
	90%-60%	3.31	3.31	0.32	0.29	0.28	0.28
120	70%-40%	3.12	3.19	0.60	0.60	0.50	0.43
	90%-60%	6.85	5.74	0.50	0.45	0.31	0.29
150	70%-40%	3.49	3.65	0.64	0.57	0.38	0.38
	90%-60%	2.91	2.89	0.51	0.48	0.30	0.31

**Table 3.3 Summary of RMSE Distribution**

	No GCPs	1 GCPs	4 GCPs	8 GCPs	12 GCPs	16 GCPs
Mean	4.26	3.96	0.57	0.52	0.41	0.37
Std Dev	1.37	0.91	0.22	0.18	0.14	0.10

On the contrary, the errors increase if selecting the higher overlapping rate, as shown in Figure 3.12, and this tendency will not have changes when applying a different number of GCPs. The reason for this may be that a high overlapping rate at a low altitude allows the SfM algorithms to have better results when using a high redundant bundle adjustment. As the flight altitude increase, the area covered by each images increase, which also means the quality of spatial resolution decrease and less visual details of individual elements can be identified. However, when the overlapping rate is low, the matching features are inadequate. The higher flight altitudes can make up for the lack of information as a compromise.

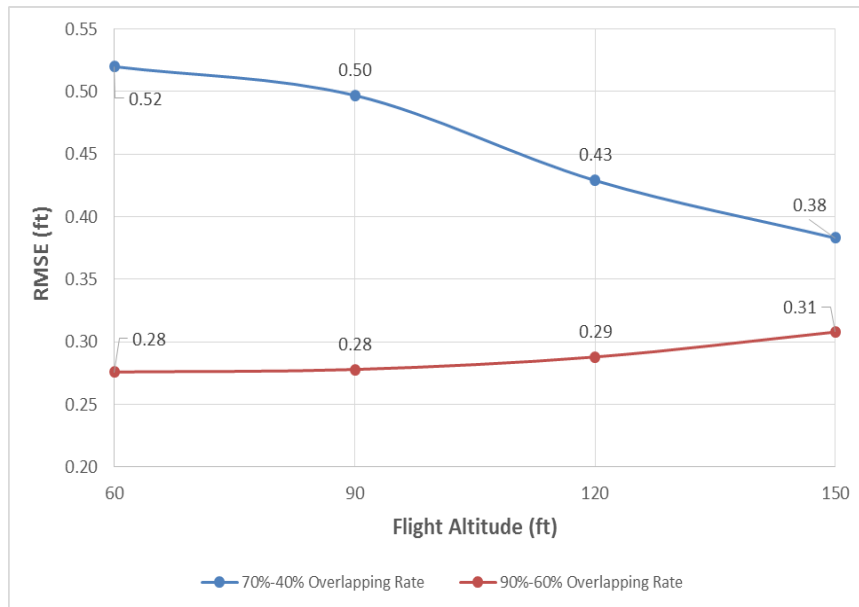


**Figure 3.12 Relationship of Overlapping Rates against Flight Altitudes and RMSE**

The results discussed above are based on applying all 16 GCPs. In order to improve the processing efficiency, it is necessary to identify how the changes in numbers of GCPs impact the position accuracy. Figure 3.13 presents the variety in RMSE when applying 0, 1, 4, 8, 12 and 16 GCPs respectively (Appendix B). It can be observed that the errors decrease as the number of GCPs increase. However, there are no significant differences in the errors between using 4 GCPs and 16 GCPs. In additions, for all flight plans, the major change in accuracy appears between using 1 GCP and 4 GCPs. Therefore, from a management perspective, unlimited number of GCPs may not result in significant improvement in the accuracy of measurement, while incurring much higher processing and data collection costs. Especially for construction management, the manager or engineer has to balance between the accuracy and productivity depending on the specific accuracy requirement.

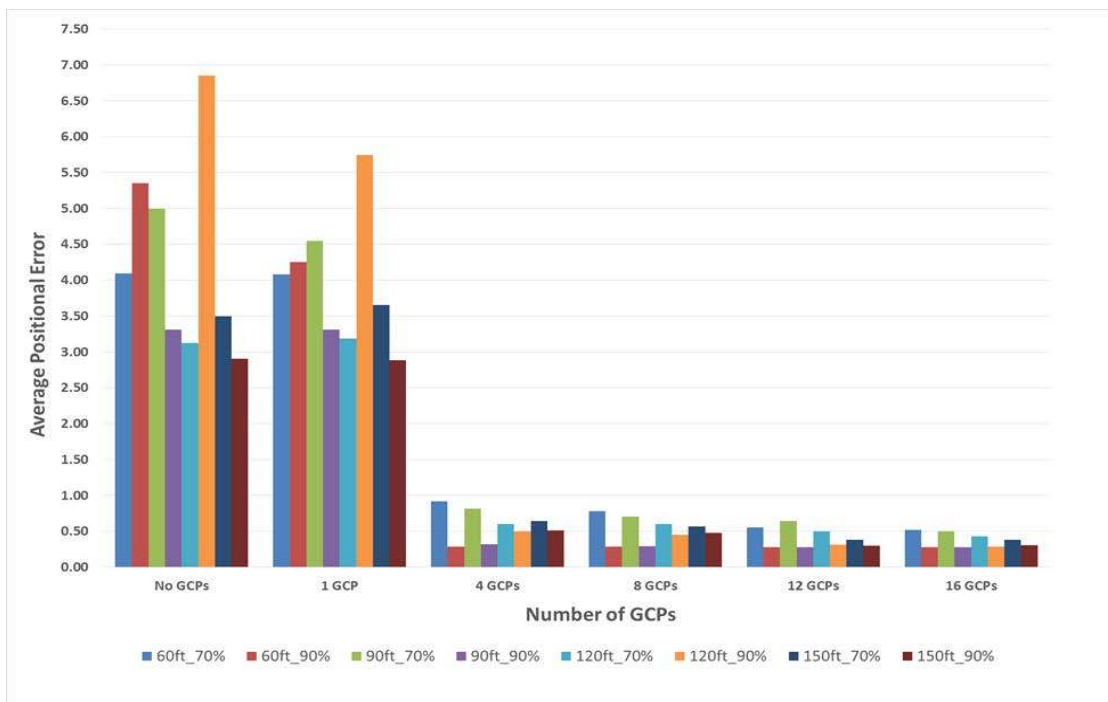


**Figure 3.13 Relationship between Number of GCPs and Average Positional Error on (1) Flight Altitude and (2) Image Overlapping Rate**

According to observations of the collected data, lower flight altitude with high image overlapping rate and the use of GCPs result in better positional accuracy. A multiple regression analysis was used to verify the results based on the observations. The multiple regression analysis is a powerful technique used for identifying the interactions between variables (Utts and Heckard, 2011). It builds an equation to “best” describe the relationship between a dependent variable  $y$  and  $K$  explanatory variables, as shown in the following equation,

$$y = b_0 + b_1x_1 + b_2x_2 + \dots + b_Kx_K$$

where  $b_0, b_1, b_2, \dots, b_k$  are the least-squares coefficient. The results are generated from F-test and t-test. In general, an F-test in regression compares the fits of different linear models. The F-test assesses multiple coefficients simultaneously. The F-test of the overall significance is a specific form of the F-test. It compares a model with no predictors, is also known as an intercept-only model, to a specified model. The hypotheses for the F-test of the overall significance are as follows (Dielman 2005):

- Null hypothesis: The fit of the intercept-only model and the specified model are equal.
- Alternative hypothesis: The fit of the intercept-only model and the specified model are NOT equal.

The t-test is used to test the significance of individual regression coefficients in the multiple linear regression model. A significant variable makes the regression model more effective. The hypotheses for the t-test are as follows (Dielman 2005):

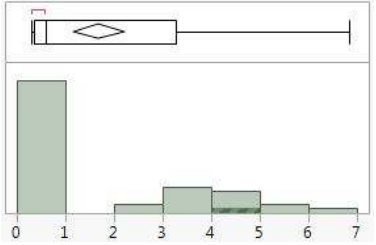
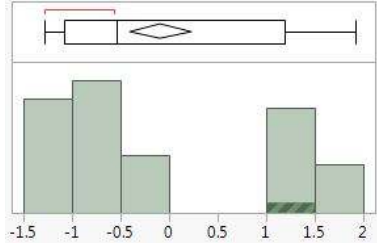
- Null hypothesis:  $b_K = 0$
- Alternative hypothesis:  $b_K \neq 0$

In this study, the RMSE of check points was the dependent variables. The flight altitude, image overlapping rate, and the use of GCPs are the independent variables. The first step of the multiple regression analysis is Transforming a variable using a mathematical operation to change its measurement scale (Beauchamp and Olson, 1973). One of the reasons to transform the variable is to reduce skewness. A distribution that is symmetric or nearly so is often easier to handle and interpret than a skewed distribution. More specifically, a normal distribution is always seen as ideal as it is assumed by many statistical methods. The logarithm and square root transformations are commonly used for positive data, and the multiplicative inverse (reciprocal) transformation can be used for non-zero data. In this case, it is necessary to decide whether the dependent variable (RMSE) should be modeled on the scale of measurement or transformed-scale by comparing the distribution and summary statistics of them respectively. From the Table 3.4, it can be observed that the distribution shape of Log (RMSE) is more symmetric than the RMSE because the mean of Log (RMSE) is closer to the center and has a smaller standard deviation. Therefore, the multiple regression analysis should consider the use of Log (RMSE).

Secondly, four interaction variables were added to the model to change the interpretation of the coefficient of each independent variable. From the statistical point of view, if there are no interaction terms, each independent variable would be interpreted as having a unique effect on the dependent variable. Thus, the interaction means that the effect of one factor on measurement accuracy is different for different values of other factors (Dielman, 2005).

For instance, the unique effect of flight altitude on accuracy is not limited to the altitude, but also depended on the values of overlapping rate, and the use of GCPs. Therefore, the 3 interaction variables included: Flight Altitude  $\times$  Overlapping rate, Overlapping rate  $\times$  GCPs, Flight Altitude  $\times$  GCPs, and Flight Altitude  $\times$  Overlapping rate  $\times$  GCPs.

**Table 3.4 Comparisons between RMSE and Log (RMSE) on the Distribution and Summary Statistic**

	RMSE	Log (RMSE)
Distribution		
Mean	1.68	-0.09
Std Dev	1.86	1.10
Std Err Mean	0.27	0.16
Upper 95% Mean	2.22	0.23
Lower 95% Mean	1.14	-0.41
N	48	48

Thirdly, the residue of the multiple regression model should be checked. Because the true disturbances cannot be observed in the regression model, they are modeled as realizations of random variable about which certain assumptions are made. The best possible estimation of population regression coefficient are obtained under a set of assumptions, which are linearity, equal variance, independence and normality. The residues can be used to conduct

assumption assessment by residual plot. If there is no assumption is violated, the residuals should be randomly distributed.

**Table 3.5 Summary of Fit in Multiple Regression Analysis**

RSquare	0.70
RSquare	0.65
Root Mean Square Error	0.65
Mean of Response	-0.09
Observations (or Sum Wgts)	48

**Table 3.6 ANOVA of Multiple Regression Analysis**

Source	DF	Sum of Squares	Mean Square	F Ratio
Model	7	40.32	5.76	13.55
Error	40	17.00	0.43	Prob > F
C. Total	47	57.33		<0.0001*

Parameter Estimates				
Term	Estimate	Std Error	t Ratio	Prob> t
Intercept	1.3955889	0.464759	3.00	0.0046*
Flight Altitude	-0.003622	0.003968	-0.91	0.3668
Overlapping Rate[90%-60%-70%-40%]	-0.349009	0.188214	-1.85	0.0711
Number of GCPs	-0.136464	0.023004	-5.93	<.0001*
(Flight Altitude-105)*Overlapping Rate[90%-60%-70%-40%]	0.0054048	0.005611	0.96	0.3412
(Flight Altitude-105)*(Number of GCPs-6.83333)	-6.181e-5	0.000686	-0.09	0.9286
Overlapping Rate[90%-60%-70%-40%]*(Number of GCPs-6.83333)	-0.034275	0.032532	-1.05	0.2984
(Flight Altitude-105)*Overlapping Rate[90%-60%-70%-40%]*(Number of GCPs-6.83333)	0.0002693	0.00097	0.28	0.7827

**Figure 3.14 Estimations of the Independent Variables Significance**

Table 3.5 displays the summary of fit of the multiple regression model. R-squared measures the proportion of the variation in the dependent variable explained by the independent

variables for a linear regression model. In this model, the R Square is 0.70, which indicates that 70 percent of variations can be explained by the independent variables. Generally, although no standard determines the minimum value of R Square, the R Square closing to 1 would result in a more convincing model. The R Square in this model is not close to 1 but larger than 0.5. Besides, there is a statistically significant predictor, the use of GCPs, whose p-value of t-test is smaller than 0.05 (Figure 3.14). It is reasonable to draw important conclusions about how changes in the predictor values are associated with changes in the response value. Regardless of the R Square, the significant coefficients still represent the mean change in the response for one unit of change in the predictor while holding other predictors in the model constant. In addition, While R-squared provides an estimate of the strength of the relationship between predictors and the response variable, it does not provide a formal hypothesis test for this relationship. The overall F-test determines whether this relationship is statistically significant. If the P value for the overall F-test is less than your significance level, you can conclude that the R-squared value is significantly different from zero.

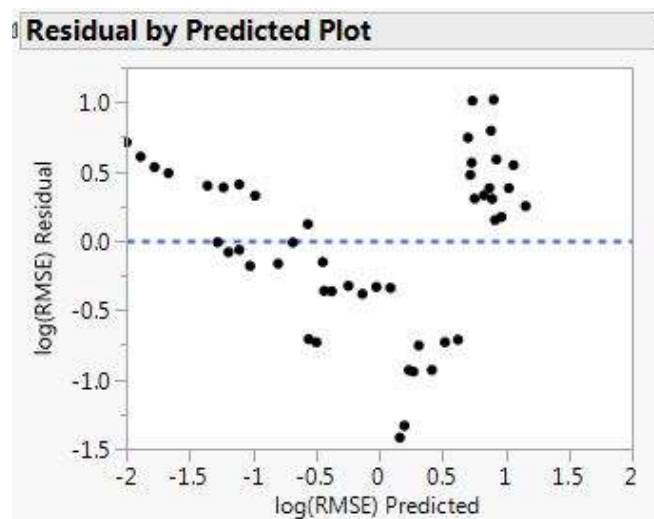


**Figure 3.15 Distribution of Residuals**



From the ANOVA of multiple regression analysis (Table 3.6), the p-value of F-test is much smaller than 0.05, which further proves that the relationship between variables are significant. Furthermore, the residuals are distributed in a random pattern (Figure 3.15), which also indicates the validity of the multiple regression model.

### 3.4.3 Soil Types

Soil type, which is the surface material, is another important factor for the measurement accuracy. In this study, the effect of soil type on the volumetric measurement accuracy was tested by modeling four samples composed of different soil types. The four soil types were sand, clay, fine grade gravel, and coarse grade gravel. The actual volumes of samples are based on the standards measured by the manufacture. All samples were piled in similar shapes under same weather and illumination conditions, as shown in Figure 3.14, and they have the same number of images captured in a circle pattern at 3.28ft (0.01in GSD) altitude for processing in the photogrammetry software (Figure 3.17). At the same time, all pictures are taken at early morning to avoid objects dropping shadows due to sun elevation arises.



**Figure 3.16 Sample Piles of Different Soil Type**

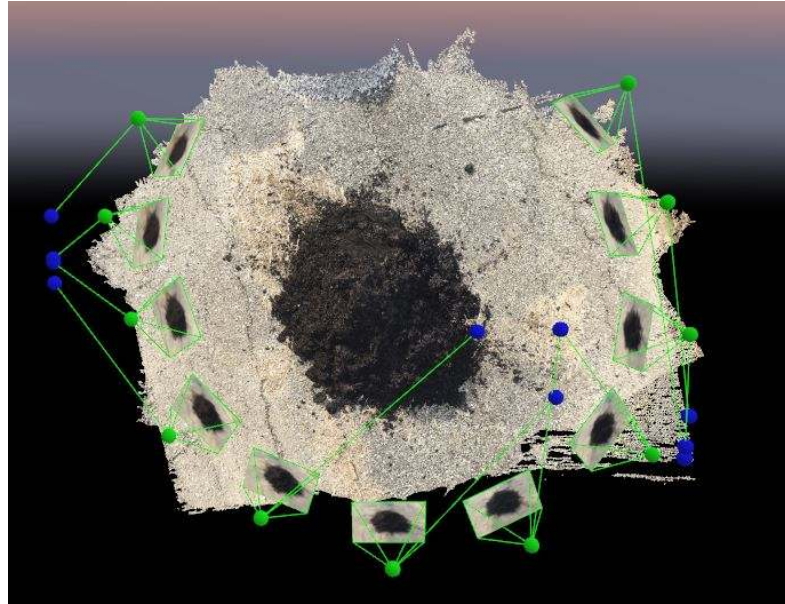


**Figure 3.17 Circle Pattern of Images Collections for Each Soil Type**

**Table 3.7 Impact of Soil Types on the Accuracy of Volumetric Measurements**

Soil Type	Number of Calibrated Photos	Actual Volume (ft <sup>3</sup> )	Computed Volume (ft <sup>3</sup> )	% Error
Clay	11	1.5	1.48	1.33
Sand	11	0.5	0.53	6.00
Gravel	10	0.5	0.47	6.00
Rock	10	0.5	0.45	10.00

Due to the size of modeling object is small, it is unfeasible to fly the UAS to capture images. In this independent experiment, pictures are captured by hand using camera. The camera is equipped with a 4.15mm f/2.2 lens, and the image resolution is 3264×2448 (RGB). Table 3.5 shows the actual volume and the % error for each soil type. The results indicate that the measured volume of clay had the smallest errors. In addition, as the soil granularity increased, and the color of material became lighter, the accuracy of measurement decrease.

The reason may be that coarse surface texture creating more noise on the surfaces of models. Also, light-colored and glossy surfaces tend to saturate images leading to difficulties in visual interpretation.

### **3.5 Conclusion**

This study aims to investigate how important flight parameters of the UAS and environmental factors impact on measurement accuracy through experimental flights and statistical analysis of positional errors computed through photogrammetry technologies. According to the literature and practical experience, the most influential factors are flight altitude, image overlapping rate, the use of GCPs and soil types. Each factor does not work independently. Therefore, it is necessary to investigate how they cooperate with each to impact on the quality of mapping and the measurement accuracy.

After detailed comparisons and analysis for each flight plan, one can derive that the combination of low flight altitudes, high image overlapping rate, the use of a proper number of GCPs and modeling surface of clay soil type can maximize the measurement accuracy. The positional errors become much smaller when more than 1 GCP is used for processing because GCPs provide an accurate orientation of the coordinate reference system. This behavior is constant independent of flight heights and image overlapping rates. With the image overlapping and flight altitudes settings, higher overlapping rates result in larger errors as the flight altitude increases, and the errors decrease if selecting the low overlapping rate. The spatial resolution and border definition improve as the altitudes decrease. This tendency will not have changes when applying a different number of GCPs. However, it does not mean it is useless to fly the UAS at high altitudes. Although GCPs is

the most influential factor based on the results of multiple regression analysis, it does not mean an unlimited number of GCPs is an optimal strategy to guarantee the accuracy. In the experiment, there are no significant differences in the errors between using 4 GCPs and 16 GCPs. The selections of parameter values largely depend on the required of accuracy by users. For example, high flight altitudes can reduce the flight durations and improve the accuracy when the overlapping percentage is low; fewer GCPs can save a lot of labor and cost especially when the topographic condition is complex.

The limitation of this study is the selection of the UAS equipment and photogrammetry software. The UAS, especially low-cost device, limit the sensor payload in weight and dimension so that usually low weight sensors like small or medium format amateur cameras are selected. When compared to large format cameras, the UAVs acquire a higher number of images in order to obtain the same image coverage and comparable image resolution. Moreover, low-cost sensors are normally less stable, which results in a low image quality. In addition, low-cost UAVs are normally equipped with less powerful engines, limiting the reachable altitude. Therefore, when processing the images collected by the UAV, this study will not concern about the difference caused by different devices. The accuracy level and hardware equipment of the selected device and photogrammetry software in this study is above the average in the market, which can be used as a reasonable reference for most researcher and practitioners. In the future, more research can be conducted regarding how different devices and other potential environmental factors impact on the measurement accuracy when the limitations of UAS technology can be solved such as inaccurate georeferencing capability and limited battery capacity.

## **4. COMPARISONS BETWEEN APPLICATIONS OF THE UAS AND CONVENTIONAL METHODS IN EARTHWORK VOLUME MEASUREMENT**

### **4.1 Introduction**

Earthwork involves moving massive quantities of soil or unformed rock. The purpose is to reconfigure the topography of a construction site to meet the design requirements (Nunnally, 2004). As an important mission of a construction project, the earthwork operation is mainly executed in the early stage of the construction process, which means the earthwork progress controls the overall project schedule. Besides, earthwork is often one of the major cost items on most construction projects because of the long operation time and cost uncertainties caused by unstable geographical conditions and construction organization plans. It is essential to make the best possible measurement of the quantities of earthwork materials that have been excavated and placed. An accurate estimation of earthwork quantity not only enables contractors to present an accurate bid, assign construction assets reasonably, and formulate a project schedule but also helps owners make correct payments. Therefore, the selection of a proper measurement method is a prerequisite to accurate estimations and cost control.

In recent years, the surveying industry has seen significant changes with the development of modern technologies. However, the implementation of advanced survey techniques in constructions is still in the early stage. According to the latest standard specifications published by the Department of Transportation (DOT) of each state, most states are predominantly using conventional methods such as tapes and manual calculation methods based on the blueprints to collect data and calculate quantities for payments in earthwork

process. As shown in Figure 4.1, 68% of states measure the roadway excavation in its original position by taking cross sections and computing the volume using the Average-End-Area (AEA) method (cross-section). The AEA method involves plotting cross sections of the existing and proposed levels at certain intervals across the construction site (Hintz and Vonderohe, 2011). The accuracy largely relies on the selected distance between the sections. Closer sections improve the estimation accuracy but require much more time for data collection. A balance has to be made between accuracy and efficiency, which could result in various levels of errors (Epps and Marion, 1990). Another common method is the grid method. When applying the grid method, the area is divided into a grid indicating the depth of cut or fill at each grid intersection. The method involves taking off the existing and proposed ground levels at each node of the grid. Similar to the AEA method, the accuracy depends on the size of grid that is used.

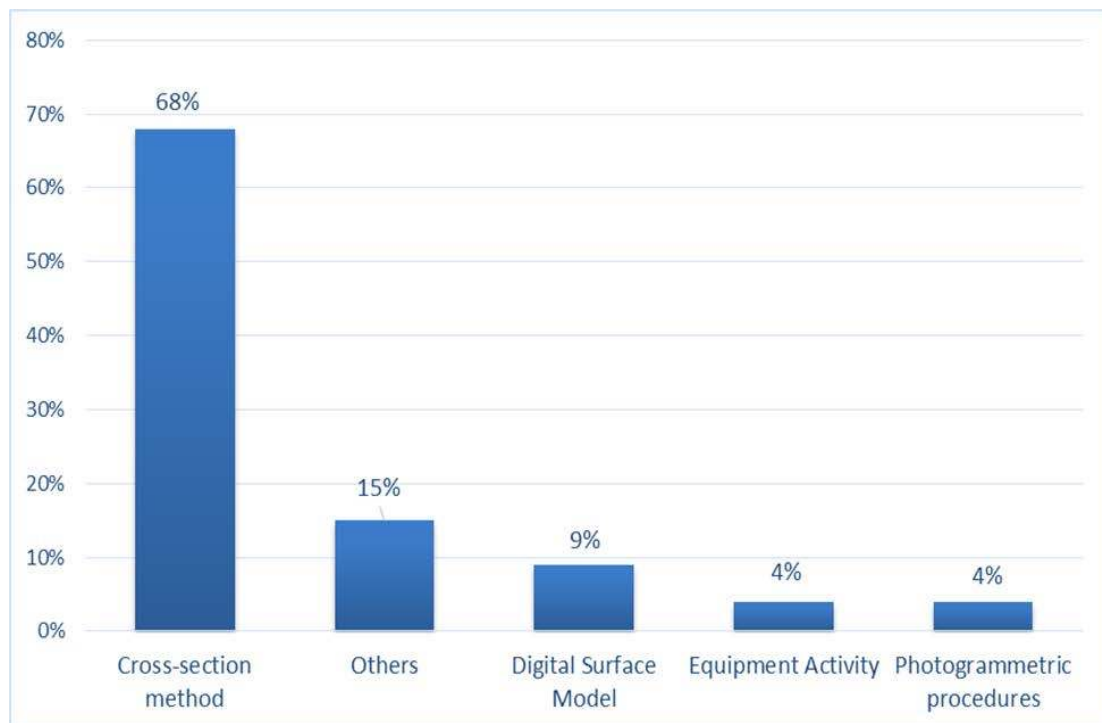


**Figure 4.1 Earthwork Volume Measurement Methods Applied by DOTs**

The methods mentioned above are inefficient as they require a large amount of time to collect data on the site and go through a tedious quantity calculation process (Yanalak 2005). Although some Departments start to use software products such as AutoCAD to make their work easier and faster, the fundamentals of manual methods are still used to find the quantities of earthwork even when using a software package. In addition, the DOTs are facing increasing budget and personnel constraints and are exploring ways to use advanced technologies to maximize productivity and leverage the decreasing number of surveying personnel on their staffs (Vincent and Ecker, 2010). Therefore, it is imperative to upgrade the current practices of data acquisition and computation methods. In this paper, the unmanned aerial systems (UAS) are introduced as tools to estimate earthwork volume with the cooperation of with digital photogrammetry. UAS, or colloquially drones, are remotely controlled aircraft equipped with various sensors such as cameras, Global Positioning System (GPS), and other communication devices. GPS technology enable the UASs to provide accurate geo-referenced visual assets (Siebert and Teizer, 2014). With the integration of digital photogrammetry, a well-established technology for obtaining three-dimension (3D) geometric information for real-world objects from single or multiple photographs, a geo-referenced three-dimensional (3D) model is generated for survey applications (Luhmann et al, 2013).

With the improvement and wide applications of UAS in recent years, the technology has become attractive for various surveying applications in civil engineering. Metni and Hamel (2007) described the dynamics of a UAS for monitoring of structures and maintenance of bridges; Morgenthal and Hallermann (2014) discussed the use of a UAS for inspection of critical structural components and hot spots that are hard to reach. Rathinam et al. (2008)

addressed the problem of monitoring civil systems such as oil-gas pipelines using an autonomous UAS based on visual feedback. In construction, Sibert and Teizer (2014) evaluated the performance of the application of the UAS in surveying earthwork projects. They developed a performance model for estimating the position error and conducted tests in several realistic construction environments. Hugenholtz et al. (2013) quantified the accuracies of an in-house developed UAS through a stockpile volumetric survey.

However, research conducted on the UAS and photogrammetry applications is still in its infancy, especially in the earthwork volume measurement application. As an emerging technology in construction, it requires much practice to reveal various possibilities in operations and prove its feasibility. This paper compares the earthwork volumes measured by using different methods on AutoCAD models in order to verify the effectiveness and accuracy of the UAS applied in earthwork volume measurement. At the same time, the results and discussions can provide managers and engineers with a reference regarding the selection of proper tools in the practice.

#### **4.2 Average-End-Area (AEA) Method and Grid Method**

The earthwork includes field volume measurements of earthen materials such as soil, gravel, or rock, which are used to determine the total material transported to and from a site (Hintz and Vonderohe, 2011). The cut volume is the extra dirt that must be removed to meet the designed elevation and grade; the fill volume is the amount of material that must be added to meet the desired elevation and grade. Before measuring the volume, especially for the highway construction, surveying personnel need to plot cross sections of



the existing and proposed levels at certain intervals across the construction site, as shown in Figure 4.2.

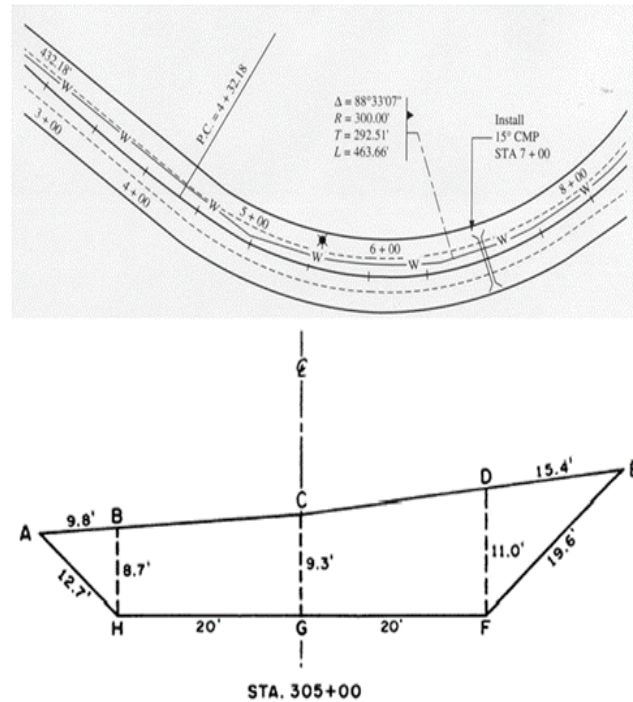


**Figure 4.2 Stations and Cross-Sections of a Highway Project**

When using AEA method, the volume between each pair of sections is computed by multiplying the distance between cross-sections by the average of the end cross-sectional area, as presented in Equation 1. The total cut or fill volumes are obtained by adding the volumes between all consecutive pairs of cross-sections.

$$V = \left( \frac{A_1 + A_2}{2} \right) \times L \quad (1)$$

where the V is the earthwork volume between the cross-sections 1 and 2, L is the distance between cross-sections, and A1, A2 are areas of the cross-sections 1 and 2. The accuracy of the AEA method largely relies on the distance between the sections, especially for the irregularly-shaped sections or sections with unequal areas of cut and fill (Epps and Marion,

1990). In other words, the measurement would be improved if the project were divided into more stations. Increasing the number of cross sections can explain more details of the topographic conditions.

The grid method is the other common method to calculate the earthwork volume, especially for large earthwork area. This method divides the site area into a grid and requires a survey of the construction site showing the elevation of the existing grade at each intersection point on the grid. The elevation of the designed grade is also plotted at each intersection point, and then the depth of cut or fill can be computed at each point from these two elevations. After determining the depth of cut or fill at each point where the grid lines intersect, which is also the station, the estimator needs to assign the depth at each station a weight or a frequency based on its location.

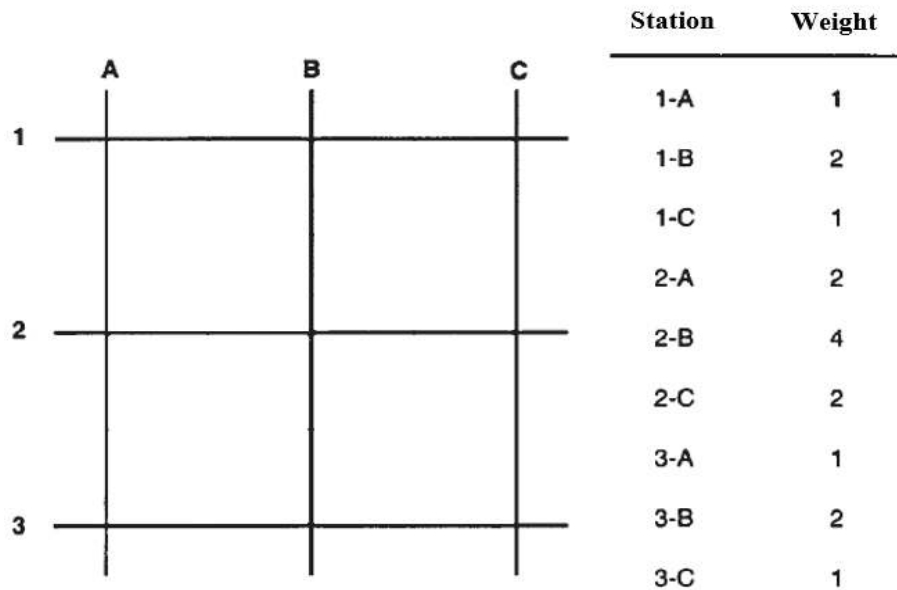


**Figure 4.3 Grid Method Calculation**

As illustrated in Figure 4.3, the interior points which are the intersection of four segments are assigned a weight of four; the exterior points which are intersections of two segments

are assigned a weight of two; the corner points are assigned a weight of one. After determining the weights and depth of each intersection, the average depth can be computed by the Equation 2, and then the earthwork volume can be obtained by multiplying the average depth by the horizontal area of the grid (Nunnally, 2011). Similar to the AEA method, the measurement accuracy depends on the grid spacing; generally, the closer the grid spacing, the more accurate the volumes are.

$$Average\ Depth = \frac{Sum\ of\ products\ of\ depth\ \times Weight}{Sum\ of\ Weight} \quad (2)$$

Both methods are commonly used to estimate the earthwork volumes. At the same time, they also have various limitations regarding accuracy and feasibility. Usually, in practice, the AEA method can provide acceptable accuracy. However, the AEA method is more accurate when the corresponding end areas of adjacent cross-sections have equal or similar surface areas (Hintz and Vonderohe, 2011). As the difference in surface area of the end areas increase, the average-end-area formula will yield volumes that are overestimated relative to the corresponding true volumes (Michael, 1993). The problem can be avoided by increasing the number of cross sections taken in a given interval, but this requires more time and labour. Similarly, the grid method also can provide better accuracy for the sites with relatively flat existing and design topographies. When the site is complex, it has to use smaller grid line spacing to guarantee the measurement accuracy but requires intense calculations. Besides two methods mentioned above, in practice, many contractors estimate the earthwork quantity based on the equipment activity. The total quantity is equal to volume per cycle multiplied by the cycles per hour. The contractor observes and records the equipment cycle time, and then estimate the total production of earthwork based on the

capacities of equipment. Various factors such as counting mistakes or selection of incorrect parameters in formulas could have an influence on the measurement accuracy in the process of earthwork. Therefore, it is necessary to update the current practices of earthwork volume estimation.

### **4.3 The UAS and Photogrammetry**

The UAS is originally developed and used in military implementation. They are remotely controlled aircraft or helicopters equipped with precision sensors. Inertial motion units and gyroscopes are used to recognize the alignment and position of the aircraft so that a pilot can control the navigation without much manual operation. Also, highly accurate and low-cost GPS can maintain the position of a UAV system in a global reference system everywhere in real time. The application and performance of the UAV are further improved when digital photos and video cameras are capable of converting UAV systems into highly mobile sensor platform. The UAS systems typically consist of UAVs and ground equipment for planning and transferring flight routes to the UAV as well as for monitoring the UAV telemetry data. In recent years, UAV systems have been utilized for diverse nonmilitary purposes such as photogrammetry for 3-D modeling (Colomina and Molina, 2014), remote sensing and mapping (Nex and Remondino, 2014). In construction, the application of the UAS and photogrammetry has been preliminarily proved. Abeid et al. (2003) developed a construction control system by combing the construction progress chart with a database of site pictures; Memon et al. (2005) prototyped a digitized construction monitoring system which is used to monitor and evaluate actual construction progress. Metni and Hamel (2007) described the dynamics of a UAS for monitoring of structures and maintenance of bridges; Zhu and Brilakis (2009) reconstructed a house and a wheel

loader as two example cases validating photogrammetry as an optical sensor-based spatial data collection method for infrastructure modelling; Sibert and Teizer (2014) evaluated the performance of the application of the UAS in surveying earthwork projects. They developed a performance model for estimating the position error and conducted tests in several realistic construction environments. Hugenholtz et al. (2014) quantified the accuracies of an in-house developed UAS through a stockpile volumetric survey. These applications proved the feasibility and use of UAS and photogrammetry technology in recording and tracking the construction progress for helping engineers and managers perform the quality control of construction projects. However, the utilization of the UAS and photogrammetry technologies in construction is still at an early stage, especially in earthwork volume estimations, even though it is one of the major components of a construction project.

Photogrammetry is a technology of image processing to interpret the shape and location of an object from one or more photographs of that object. This study uses a UAS to capture images of the site. Generally, the process begins with the flight mission planning. Once all the requirement and parameters are defined for the flight mission, a flight plan or an image acquisition plan is developed and aerial imagery is collected based on the project specifications. At the same time, a ground control survey needs to be conducted to improve the positional accuracy of the 3D outputs. After the image acquisitions and the ground control survey, methods of image interpretation and measurement are required to complete the transformation between images and object. To be more specific, the photogrammetry software first identifies and measures conjugate points in the overlapping photographs (Schenk, 1997). During this process, Automatic Aerial Triangulation (AAT) is the basic

method to analyze and perform exterior orientation of aerial images to calculate the 3D coordinate of object points (Yuan et al, 2015). In other words, the AAT represents the mathematical process of establishing accurate relationships between the individual image coordinate systems and a defined datum and projection on the ground (Tang et al., 1997). The main objective is to ensure that each model can be oriented accurately as required. At the same time, the Bundle Block Adjustment (BBA), another basic method cooperating with the AAT to produce the final three-dimensional coordinates of all the measured points, is performed by Structure from Motion (SfM) algorithm. Using the UAS platforms, the SfM is operated using highly redundant information extracted from a group of high percentage overlaps that register the 3D structure of an object (Snavely et al., 2006). SfM extract features in each image of the photogrammetric block, which is matched to their corresponding features in another image. These matched features are used to compute the relative position of the camera sensor during the flight operations thus the orientation of each sensor can be calculated (Westoby et al, 2012).

The major output of the photogrammetric process is a point cloud model. A point cloud is a set of data points in a three-dimensional coordinate system, and each point is defined by X, Y, and Z coordinates. The point cloud is normally used to represent the external surface of an object. For more realistic visual operations, the triangle mesh should be generated. Although triangle mesh model is optimal for visualization, it is infeasible for detailed modifications on a small scale. Therefore, most operations are performed on the point cloud model. Nowadays, as the development of three-dimension (3D) modelling technologies, the compatibility of outputs generated from different platforms is also improved. For

example, the point cloud model can be imported into Autodesk software for various purposes such as surface reconstruction or inspections.

## **4.4 Case Study**

### **4.4.1 Project Description**

The Virginia Department of Transportation's U.S. Route 460 Connector Phase II project is located between U.S. 460 Connector Phase I ("Phase I") near Breaks Interstate Park and the proposed Coalfields Expressway ("CFX") corridor, as shown in Figure 4.4. The Project is a limited access facility located in Buchanan County, Virginia and totals approximately 6.2 miles with over 15 million cubic yards of material to be moved during construction and includes an at-grade intersection with Route 609. The Project features an alignment proposed by Design-Builder (through its predecessors) in an unsolicited proposal submitted to Department using a Coal Synergy, sole source procurement for Project development. The Project is tied to a transportation initiative known as Corridor Q of the Appalachian Development Highway System (ADHS), in conjunction with the economic development program of the Appalachian Regional Commission (ARC). The Phase II design-build contract with Bizzack Construction, LLC, Lexington, KY., uses the coal synergy concept to provide a road to rough grade at a reduction in costs (VDOT, 2018).

In this study, a partial area of the project which is under earthwork is selected to investigate the earthwork measurement accuracy of the UAS technology compared with another two conventional methods. The size of test area is 64,057.24 square feet. The earthwork of this sub-project lasts five months from early October 2017 to late January 2018. The project team visits the site two times to investigate the earthwork changes during the construction.

The first visit aims to record the original topographic conditions of the site as the reference for later calculations and comparisons. The purpose of the second visit is to investigate the earthwork-completed site through different methods. After the field investigations, the earthwork volumes can be calculated in the AutoCAD models and thus the accuracy of different measurements methods can be measured and compared.

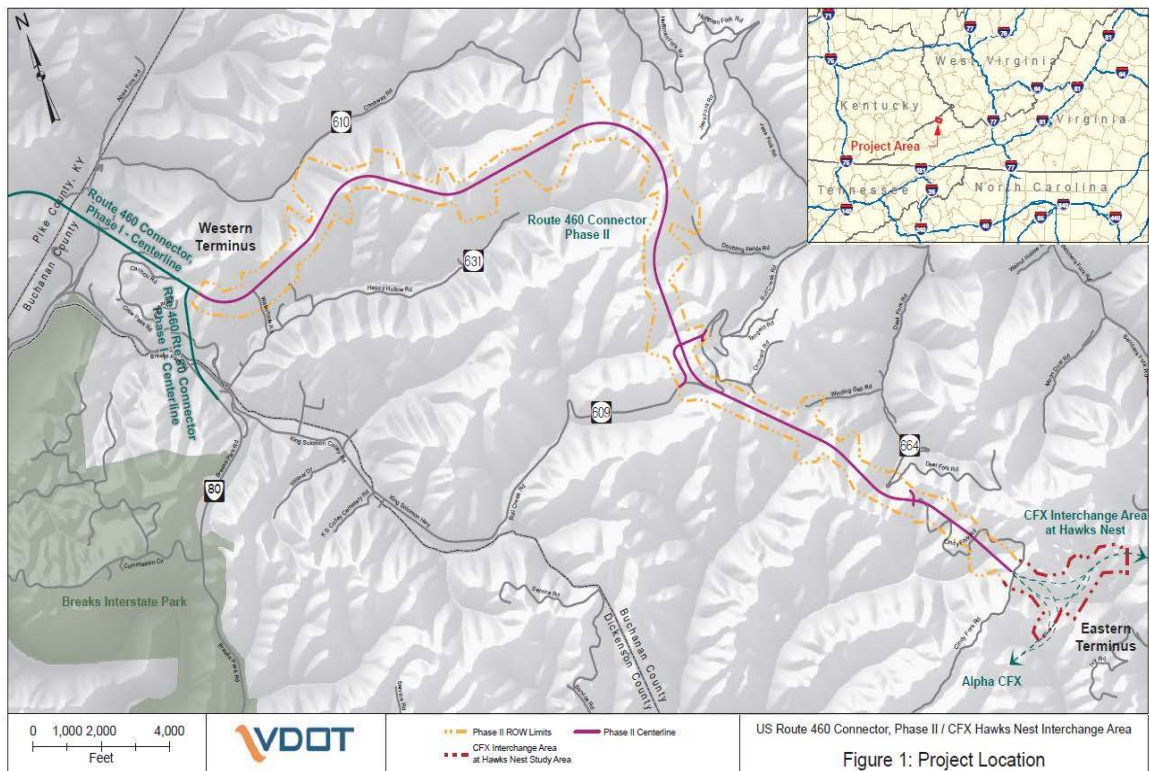


**Figure 4.4 Project Location (VDOT, 2018)**

#### 4.4.2 Methodology

The project team visit the site to investigate the original topographic conditions before the earthwork starts. Figure 4.5 shows the 3D contour map of the site created after the survey of the first visit, which is used as the base model for volume calculations.



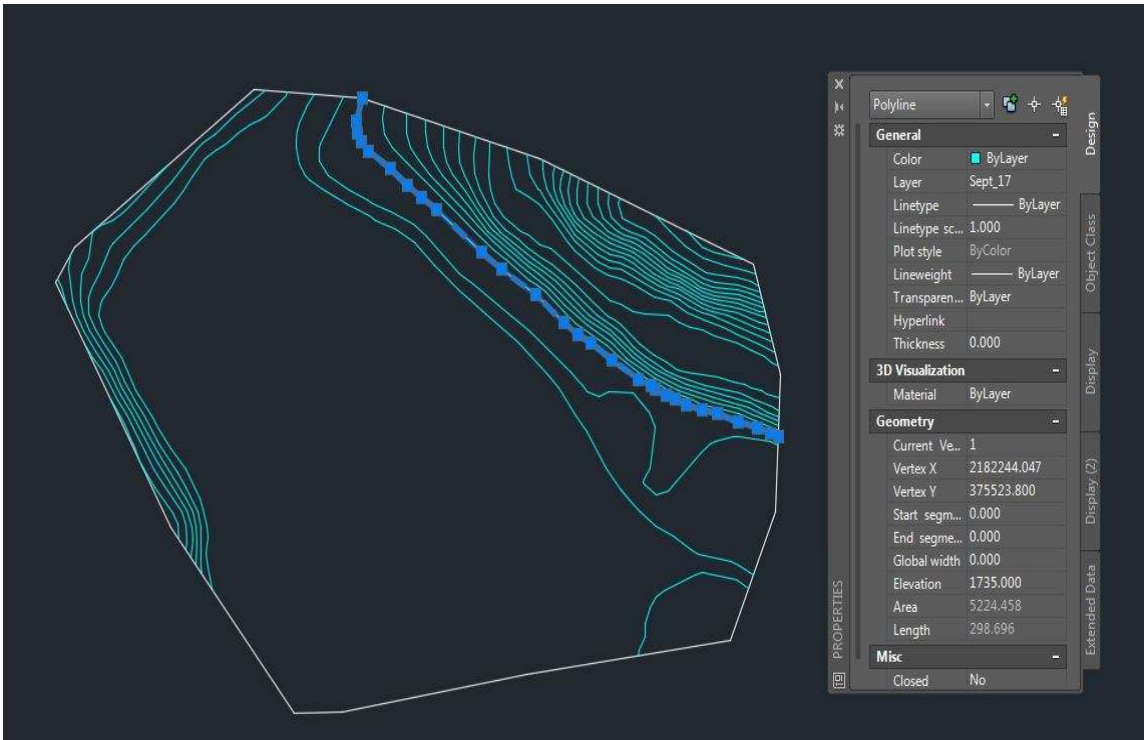


**Figure 4.5 3D Contour Map and Properties of the Site after 1st Visit**

The UAS used in this study is equipped with Sony UMC-R10C camera that has a large Exmor APS-C Sensor that captures 20 megapixels of colour detail to accurately calculate volumes. With this sensor, the flight duration is approximately 30 minutes. The system has a maximum payload of 2kg and its wind tolerance is 30 mph (Kespry, 2018). Approximately 280 images are captured by the UAS during the second visit and then processed in the Autodesk ReCap Photo to generate a point cloud of the site. In order to perform complex measurements such as volumes, the point cloud model needs to be imported into Autodesk Civil 3D to display the 3D contour data of the construction site, as shown in Figure 4.6. In order to verify the measurement accuracy based on the model created through UAS platform, a total of 408 survey points are collected using the GNSS receiver, and the point map and point examples are shown in Figure 4.7 and Figure 4.8.

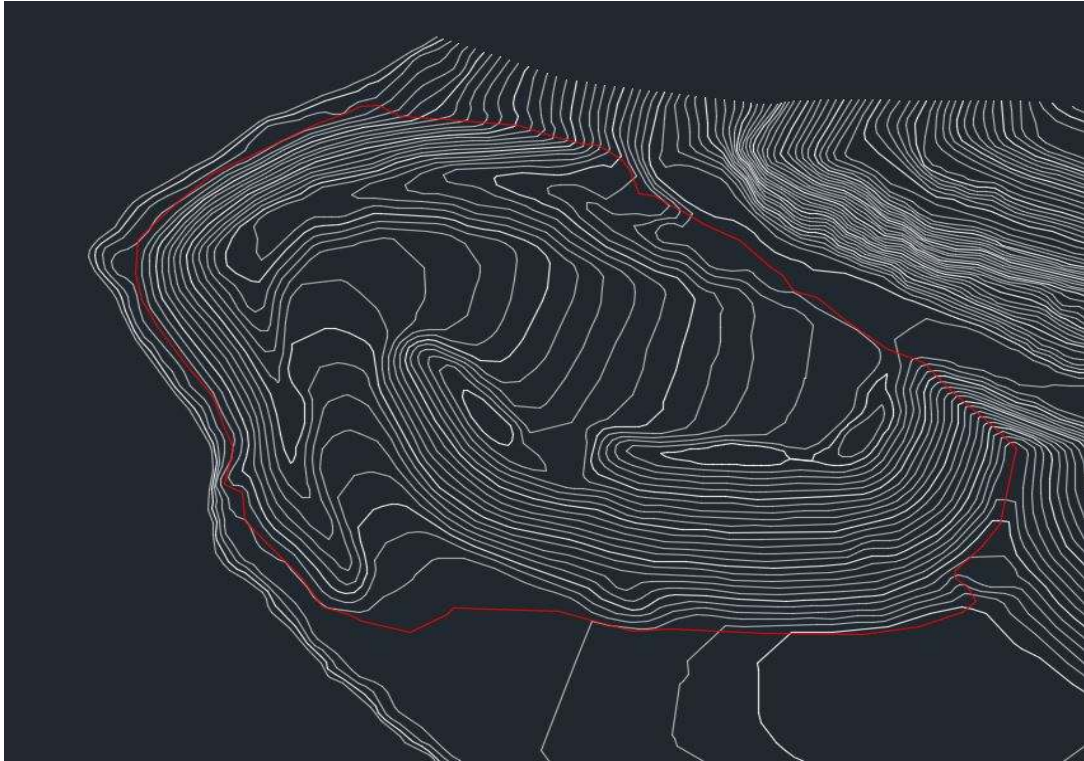


**Figure 4.6 3D Contour Map of the Site after 2nd Visit**

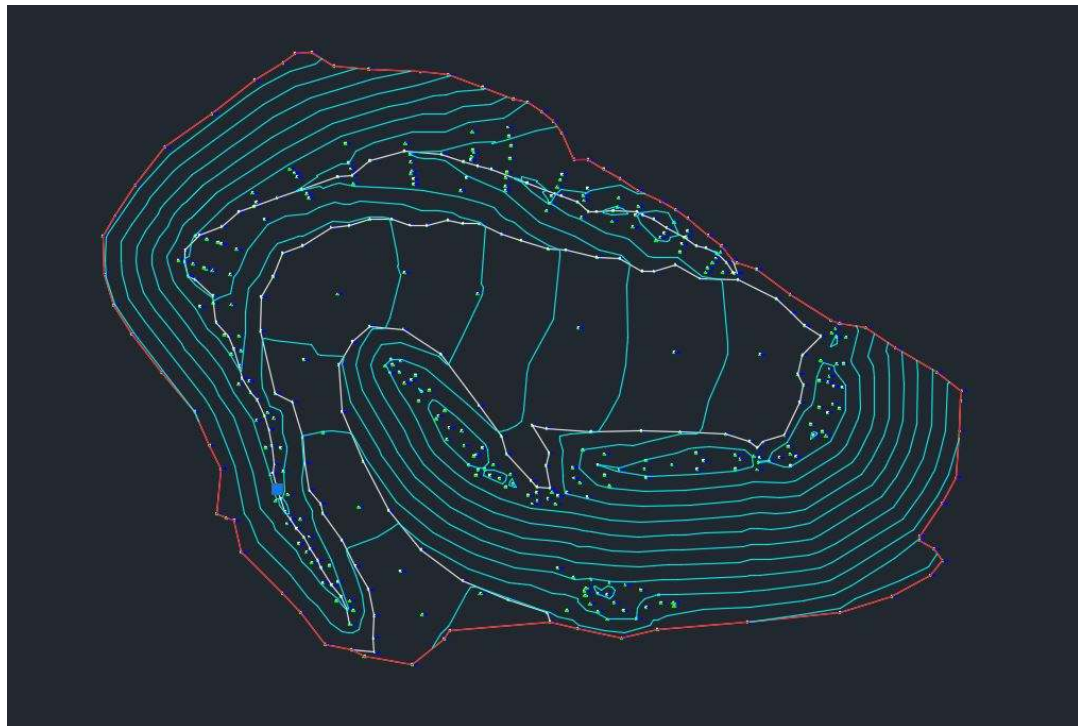


**Figure 4.7 Map of Survey Points**

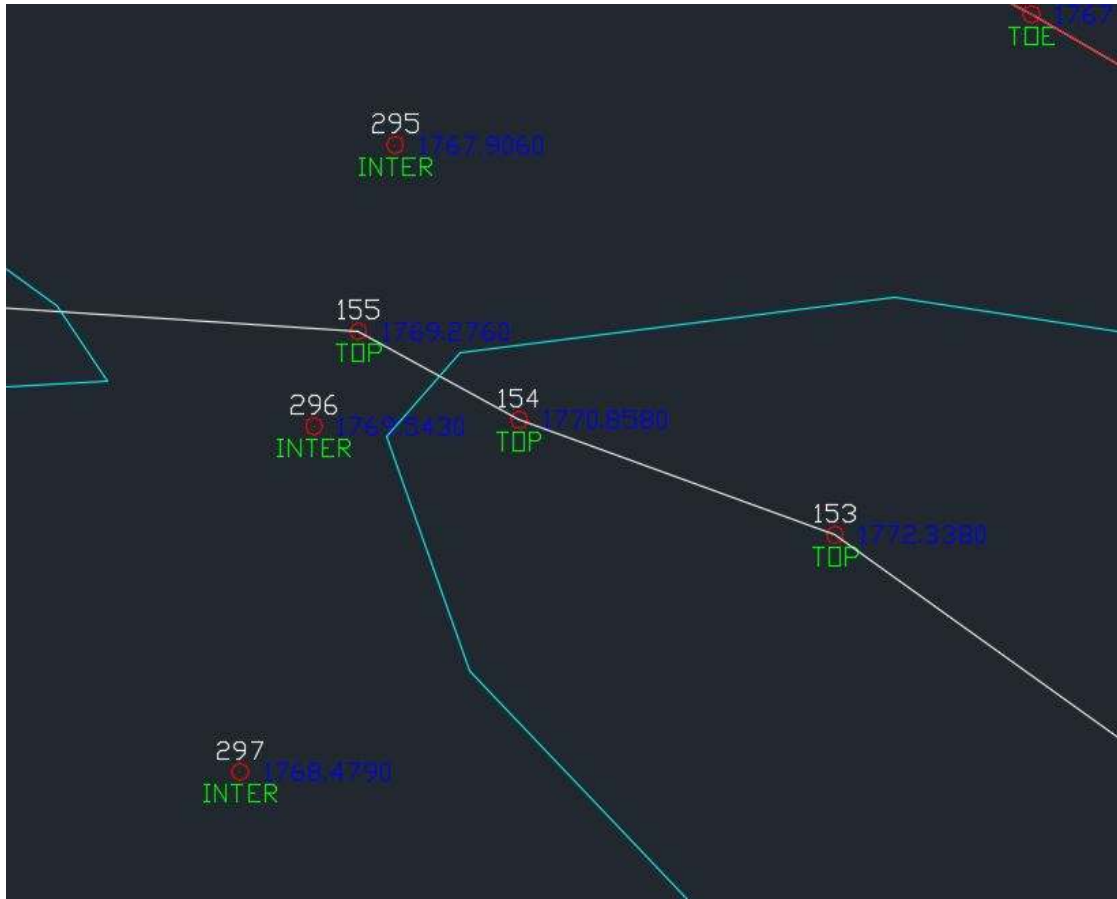


**Figure 4.8 Information of Survey Points**

The earthwork volumes can be estimated through 3D contour maps obtained after two visits. In Autodesk Civil 3D, the volume changes between two models can be calculated after creating Triangulated Irregular Network (TIN) surfaces for each contour map. Thus, the volumetric measurements based on the model of the UAS platform can be used to compare with the results obtained by other methods. The other two measurement methods, which are AEA method and grid methods, are applied to calculate the volume of same earthwork area based on the survey points collected during the second visit. As discussed earlier, the accuracy of these two methods largely depends on the distance between cross-sections and the size of the grid. In this study, volumes are calculated at cross-section intervals and the grid of 10ft, 30ft, 50ft, and 100ft for detailed comparisons. In Figure 4.9, the green

boundary line indicates the original area before earthwork; the orange boundary line indicates the earthwork area; the red line in horizontal direction is the centreline of the site, and the 43 blue lines in vertical direction indicate the intervals between each pair of cross-sections along the site used for AEA method.

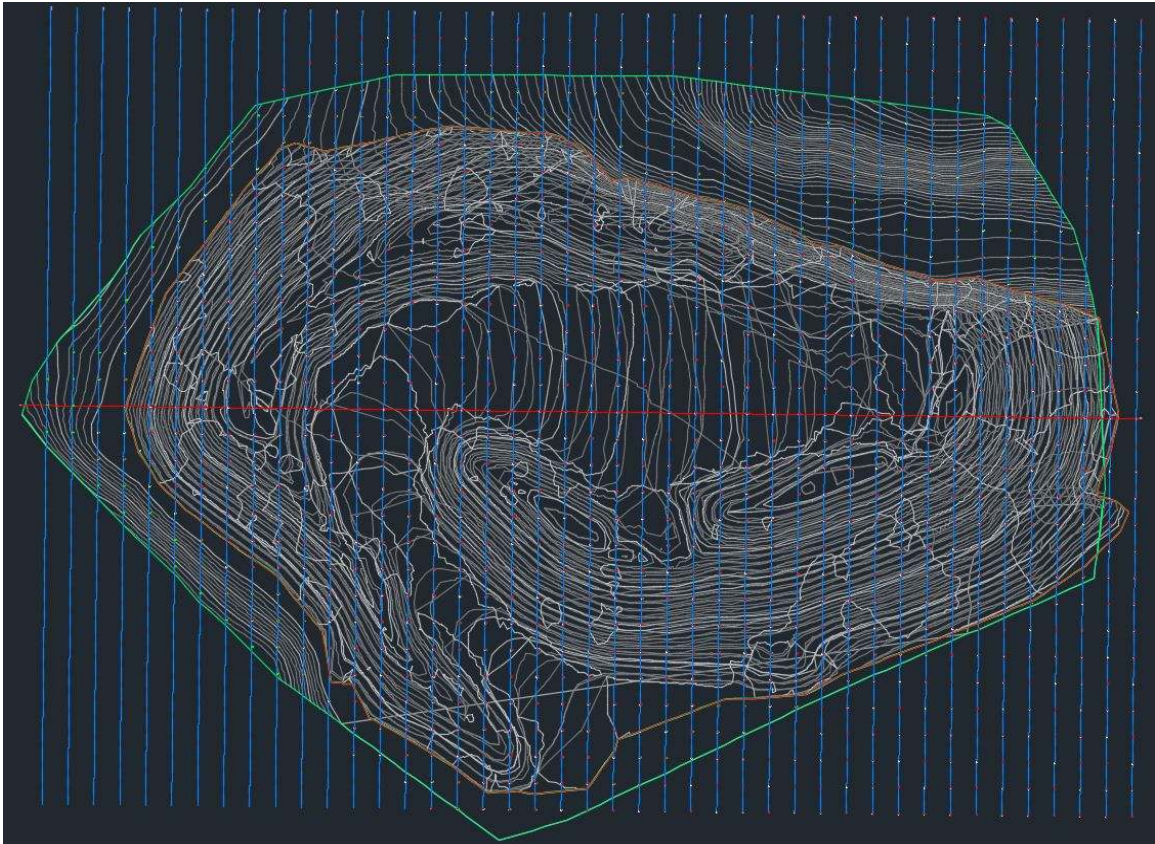


**Figure 4.9 Overlay of Multiple 3D Contour Map and Cross-sections Intervals**

The Figure 4.10 shows the grid pattern of the earthwork area created for applying the grid method. The size of each grid is 100 square feet. Once the grid size is determined, the elevation at each grid intersections can be calculated based on the surfaces of each contour layer. As shown in the Figure 4.11, there are three elevations in different colours for each intersection. They represent the elevations of points in the base model (green), model

created by the UAS platform (red), and survey data map (blue). The elevations of each intersection are recorded in Appendix B.

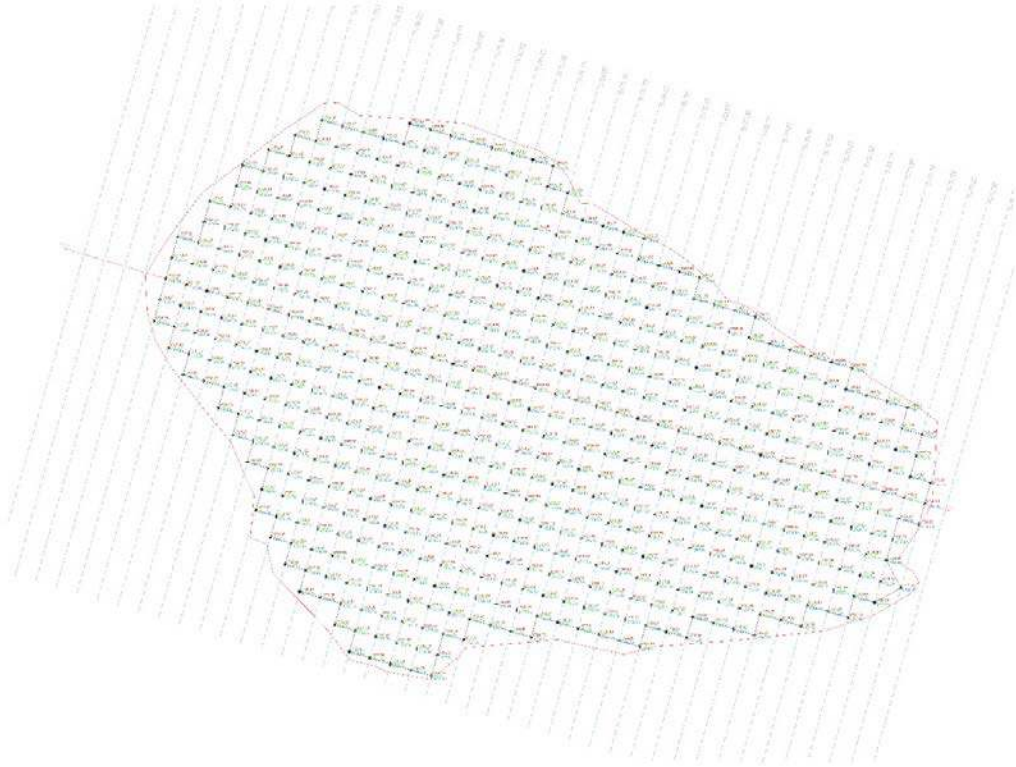


**Figure 4.10 Grid Pattern (10ft) of the Earthwork Area**

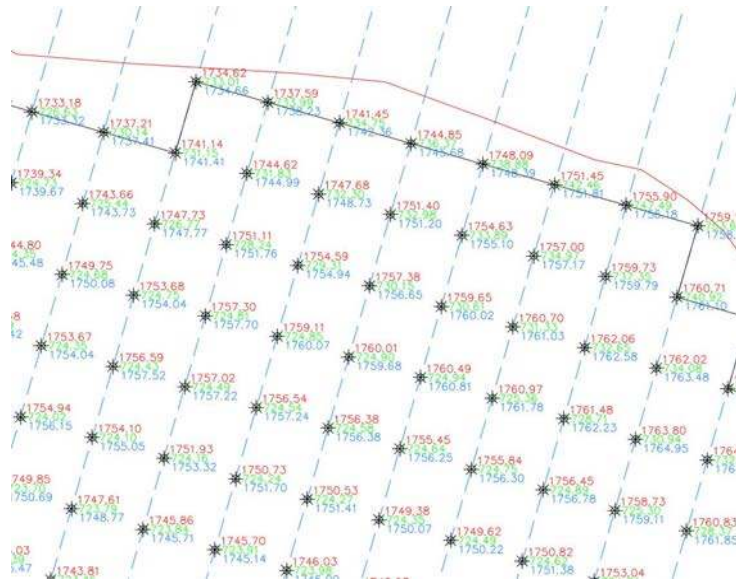


**Figure 4.11 Elevations of each Grid Intersection**

### 4.4.3 Results

Earthwork volumes are computed using the 3D contour map created by the UAS platform, AEA method and grid method. All volume analyses were conducted using Autodesk's AutoCAD Civil 3D 2015. Although no true values for the volumes were available, the volume calculated by the survey points could be an objective reference for comparisons. Because the accuracy of the AEA method and grid methods largely depend on cross-section intervals and the size of grid, in this study, the volumes are computed via the AEA method at a cross-section interval of 10-, 30-, 50-, and 100-ft intervals respectively. Similarly, the volumes are calculated via the grid method using the grid spacings of 10, 30, 50, and 100ft respectively. The results are shown in Table 4.1:

**Table 4.1 Comparisons of Earthwork Volumes Computed by Different Methods**

	Survey	UAS	Average-End-Area Method (10 <sup>3</sup> Cubic Yard)				Grid Method (10 <sup>3</sup> Cubic Yard)			
	-	-	10ft	30ft	50ft	100ft	10ft	30ft	50ft	100ft
Fill	54.20	53.59	54.18	54.35	52.94	46.27	54.02	50.51	43.65	39.11
Cut	0.004	0.003	0.004	0.002	0.003	0.007	0	0	0	0
Net	54.20	53.59	54.18	54.35	52.94	46.27	54.02	50.51	43.65	39.11
*Percentage Difference (%)	-	1.11	0.03	0.28	2.32	14.62	0.33	6.8	19.46	27.83

\*Percentage Difference is the earthwork volumes measured by other methods different from the volume calculated by the survey points.

As to the AEA method, the area and volumes for each cross-section are recorded in the Appendix B.

It can be observed that the grid method with 10ft grid spacing and the AEA method with 10ft and 30ft intervals generate better results than the volumes calculated based on the model of UAS platform. However, when cross-sections interval was larger than 30ft and the grid spacing was larger than 10ft, the UAS platform shows a significant advantage in accuracy over the other two methods. In practice, due to the nature of the earthwork job on a construction site, no method can be used to identify the true earthwork volumes with 100 percent accuracy; therefore, a reasonable scale of errors is always acceptable. The tolerance for errors varies by owners and projects; there is no uniform standard to determine required measurement accuracy. A few state DOTs provide references regarding the authorized adjustments of earthwork quantity in the design. For instance, the Kentucky Transportation Cabinet requires corrections of major errors on the Plans, which are defined as mistakes of 3 percent or more in the quantity of earthwork (KYTC, 2012); The Indiana DOT requires detailed checks on areas to determine whether the planned quantity needs to be adjusted for areas varying more than 10% from the area indicated on the plans (INDOT, 2018). The volumes measured by the UAS platform are 1.11% different from the volumes of survey data. Although the accuracy is not optimal, it is a more efficient method to measure the earthwork volume based on the comparison between UAS and conventional survey methods regarding time and cost displayed in Table 4.2 and Table 4.3

**Table 4.2 Comparisons of Labor Hours between UAS and Conventional Survey Methods**

	Area (acre)	Number of Crew	Labor-Hours (per acre)	Total Hours
UAS	1.47	1-2	0.35	0.51
Conventional	1.47	4	7.27	10.69

**Table 4.3 Comparisons of Cost between UAS and Conventional Survey Methods**

	Area (acre)	Number of Crew	Cost (dollars per acre)	Total Cost (dollars)
UAS	1.47	1-2	440	646.80
Conventional	1.47	4	545	801.15

According to the RS Means manual, the unit surveying labor-hour and cost of UAS method is much smaller than conventional method. As the distance between cross-sections or the grid spacing decrease, the accuracy of the calculation is improved, but the time and labor for surveying the site will significantly increase and the computation becomes much more complicated. In practice, the owner or project manager aims to reach a balance between the measurement accuracy and the productivity concerning the time and cost. In this study, the UAS is proved to be an effective and efficient method in the process of earthwork volume measurement.

#### **4.5 Conclusion**

Earthwork is one of the major cost items for a construction project. It is crucial to have an accurate measurement of earthwork materials quantity for payments. The current practices of earthwork measurement at most DOTs need to be improved due to issues such as shortage of staff or inefficiency of conventional methods. As the surveying technologies develop in recent years, applications of the UAS become popular in many areas. This study aims to prove the effectiveness and efficiency of using the UAS platform to measure the earthwork volume by comparing with the other two most commonly used methods, Average-End-Area (AEA) method and grid method, in a highway project. This study uses the UAS as the survey method to collect images of the earthwork area and creates 3D



contour map for computing the volumes by the Autodesk Civil 3D software. The volumes of same earthwork area are calculated by the AEA method and grid method using different intervals and grid spacing. Due to no true volumes available, a 3D contour map created based on more than 400 survey points measured by an accurate GPS rover is used as the criteria for comparing the volumes calculated by different methods. The results indicate that decreasing the cross-section interval used in AEA method and the grid size used in the grid method leads to smaller percentage differences from the criteria volume measurement. However, the optimal intervals and the grid spacing are not feasible in practice due to intense calculations and a large amount of survey works. The UAS provides a balance between accuracy and efficiency, even though its percentage difference is larger than the other two methods using the minimum distance (10ft).

Overall, the UAS is proved to be an effective tool in the process of earthwork measurement. This study aims to provide a reference for engineers or managers regarding the selections of earthwork volume measurement methods. The selection always depends on the required accuracy and budget of a project. For instance, the UAS may have better performance when estimating the earthwork of large construction area because it decreases the survey time and also reduces the risk of safety. For small earthwork area, conventional methods may be the better option because the small area may require less cost. In the future, more research can be conducted to compare the performance of different types of the UAS in various construction situations. In addition, besides the Autodesk software, the data can be operated on other platforms to test the compatibility between different devices. Furthermore, it is necessary to conduct productivity analysis of this emerging technology from management and economic perspectives.

## 5. CONCLUSION

This dissertation discusses using the UAS and photogrammetry technology to estimate the earthwork volume of construction projects. The research is composed of three sections: (1) estimate earthwork volumes of a highway project on Newtown Pike in Lexington through the UAS and photogrammetry to preliminarily prove the effectiveness of this emerging technology; (2) Analyze the influence of different flight parameters and processing factors on the measurement accuracy through multiple flight tests on the UK Coldstream farm at Lexington; (3) Compare the earthwork volumes of a highway project in Virginia measured by traditional methods (Average-End-Area method and grid method) and UAS photogrammetry technology through models in AutoCAD to further prove the effectiveness and efficiency of the UAS platform. The findings of each section are summarized as follows,

- **Chapter 2: the results preliminarily support the accuracy and mapping suitability of UAS and photogrammetry applications in earthwork construction.** In this chapter, the research follows the basic procedures of photo collection by the UAS and image processing in photogrammetry to estimate earthwork volumes of a construction project. The average errors of measurements, which are 7% and 0.9% for the stockpile and trench respectively, are smaller than 11% which is the result of the most cited literature applying same procedures and methods as this study. The trench volume error is smaller than 4.5% which is the error if using conventional cross-section method.

- Chapter 3: the results indicate that the combination of low flight altitudes, high image overlapping rate, the use of a proper number of GCPs and modeling surface of a clay soil type can maximize the measurement accuracy, after detailed comparisons and analysis for multiple flight plans.** The purpose of Chapter 3 is to investigate how important factors, including flight altitude, image overlapping rate, the use of GCPs, and soil types, impact on measurement accuracy through experimental flights and statistical analysis of positional errors. After image processing, it is observed that flying the UAS at 60ft or 90ft altitude with 90%-60% image overlapping rate and applying 8 to 16 GCPs has the smallest positional error (RMSE = 0.28ft). Among all the factors, the use of GCPs is the most influential factor due to it has the smallest p-value (<0.0001) of the multiple regression model. In addition, the measured volume of clay has the smallest error (1.33%) compared with other soil types.
- Chapter 4: the results indicate that the UAS obtains less accurate measurements than the other two conventional methods when using minimum cross-section intervals and grid spacing, but the UAS provides a balance between accuracy and efficiency.** Chapter 4 aims to further prove the effectiveness and efficiency of using the UAS platform to measure the earthwork volumes by comparing with the other two most commonly used methods, Average-End-Area (AEA) method and grid method, in a highway project. The volumes of the same earthwork area are calculated by conventional methods using different intervals and grid spacing. Due to there is no feasible way to obtain true volumes, a 3D contour map created based on more than 400 survey points measured by an

accurate GPS rover is used as the criteria for comparing the volumes calculated by different methods. The errors of AEA method using 10ft and 30ft cross-sections distance are 0.03% and 0.28% respectively; the error of grid method using 10ft grid spacing is 0.33%; and the UAS method has the error of 1.11%. Although the accuracy of UAS method is not optimal, it save more time and labor than the other two method when using 10ft or 30ft. Besides, its accuracy is significantly higher when applying large cross-section distance and grid spacing.

The limitation of this study is the selection of the UAS device and photogrammetry software. Low cost UAS limits the sensor payload in weight and dimension so that usually low weight sensors like small or medium format amateur cameras are selected. When compared to large format cameras, the UAS acquire a higher number of images in order to obtain the same image coverage and comparable image resolution. Moreover, low-cost sensors are normally less stable, which results in a low image quality. In addition, low-cost UAVs are normally equipped with less powerful engines, limiting the reachable altitude. Therefore, when processing the images collected by the UAS, this study will not concern about the difference caused by different devices. Although the accuracy and hardware equipment of the selected device and photogrammetry software in this study is above the average in the market, which can be used as a reasonable reference for most researcher and practitioners, more research should be conducted regarding how different equipment impact on the measurement accuracy. Besides, compatibility of outputs created by the UAS and photogrammetry is another potential topic for the future research. For instance, the smooth corporations between the point cloud model and BIM model may significantly improve the construction management process. In addition, some technical limitations such

as inaccurate geo-referencing capability and limited battery capacity need to be solved for better flight performance. Last but not least, more research can be conducted regarding the safety and productivity performance of the UAS and photogrammetry method in earthwork estimation or other construction activities. In conclusion, although the selection of measurement methods always depends on the required accuracy and budget of a project, the UAS is definitely an effective one to be considered.

## APPENDICES

### Appendix A. Positional Errors Analysis Results of Flight Plans

The Table 6.1 displays the coordinates of GCPs measured by the GPS rover in X, Y, and Z directions. The Table 6.2 display the point positional errors in three dimensions and the average errors of each flight plan when processing images with different number of GCPs. The name of flight plan is composed of the flight altitude and image overlapping rate. For instance, 60ft\_70% indicates flying the UAS at 60ft altitudes with 70% image overlapping rate. The Table 6.3 shows the multiple regression analysis results in JMP.

**Table 6.1 Coordinates of GCPs (ft)**

<b>Name of Points</b>	<b>X</b>	<b>Y</b>	<b>Z</b>
GCP 1	1564429.80	222785.90	571.30
GCP 2	1564355.29	222724.08	571.97
GCP 3	1564286.81	222668.89	570.45
GCP 4	1564331.59	222607.21	572.03
GCP 5	1564378.29	222548.07	570.39
GCP 6	1564422.52	222498.41	568.16
GCP 7	1564467.30	222440.49	564.93
GCP 8	1564532.67	222501.60	566.49
GCP 9	1564607.13	222565.46	566.72
GCP 10	1564561.87	222607.23	566.76
GCP 11	1564501.44	222549.95	567.17
GCP 12	1564474.38	222585.07	570.03
GCP 13	1564462.25	222607.89	571.03
GCP 14	1564543.14	222656.15	570.08
GCP 15	1564480.61	222708.31	571.39
GCP 16	1564427.69	222666.94	572.09

**Table 6.2 Residue Values of Each Flight Plan When Applying Different Number of GCPs (ft)**

	<b>Residual Values (No GCPs)</b>			
<b>Flight Plan</b>	<b>Error in x</b>	<b>Error in y</b>	<b>Error in z</b>	<b>Average error</b>
60 ft_70%	7.19	4.21	0.89	4.09
60 ft_90%	4.50	3.95	7.61	5.35
90 ft_70%	5.91	4.80	4.28	5.00
90 ft_90%	3.72	3.49	2.73	3.31
120 ft_70%	3.30	2.17	3.90	3.12
120 ft_90%	2.20	14.68	3.67	6.85
150 ft_70%	4.20	5.20	1.08	3.49
150 ft_90%	2.72	3.51	2.48	2.90
	<b>Residual Values (1 GCPs)</b>			
<b>Flight Plan</b>	<b>Error in x</b>	<b>Error in y</b>	<b>Error in z</b>	<b>Average error</b>
60 ft_70%	1.79	3.84	6.60	4.08
60 ft_90%	4.96	4.55	3.26	4.25
90 ft_70%	6.56	4.75	2.33	4.55
90 ft_90%	4.26	3.83	1.84	3.31
120 ft_70%	2.22	2.33	5.00	3.19
120 ft_90%	6.23	5.95	5.04	5.74
150 ft_70%	3.44	2.77	4.75	3.65
150 ft_90%	2.67	3.43	2.56	2.89
	<b>Residual Values (4 GCPs)</b>			
<b>Flight Plan</b>	<b>Error in x</b>	<b>Error in y</b>	<b>Error in z</b>	<b>Average error</b>
60 ft_70%	0.40	0.86	1.48	0.92
60 ft_90%	0.33	0.30	0.22	0.29
90 ft_70%	1.17	0.85	0.42	0.81
90 ft_90%	0.41	0.37	0.18	0.32
120 ft_70%	0.42	0.44	0.94	0.60
120 ft_90%	0.54	0.52	0.44	0.50
150 ft_70%	0.61	0.49	0.84	0.64
150 ft_90%	0.47	0.61	0.45	0.51
	<b>Residual Values (8 GCPs)</b>			
<b>Flight Plan</b>	<b>Error in x</b>	<b>Error in y</b>	<b>Error in z</b>	<b>Average error</b>
60 ft_70%	0.34	0.73	1.26	0.78
60 ft_90%	0.33	0.30	0.22	0.28
90 ft_70%	1.01	0.73	0.36	0.70

90 ft_90%	0.38	0.34	0.16	0.29
120 ft_70%	0.42	0.44	0.94	0.60
120 ft_90%	0.49	0.47	0.40	0.45
150 ft_70%	0.53	0.43	0.74	0.57
150 ft_90%	0.44	0.57	0.42	0.48
<b>Residual Values (12 GCPs)</b>				
<b>Flight Plan</b>	<b>Error in x</b>	<b>Error in y</b>	<b>Error in z</b>	<b>Average error</b>
60 ft_70%	0.24	0.52	0.89	0.55
60 ft_90%	0.32	0.30	0.21	0.28
90 ft_70%	0.93	0.67	0.33	0.64
90 ft_90%	0.36	0.32	0.16	0.28
120 ft_70%	0.35	0.37	0.79	0.50
120 ft_90%	0.34	0.32	0.27	0.31
150 ft_70%	0.36	0.29	0.50	0.38
150 ft_90%	0.28	0.36	0.27	0.30
<b>Residual Values (16 GCPs)</b>				
<b>Flight Plan</b>	<b>Error in x</b>	<b>Error in y</b>	<b>Error in z</b>	<b>Average error</b>
60 ft_70%	0.23	0.49	0.84	0.52
60 ft_90%	0.32	0.30	0.21	0.28
90 ft_70%	0.72	0.52	0.25	0.50
90 ft_90%	0.36	0.32	0.15	0.28
120 ft_70%	0.30	0.31	0.67	0.43
120 ft_90%	0.31	0.30	0.25	0.29
150 ft_70%	0.36	0.29	0.50	0.38
150 ft_90%	0.29	0.37	0.27	0.31



**Appendix B. Earthwork Volumes Calculated by Average-End-Area Method and Grid Method.**

In this appendix, Table 6.4 shows the area and volume of each cross-sections (10ft) when using different data resource. UAS\_Cut and UAS\_Fill indicates the cut and fill earthwork volumes of the model created by the UAS platform. Survey\_Cut and Survey\_Fill indicates the cut and fill earthwork volume computed by using the survey point data. Table 6.5 displays the elevations at each grid intersection when applying 10ft grid spacing. The station indicates the location of each grid intersection. The first part indicates the cross-section lines across the area; the second part is the offset from the central line. For example, 1+00 80 represent the intersection located at 1+00 section and 80ft to the right of the centerline when traveling in the direction of the station increasing; if the 80ft to the left, it's going to be a 1+00 -80. This is the standard name in civil engineering for points at left or right of a centerline and it is numbered the same way on the sections. The “UAS” column displays the elevations in the model created through the UAS platform; the “Survey” column dispays the elevations in the model created based on the survey points; the “Base” are the elevations of each point before earthwork.

**Table 6.3 Results of Average-End-Area Method**

	<b>Section Type</b>	<b>Area (ft<sup>2</sup>)</b>	<b>Volume (cy)</b>	<b>Cumulative Volume</b>
Station: 10.00	UAS_Cut	0.00	0.00	0.00
	UAS_Fill	0.00	0.00	0.00
	Survey_Cut	0.00	0.00	0.00
	Survey_Fill	0.00	0.00	0.00
Station: 20.00	UAS_Cut	0.00	0.00	0.00
	UAS_Fill	0.00	0.00	0.00
	Survey_Cut	0.00	0.00	0.00
	Survey_Fill	0.00	0.00	0.00
Station: 30.00	UAS_Cut	0.00	0.00	0.00

	UAS_Fill	0.00	0.00	0.00
	Survey_Cut	0.00	0.00	0.00
	Survey_Fill	0.00	0.00	0.00
Station: 40.00	UAS_Cut	0.00	0.00	0.00
	UAS_Fill	0.00	0.00	0.00
	Survey_Cut	0.00	0.00	0.00
	Survey_Fill	0.00	0.00	0.00
Station: 50.00	UAS_Cut	0.00	0.00	0.00
	UAS_Fill	336.43	62.30	62.30
	Survey_Cut	0.00	0.00	0.00
	Survey_Fill	363.38	67.29	67.29
Station: 60.00	UAS_Cut	0.00	0.00	0.00
	UAS_Fill	893.83	227.83	290.13
	Survey_Cut	904.86	234.86	302.15
	Survey_Fill	904.86	234.86	302.15
Station: 70.00	UAS_Cut	0.00	0.00	0.00
	UAS_Fill	1525.71	448.06	738.19
	Survey_Cut	0.00	0.00	0.00
	Survey_Fill	1517.10	448.51	750.66
Station: 80.00	UAS_Cut	0.00	0.00	0.00
	UAS_Fill	2206.47	691.14	1429.33
	Survey_Cut	0.00	0.00	0.00
	Survey_Fill	2168.48	582.51	1433.17
Station: 90.00	UAS_Cut	0.00	0.00	0.00
	UAS_Fill	2791.16	925.49	2354.82
	Survey_Cut	0.00	0.00	0.00
	Survey_Fill	2763.72	913.37	2346.54
Station: 100.00	UAS_Cut	0.00	0.00	0.00
	UAS_Fill	3224.75	1114.06	3468.88
	Survey_Cut	0.00	0.00	0.00
	Survey_Fill	3207.98	1105.87	3452.41
Station: 110.00	UAS_Cut	0.00	0.00	0.00
	UAS_Fill	3373.14	1221.83	4690.71
	Survey_Cut	0.00	0.00	0.00
	Survey_Fill	3406.65	1224.93	4677.34
Station: 120.00	UAS_Cut	0.00	0.00	0.00
	UAS_Fill	3597.85	1290.93	5981.64
	Survey_Cut	0.00	0.00	0.00
	Survey_Fill	3598.78	1297.30	5981.64
Station: 130.00	UAS_Cut	0.00	0.00	0.00
	UAS_Fill	3833.30	1376.14	7357.78
	Survey_Cut	0.00	0.00	0.00
	Survey_Fill	3838.10	1377.20	7351.84
Station: 140.00	UAS_Cut	0.00	0.00	0.00
	UAS_Fill	4095.86	1468.36	8826.14

	Survey_Cut	0.00	0.00	0.00
	Survey_Fill	4165.12	1482.08	8833.92
Station: 150.00	UAS_Cut	0.00	0.00	0.00
	UAS_Fill	4151.52	1527.29	10353.42
	Survey_Cut	0.00	0.00	0.00
	Survey_Fill	4214.57	1551.80	10385.71
Station: 160.00	UAS_Cut	0.00	0.00	0.00
	UAS_Fill	4315.85	1586.03	11921.46
	Survey_Cut	0.00	0.00	0.00
	Survey_Fill	4401.84	1595.63	11981.35
Station: 170.00	UAS_Cut	0.00	0.00	0.00
	UAS_Fill	4696.51	1668.95	13590.42
	Survey_Cut	0.00	0.00	0.00
	Survey_Fill	4753.81	1695.49	13676.84
Station: 180.00	UAS_Cut	0.00	0.00	0.00
	UAS_Fill	5006.05	1796.77	15387.19
	Survey_Cut	0.00	0.00	0.00
	Survey_Fill	5108.12	1826.28	15503.12
Station: 190.000	UAS_Cut	0.00	0.00	0.00
	UAS_Fill	5201.32	1890.25	17277.44
	Survey_Cut	0.00	0.00	0.00
	Survey_Fill	5333.79	1933.69	17436.80
Station: 200.00	UAS_Cut	0.00	0.00	0.00
	UAS_Fill	5326.29	1949.56	19227.00
	Survey_Cut	0.00	0.00	0.00
	Survey_Fill	5457.09	1998.31	19435.12
Station: 210.00	UAS_Cut	0.00	0.00	0.00
	UAS_Fill	5452.59	1996.09	21223.09
	Survey_Cut	0.00	0.00	0.00
	Survey_Fill	5598.15	2047.27	21482.38
Station: 220.00	UAS_Cut	0.00	0.00	0.00
	UAS_Fill	5467.50	2022.24	23245.33
	Survey_Cut	0.00	0.00	0.00
	Survey_Fill	5598.17	2073.39	23555.77
Station: 230.00	UAS_Cut	0.00	0.00	0.00
	UAS_Fill	5377.66	2008.36	25253.69
	Survey_Cut	0.00	0.00	0.00
	Survey_Fill	5468.70	2049.42	25605.19
Station: 240.00	UAS_Cut	0.00	0.00	0.00
	UAS_Fill	5390.14	1994.04	27247.73
	Survey_Cut	0.00	0.00	0.00
	Survey_Fill	5450.81	2022.13	27627.32
Station: 250.00	UAS_Cut	0.00	0.00	0.00
	UAS_Fill	5383.86	1995.19	29242.91
	Survey_Cut	0.00	0.00	0.00

	Survey_Fill	5469.72	2022.32	29649.64
Station: 260.00	UAS_Cut	0.00	0.00	0.00
	UAS_Fill	5379.89	1993.29	31236.20
	Survey_Cut	0.00	0.00	0.00
	Survey_Fill	5510.68	2033.41	31683.05
Station: 270.00	UAS_Cut	0.00	0.00	0.00
	UAS_Fill	5444.39	2004.50	33240.70
	Survey_Cut	0.00	0.00	0.00
	Survey_Fill	5594.55	2056.52	33739.57
Station: 280.00	UAS_Cut	0.00	0.00	0.00
	UAS_Fill	5403.31	2008.83	35249.53
	Survey_Cut	0.00	0.00	0.00
	Survey_Fill	5483.95	2051.57	35791.15
Station: 290.00	UAS_Cut	0.00	0.00	0.00
	UAS_Fill	5353.55	1992.01	37241.54
	Survey_Cut	0.00	0.00	0.00
	Survey_Fill	5427.62	2020.66	37811.81
Station: 300.00	UAS_Cut	0.00	0.00	0.00
	UAS_Fill	5234.93	1960.83	39202.37
	Survey_Cut	0.00	0.00	0.00
	Survey_Fill	5289.10	1984.58	39796.39
Station: 310.00	UAS_Cut	0.00	0.00	0.00
	UAS_Fill	4999.41	1895.25	41097.62
	Survey_Cut	0.00	0.00	0.00
	Survey_Fill	5022.03	1909.47	41705.85
Station: 320.00	UAS_Cut	0.00	0.00	0.00
	UAS_Fill	4741.81	1803.93	42901.55
	Survey_Cut	0.00	0.00	0.00
	Survey_Fill	4780.65	1815.31	43521.17
Station: 330.00	UAS_Cut	0.00	0.00	0.00
	UAS_Fill	4505.22	1712.41	44613.96
	Survey_Cut	0.00	0.00	0.00
	Survey_Fill	4501.42	1718.90	45240.07
Station: 340.00	UAS_Cut	0.00	0.00	0.00
	UAS_Fill	4208.37	1613.63	46227.59
	Survey_Cut	0.00	0.00	0.00
	Survey_Fill	4162.93	1604.51	46844.58
Station: 350.00	UAS_Cut	0.00	0.00	0.00
	UAS_Fill	3933.02	1507.66	47735.25
	Survey_Cut	0.00	0.00	0.00
	Survey_Fill	3943.44	1501.18	48345.76
Station: 360.00	UAS_Cut	0.04	0.00	0.00
	UAS_Fill	3774.90	1427.39	49162.64
	Survey_Cut	0.03	0.00	0.00
	Survey_Fill	3939.39	1441.26	49787.02

Station: 370.00	UAS_Cut	0.16	0.04	0.05
	UAS_Fill	3319.92	1313.86	50476.50
	Survey_Cut	0.13	0.03	0.04
	Survey_Fill	3343.74	1330.21	51117.23
Station: 380.00	UAS_Cut	0.43	0.11	0.16
	UAS_Fill	2641.59	1103.98	51580.48
	Survey_Cut	0.42	0.10	0.14
	Survey_Fill	2683.09	1116.08	52233.31
Station: 390.00	UAS_Cut	1.38	0.33	0.49
	UAS_Fill	2031.11	865.31	52445.80
	Survey_Cut	0.96	0.25	0.39
	Survey_Fill	1991.64	865.69	53099.00
Station: 400.00	UAS_Cut	1.30	0.50	0.99
	UAS_Fill	1373.69	630.52	53076.32
	Survey_Cut	3.73	0.87	1.26
	Survey_Fill	1283.47	606.50	53705.50
Station: 410.00	UAS_Cut	4.77	1.12	2.11
	UAS_Fill	691.70	382.48	53458.80
	Survey_Cut	6.08	1.82	3.07
	Survey_Fill	641.51	356.48	54061.98
Station: 420.00	UAS_Cut	0.00	0.88	2.99
	UAS_Fill	0.00	128.09	53586.89
	Survey_Cut	0.00	1.13	4.20
	Survey_Fill	0.00	118.80	54180.78
Station: 430.00	UAS_Cut	0.00	0.00	2.99
	UAS_Fill	0.00	0.00	53586.89
	Survey_Cut	0.00	0.00	4.20
	Survey_Fill	0.00	0.00	54180.78

**Table 6.4 Elevations of Grid Intersections (ft)**

<b>Station</b>	<b>UAS</b>	<b>Survey</b>	<b>Base</b>
0+50 -20	1725.38	1725.89	1720.86
0+50 -10	1727.66	1728.35	1721.07
0+50 0	1729.57	1730.49	1720.92
0+50 10	1728.71	1729.19	1720.64
0+50 20	1725.76	1726.08	1720.35
0+60 -40	1725.71	1726.23	1720.95
0+60 -30	1729.55	1729.86	1721.33
0+60 -20	1733.32	1733.37	1721.53
0+60 -10	1735.82	1735.62	1721.43
0+60 0	1737.29	1737.69	1721.15
0+60 10	1735.95	1736.23	1720.85
0+60 20	1732.00	1732.32	1720.60
0+60 30	1727.43	1727.15	1720.35
0+70 -60	1723.46	1723.30	1720.93
0+70 -50	1727.85	1727.78	1721.26
0+70 -40	1732.33	1732.33	1721.76
0+70 -30	1736.83	1736.61	1721.94
0+70 -20	1740.43	1740.56	1721.93
0+70 -10	1742.95	1742.17	1721.65
0+70 0	1744.81	1744.84	1721.36
0+70 10	1742.80	1742.49	1721.36
0+70 20	1738.27	1737.76	1720.87
0+70 30	1732.17	1731.94	1720.58
0+70 40	1726.19	1725.93	1720.30
0+80 -70	1725.35	1724.66	1721.57
0+80 -60	1729.98	1729.18	1721.78
0+80 -50	1734.46	1733.90	1722.09
0+80 -40	1739.20	1738.38	1722.38
0+80 -30	1743.71	1743.30	1722.43
0+80 -20	1747.29	1747.02	1722.16
0+80 -10	1749.98	1750.67	1721.88
0+80 0	1750.07	1750.42	1721.63
0+80 10	1748.26	1748.35	1721.36
0+80 20	1742.64	1742.23	1721.08
0+80 30	1736.57	1736.15	1720.80
0+80 40	1730.40	1730.29	1720.52
0+90 -80	1725.74	1725.65	1721.97
0+90 -70	1731.23	1730.39	1722.49
0+90 -60	1736.14	1734.80	1722.40
0+90 -50	1740.95	1739.69	1722.84

0+90 -40	1745.61	1744.40	1722.94
0+90 -30	1749.86	1749.45	1722.66
0+90 -20	1752.01	1753.77	1722.40
0+90 -10	1752.01	1752.17	1722.14
0+90 0	1751.63	1751.47	1721.86
0+90 10	1750.09	1750.35	1721.58
0+90 20	1746.32	1746.33	1721.29
0+90 30	1740.58	1740.76	1721.01
0+90 40	1734.50	1734.63	1720.73
0+90 50	1728.69	1728.61	1720.45
1+00 -90	1724.96	1725.17	1722.51
1+00 -80	1730.68	1730.57	1722.98
1+00 -70	1736.07	1735.61	1723.19
1+00 -60	1741.30	1740.49	1723.24
1+00 -50	1746.56	1745.25	1723.43
1+00 -40	1751.02	1750.10	1723.17
1+00 -30	1752.28	1753.97	1722.91
1+00 -20	1752.01	1751.96	1722.64
1+00 -10	1751.48	1751.31	1722.36
1+00 0	1750.05	1750.41	1722.05
1+00 10	1749.08	1750.00	1721.78
1+00 20	1748.64	1748.67	1721.48
1+00 30	1744.87	1744.75	1721.20
1+00 40	1738.83	1738.72	1720.91
1+00 50	1732.95	1732.83	1720.61
1+00 60	1727.15	1726.93	1720.33
1+10 -90	1729.01	1729.24	1724.11
1+10 -80	1735.19	1735.51	1723.97
1+10 -70	1740.79	1740.51	1723.55
1+10 -60	1745.25	1745.60	1723.91
1+10 -50	1750.72	1750.67	1723.68
1+10 -40	1753.28	1753.55	1723.42
1+10 -30	1752.10	1751.75	1723.14
1+10 -20	1747.85	1747.88	1722.82
1+10 -10	1745.47	1745.85	1722.54
1+10 0	1743.92	1744.81	1722.23
1+10 10	1743.15	1743.53	1721.93
1+10 20	1744.55	1745.05	1721.64
1+10 30	1746.10	1746.09	1721.34
1+10 40	1743.18	1743.51	1721.03
1+10 50	1737.87	1738.11	1720.79
1+10 60	1732.33	1732.08	1720.55
1+10 70	1727.35	1727.51	1720.28

1+20 -90	1733.18	1733.32	1726.63
1+20 -80	1739.34	1739.67	1724.73
1+20 -70	1744.80	1745.48	1724.35
1+20 -60	1749.48	1750.42	1724.19
1+20 -50	1753.77	1754.21	1723.91
1+20 -40	1753.05	1753.74	1723.59
1+20 -30	1749.49	1749.18	1723.27
1+20 -20	1744.26	1744.71	1722.98
1+20 -10	1742.95	1742.33	1722.67
1+20 0	1741.85	1741.83	1722.35
1+20 10	1741.21	1740.88	1722.06
1+20 20	1741.11	1740.32	1721.73
1+20 30	1740.40	1740.21	1721.49
1+20 40	1742.14	1741.58	1721.24
1+20 50	1741.99	1742.51	1720.93
1+20 60	1737.59	1737.46	1720.69
1+20 70	1732.77	1732.98	1720.48
1+20 80	1728.51	1728.61	1720.31
1+20 90	1727.10	1726.66	1720.15
1+30 -90	1737.21	1737.41	1730.14
1+30 -80	1743.66	1743.73	1725.44
1+30 -70	1749.75	1750.08	1724.68
1+30 -60	1753.67	1754.04	1724.35
1+30 -50	1754.94	1756.15	1724.02
1+30 -40	1749.85	1750.69	1723.70
1+30 -30	1745.03	1745.47	1723.39
1+30 -20	1743.41	1742.99	1723.07
1+30 -10	1742.42	1742.60	1722.76
1+30 0	1741.47	1742.09	1722.44
1+30 10	1740.69	1741.14	1722.19
1+30 20	1739.97	1740.20	1721.91
1+30 30	1739.14	1739.16	1721.60
1+30 40	1738.98	1737.96	1721.33
1+30 50	1740.00	1739.45	1721.09
1+30 60	1741.32	1742.36	1720.89
1+30 70	1739.07	1738.89	1720.71
1+30 80	1735.61	1734.81	1720.49
1+30 90	1732.67	1731.48	1720.42
1+30 100	1729.03	1728.30	1720.33
1+40 -100	1734.62	1734.66	1733.01
1+40 -90	1741.14	1741.41	1731.15
1+40 -80	1747.73	1747.77	1726.77
1+40 -70	1753.68	1754.04	1724.75



1+40 -60	1756.59	1757.52	1724.43
1+40 -50	1754.10	1755.05	1724.10
1+40 -40	1747.61	1748.77	1723.79
1+40 -30	1743.81	1743.84	1723.46
1+40 -20	1743.16	1743.35	1723.14
1+40 -10	1742.51	1742.88	1722.90
1+40 0	1741.79	1742.35	1722.58
1+40 10	1740.77	1741.32	1722.27
1+40 20	1739.54	1740.15	1721.98
1+40 30	1738.33	1738.93	1721.74
1+40 40	1737.43	1737.68	1721.49
1+40 50	1737.30	1736.87	1721.30
1+40 60	1739.32	1739.02	1721.10
1+40 70	1740.27	1741.93	1720.84
1+40 80	1740.38	1740.62	1720.75
1+40 90	1738.01	1737.53	1720.66
1+40 100	1733.63	1732.95	1720.55
1+40 110	1729.49	1729.14	1720.36
1+50 -100	1737.59	1738.23	1733.99
1+50 -90	1744.62	1744.99	1731.83
1+50 -80	1751.11	1751.76	1728.24
1+50 -70	1757.30	1757.70	1724.81
1+50 -60	1757.02	1757.22	1724.49
1+50 -50	1751.93	1753.32	1724.16
1+50 -40	1745.86	1745.71	1723.84
1+50 -30	1744.30	1744.38	1723.57
1+50 -20	1743.49	1743.93	1723.25
1+50 -10	1742.93	1743.42	1722.94
1+50 0	1742.41	1743.08	1722.64
1+50 10	1741.41	1741.86	1722.38
1+50 20	1739.82	1740.87	1722.13
1+50 30	1738.22	1738.53	1721.89
1+50 40	1736.64	1737.23	1721.69
1+50 50	1735.67	1735.97	1721.47
1+50 60	1735.27	1734.95	1721.20
1+50 70	1735.07	1735.30	1721.08
1+50 80	1736.34	1736.83	1721.00
1+50 90	1738.69	1739.40	1720.88
1+50 100	1737.21	1736.85	1720.70
1+50 110	1733.38	1731.98	1720.28
1+50 120	1728.24	1727.09	1720.00
1+60 -100	1741.45	1742.36	1734.75
1+60 -90	1747.68	1748.73	1732.3

1+60 -80	1754.59	1754.94	1729.31
1+60 -70	1759.11	1760.07	1724.85
1+60 -60	1756.54	1757.24	1724.54
1+60 -50	1750.73	1751.70	1724.24
1+60 -40	1745.70	1745.14	1723.91
1+60 -30	1744.67	1744.86	1723.61
1+60 -20	1744.07	1744.55	1723.31
1+60 -10	1743.69	1744.17	1723.04
1+60 0	1743.52	1743.99	1722.78
1+60 10	1743.62	1743.17	1722.52
1+60 20	1743.76	1744.27	1722.28
1+60 30	1741.24	1741.79	1722.07
1+60 40	1737.75	1737.68	1721.84
1+60 50	1735.43	1735.47	1721.57
1+60 60	1733.98	1734.73	1721.40
1+60 70	1733.28	1734.10	1721.33
1+60 80	1733.24	1733.10	1721.22
1+60 90	1734.25	1735.25	1721.03
1+60 100	1737.50	1737.63	1720.77
1+60 110	1735.80	1735.00	1720.19
1+60 120	1730.36	1730.09	1720.00
1+70 -100	1744.85	1745.68	1736.37
1+70 -90	1751.40	1751.20	1732.98
1+70 -80	1757.38	1756.65	1730.15
1+70 -70	1760.01	1759.68	1724.90
1+70 -60	1756.38	1756.38	1724.58
1+70 -50	1750.53	1751.41	1724.27
1+70 -40	1746.03	1746.00	1723.98
1+70 -30	1745.29	1745.67	1723.70
1+70 -20	1744.97	1745.18	1723.43
1+70 -10	1744.70	1745.17	1723.18
1+70 0	1745.25	1745.11	1722.91
1+70 10	1748.45	1748.37	1722.69
1+70 20	1751.84	1752.30	1722.47
1+70 30	1748.00	1748.66	1722.21
1+70 40	1742.51	1743.42	1721.94
1+70 50	1737.42	1738.06	1721.75
1+70 60	1734.15	1734.29	1721.66
1+70 70	1732.84	1733.45	1721.55
1+70 80	1731.91	1732.52	1721.35
1+70 90	1731.69	1731.49	1721.17
1+70 100	1733.43	1733.59	1720.68
1+70 110	1736.35	1737.35	1720.10

1+70 120	1733.64	1733.63	1720.00
1+70 130	1728.32	1728.41	1720.00
1+80 -100	1748.09	1748.39	1738.88
1+80 -90	1754.63	1755.10	1733.89
1+80 -80	1759.65	1760.02	1730.61
1+80 -70	1760.49	1760.81	1724.94
1+80 -60	1755.45	1756.25	1724.64
1+80 -50	1749.38	1750.07	1724.35
1+80 -40	1746.93	1747.31	1724.09
1+80 -30	1746.05	1746.93	1723.83
1+80 -20	1745.90	1746.56	1723.57
1+80 -10	1745.72	1746.64	1723.31
1+80 0	1746.32	1746.74	1723.09
1+80 10	1749.91	1750.19	1722.84
1+80 20	1756.10	1756.83	1722.58
1+80 30	1753.64	1753.95	1722.31
1+80 40	1748.07	1748.57	1722.11
1+80 50	1742.28	1743.20	1722.00
1+80 60	1736.86	1738.00	1721.88
1+80 70	1733.39	1732.76	1721.68
1+80 80	1731.28	1731.59	1721.49
1+80 90	1730.40	1730.76	1721.17
1+80 100	1730.42	1730.04	1720.59
1+80 110	1732.49	1732.51	1720.01
1+80 120	1734.88	1735.24	1720.00
1+80 130	1731.44	1731.58	1720.00
1+80 140	1727.00	1726.80	1720.00
1+90 -100	1751.45	1751.81	1742.46
1+90 -90	1757.00	1757.17	1734.97
1+90 -80	1760.70	1761.03	1731.33
1+90 -70	1760.97	1761.78	1725.36
1+90 -60	1755.84	1756.30	1724.75
1+90 -50	1749.62	1750.22	1724.49
1+90 -40	1747.79	1748.67	1724.23
1+90 -30	1747.39	1748.30	1723.96
1+90 -20	1747.13	1747.93	1723.70
1+90 -10	1746.97	1748.09	1723.46
1+90 0	1747.31	1748.19	1723.21
1+90 10	1749.60	1749.64	1722.95
1+90 20	1756.36	1756.56	1722.68
1+90 30	1758.42	1758.58	1722.45
1+90 40	1753.23	1753.58	1722.33
1+90 50	1747.49	1748.54	1722.22

1+90 60	1742.24	1742.94	1722.01
1+90 70	1736.13	1736.70	1721.82
1+90 80	1731.34	1731.09	1721.64
1+90 90	1729.55	1730.19	1721.08
1+90 100	1728.75	1729.36	1720.50
1+90 110	1728.91	1728.59	1720.00
1+90 120	1731.10	1731.09	1720.00
1+90 130	1731.62	1732.56	1720.00
1+90 140	1727.30	1727.56	1720.00
2+00 -100	1755.90	1756.18	1747.49
2+00 -90	1759.73	1759.79	1737.35
2+00 -80	1762.06	1762.58	1732.65
2+00 -70	1761.48	1762.23	1728.71
2+00 -60	1756.45	1756.78	1724.89
2+00 -50	1750.82	1751.38	1724.62
2+00 -40	1749.18	1750.01	1724.35
2+00 -30	1748.75	1749.70	1724.09
2+00 -20	1748.52	1749.31	1723.83
2+00 -10	1748.42	1749.52	1723.58
2+00 0	1748.61	1749.73	1723.32
2+00 10	1749.75	1750.02	1723.05
2+00 20	1753.71	1753.94	1722.79
2+00 30	1759.20	1759.98	1722.66
2+00 40	1758.43	1759.14	1722.55
2+00 50	1752.35	1754.10	1722.34
2+00 60	1746.54	1747.85	1722.15
2+00 70	1740.75	1741.01	1721.96
2+00 80	1733.79	1734.02	1721.57
2+00 90	1729.22	1729.30	1720.99
2+00 100	1727.74	1728.51	1720.41
2+00 110	1727.24	1727.75	1720.00
2+00 120	1727.27	1727.15	1720.00
2+00 130	1726.87	1726.46	1720.00
2+00 140	1725.79	1725.56	1720.00
2+10 -100	1759.00	1758.76	1753.63
2+10 -90	1760.71	1761.10	1740.92
2+10 -80	1762.02	1763.48	1734.08
2+10 -70	1763.80	1764.95	1730.94
2+10 -60	1758.73	1759.11	1725.03
2+10 -50	1753.04	1753.24	1724.74
2+10 -40	1750.69	1751.34	1724.49
2+10 -30	1750.23	1751.05	1724.22
2+10 -20	1750.14	1750.81	1723.95

2+10 -10	1750.11	1751.05	1723.68
2+10 0	1750.20	1751.31	1723.41
2+10 10	1750.70	1751.58	1723.16
2+10 20	1752.19	1751.94	1722.99
2+10 30	1757.40	1757.30	1722.89
2+10 40	1760.00	1762.77	1722.67
2+10 50	1757.55	1758.17	1722.48
2+10 60	1750.37	1751.30	1722.29
2+10 70	1743.75	1744.12	1722.06
2+10 80	1737.02	1737.15	1721.48
2+10 90	1729.68	1730.19	1720.90
2+10 100	1726.88	1727.53	1720.32
2+10 110	1726.24	1727.04	1720.00
2+10 120	1725.96	1726.48	1720.00
2+10 130	1725.79	1725.91	1720.00
2+10 140	1725.48	1725.54	1720.00
2+20 -90	1761.89	1761.50	1748.22
2+20 -80	1762.61	1763.27	1736.12
2+20 -70	1764.62	1764.89	1732.35
2+20 -60	1760.82	1761.85	1728.37
2+20 -50	1754.27	1755.07	1724.86
2+20 -40	1752.23	1752.86	1724.59
2+20 -30	1751.86	1752.62	1724.32
2+20 -20	1751.81	1752.37	1724.05
2+20 -10	1751.75	1752.61	1723.78
2+20 0	1751.71	1752.90	1723.52
2+20 10	1752.11	1753.12	1723.32
2+20 20	1752.65	1753.38	1723.22
2+20 30	1754.41	1754.36	1723.00
2+20 40	1760.00	1760.21	1722.80
2+20 50	1760.00	1760.89	1722.61
2+20 60	1753.83	1754.20	1722.44
2+20 70	1746.31	1746.96	1721.98
2+20 80	1739.46	1739.52	1721.40
2+20 90	1731.54	1731.90	1720.82
2+20 100	1726.42	1726.67	1720.24
2+20 110	1725.66	1726.21	1720.00
2+20 120	1725.48	1725.81	1720.00
2+20 130	1725.37	1725.61	1720.00
2+20 140	1725.30	1725.42	1720.00
2+30 -80	1762.84	1762.98	1739.76
2+30 -70	1765.74	1767.04	1733.48
2+30 -60	1762.25	1762.74	1730.28

2+30 -50	1755.80	1756.17	1724.95
2+30 -40	1754.00	1754.44	1724.69
2+30 -30	1753.56	1754.18	1724.42
2+30 -20	1753.46	1753.92	1724.15
2+30 -10	1753.37	1754.15	1723.89
2+30 0	1753.39	1754.47	1723.67
2+30 10	1753.53	1754.64	1723.55
2+30 20	1753.74	1754.53	1723.33
2+30 30	1754.53	1754.67	1723.13
2+30 40	1756.36	1756.43	1722.94
2+30 50	1759.10	1759.45	1722.76
2+30 60	1756.15	1756.08	1722.47
2+30 70	1748.49	1748.52	1721.89
2+30 80	1741.10	1741.02	1721.31
2+30 90	1732.73	1733.57	1720.73
2+30 100	1725.94	1726.07	1720.15
2+30 110	1725.48	1725.29	1720.00
2+30 120	1725.04	1725.08	1720.00
2+40 -80	1764.31	1763.99	1745.97
2+40 -70	1767.46	1767.90	1734.57
2+40 -60	1763.35	1763.58	1731.38
2+40 -50	1757.25	1757.27	1726.41
2+40 -40	1755.43	1756.19	1724.79
2+40 -30	1755.08	1755.76	1724.52
2+40 -20	1755.02	1755.48	1724.26
2+40 -10	1754.97	1755.69	1724.03
2+40 0	1754.96	1755.79	1723.88
2+40 10	1755.04	1755.83	1723.66
2+40 20	1755.16	1755.81	1723.46
2+40 30	1755.66	1755.35	1723.27
2+40 40	1756.54	1755.57	1723.08
2+40 50	1757.89	1757.74	1722.91
2+40 60	1756.30	1756.99	1722.38
2+40 70	1748.83	1749.32	1721.80
2+40 80	1741.53	1741.63	1721.22
2+40 90	1732.88	1734.19	1720.64
2+40 100	1725.90	1726.65	1720.06
2+40 110	1725.31	1724.92	1720.00
2+50 -80	1767.47	1766.03	1753.68
2+50 -70	1767.90	1770.54	1736.51
2+50 -60	1764.03	1764.66	1732.36
2+50 -50	1758.22	1758.35	1728.62
2+50 -40	1756.91	1757.79	1724.89

2+50 -30	1756.61	1757.37	1724.62
2+50 -20	1756.55	1757.05	1724.39
2+50 -10	1756.51	1756.99	1724.21
2+50 0	1756.41	1757.05	1723.99
2+50 10	1756.49	1757.08	1723.79
2+50 20	1756.69	1757.30	1723.60
2+50 30	1757.33	1757.72	1723.40
2+50 40	1757.26	1755.60	1723.23
2+50 50	1757.42	1755.64	1722.87
2+50 60	1756.05	1756.85	1722.29
2+50 70	1748.20	1749.29	1721.71
2+50 80	1740.46	1741.95	1721.13
2+50 90	1732.94	1734.52	1720.55
2+50 100	1725.98	1727.03	1720.00
2+50 110	1725.09	1724.86	1720.00
2+60 -80	1765.37	1765.70	1760.35
2+60 -70	1767.28	1769.64	1739.92
2+60 -60	1764.38	1764.92	1733.23
2+60 -50	1759.47	1759.45	1730.27
2+60 -40	1758.49	1759.36	1724.99
2+60 -30	1758.23	1758.96	1724.74
2+60 -20	1758.09	1758.49	1724.55
2+60 -10	1757.88	1758.25	1724.32
2+60 0	1757.72	1758.30	1724.11
2+60 10	1757.79	1758.34	1723.93
2+60 20	1758.45	1758.58	1723.73
2+60 30	1760.81	1762.17	1723.55
2+60 40	1760.85	1761.43	1723.36
2+60 50	1758.57	1759.17	1722.78
2+60 60	1754.93	1755.67	1722.20
2+60 70	1746.91	1748.25	1721.62
2+60 80	1739.33	1740.79	1721.04
2+60 90	1732.83	1733.50	1720.46
2+60 100	1726.34	1726.90	1720.00
2+60 110	1724.74	1724.53	1720.00
2+70 -70	1768.02	1771.96	1745.92
2+70 -60	1766.80	1767.72	1734.41
2+70 -50	1761.30	1761.49	1731.45
2+70 -40	1760.05	1760.66	1727.30
2+70 -30	1759.75	1760.35	1724.88
2+70 -20	1759.55	1759.92	1724.65
2+70 -10	1759.31	1759.67	1724.44
2+70 0	1759.17	1759.55	1724.25

2+70 10	1759.07	1759.62	1724.06
2+70 20	1759.66	1759.95	1723.88
2+70 30	1764.49	1765.04	1723.71
2+70 40	1766.27	1766.74	1723.27
2+70 50	1760.28	1760.98	1722.69
2+70 60	1752.92	1754.53	1722.11
2+70 70	1745.90	1747.05	1721.53
2+70 80	1738.44	1739.73	1720.95
2+70 90	1732.50	1733.00	1720.37
2+70 100	1726.30	1727.12	1720.00
2+80 -70	1767.88	1769.14	1754.25
2+80 -60	1765.78	1765.87	1737.71
2+80 -50	1762.43	1762.89	1732.73
2+80 -40	1761.63	1762.02	1729.62
2+80 -30	1761.18	1761.72	1724.98
2+80 -20	1760.93	1761.36	1724.77
2+80 -10	1760.71	1761.13	1724.58
2+80 0	1760.56	1760.96	1724.39
2+80 10	1760.39	1760.79	1724.20
2+80 20	1761.38	1761.20	1724.03
2+80 30	1766.74	1767.07	1723.77
2+80 40	1767.60	1768.32	1723.19
2+80 50	1760.60	1761.29	1722.61
2+80 60	1753.06	1753.76	1722.03
2+80 70	1745.47	1746.26	1721.45
2+80 80	1738.19	1739.13	1720.87
2+80 90	1732.73	1732.89	1720.29
2+80 100	1727.21	1727.01	1720.00
2+90 -70	1767.31	1767.78	1761.19
2+90 -60	1766.55	1766.85	1743.27
2+90 -50	1763.57	1763.84	1733.81
2+90 -40	1763.06	1763.51	1730.96
2+90 -30	1762.54	1763.15	1727.09
2+90 -20	1762.26	1762.79	1724.91
2+90 -10	1762.01	1762.59	1724.72
2+90 0	1761.86	1762.41	1724.52
2+90 10	1761.78	1762.24	1724.35
2+90 20	1763.66	1764.07	1724.18
2+90 30	1769.10	1769.77	1723.68
2+90 40	1767.30	1767.30	1723.10
2+90 50	1759.85	1760.03	1722.52
2+90 60	1752.50	1752.64	1721.94
2+90 70	1744.48	1745.30	1721.36



2+90 80	1737.58	1737.81	1720.78
2+90 90	1734.16	1735.05	1720.20
2+90 100	1728.46	1728.68	1720.00
3+00 -60	1767.53	1768.04	1749.12
3+00 -50	1765.03	1764.67	1734.53
3+00 -40	1764.28	1764.34	1732.03
3+00 -30	1763.88	1764.00	1729.37
3+00 -20	1763.49	1763.74	1725.87
3+00 -10	1763.23	1763.81	1724.85
3+00 0	1763.21	1763.72	1724.67
3+00 10	1763.43	1763.63	1724.50
3+00 20	1766.79	1767.27	1724.17
3+00 30	1770.00	1770.62	1723.59
3+00 40	1764.90	1765.56	1723.01
3+00 50	1757.58	1758.22	1722.43
3+00 60	1750.49	1750.83	1721.85
3+00 70	1743.40	1743.46	1721.27
3+00 80	1736.25	1736.05	1720.69
3+00 90	1732.91	1733.50	1720.11
3+00 100	1728.08	1728.36	1720.00
3+10 -60	1767.47	1767.54	1754.78
3+10 -50	1765.41	1765.36	1736.78
3+10 -40	1765.03	1765.09	1732.72
3+10 -30	1764.72	1764.81	1730.30
3+10 -20	1764.51	1764.67	1727.51
3+10 -10	1764.37	1764.79	1724.99
3+10 0	1764.46	1764.83	1724.82
3+10 10	1765.45	1764.82	1724.65
3+10 20	1770.00	1770.96	1724.08
3+10 30	1770.00	1770.01	1723.50
3+10 40	1762.62	1763.09	1722.92
3+10 50	1755.74	1755.76	1722.34
3+10 60	1748.37	1748.21	1721.76
3+10 70	1740.94	1740.85	1721.18
3+10 80	1733.89	1733.60	1720.60
3+10 90	1728.71	1728.44	1720.02
3+10 100	1724.72	1724.76	1720.00
3+20 -60	1768.79	1768.83	1762.21
3+20 -50	1766.13	1765.91	1742.60
3+20 -40	1765.82	1765.81	1732.58
3+20 -30	1765.57	1765.66	1729.35
3+20 -20	1765.37	1765.58	1727.59
3+20 -10	1765.30	1765.56	1725.96

3+20 0	1765.43	1765.81	1724.98
3+20 10	1766.71	1766.42	1724.57
3+20 20	1770.00	1771.27	1723.99
3+20 30	1767.37	1767.78	1723.41
3+20 40	1759.79	1760.54	1722.83
3+20 50	1753.26	1753.19	1722.25
3+20 60	1745.93	1745.91	1721.67
3+20 70	1738.52	1738.56	1721.09
3+20 80	1731.03	1731.11	1720.51
3+20 90	1724.81	1725.49	1720.00
3+30 -50	1767.13	1766.16	1749.15
3+30 -40	1766.62	1766.10	1733.01
3+30 -30	1766.4	1766.22	1729.31
3+30 -20	1766.27	1766.31	1727.97
3+30 -10	1766.23	1766.23	1727.13
3+30 0	1766.40	1766.56	1726.12
3+30 10	1767.93	1767.75	1724.61
3+30 20	1770.00	1771.07	1723.90
3+30 30	1764.63	1764.93	1723.32
3+30 40	1757.79	1757.80	1722.74
3+30 50	1750.87	1750.47	1722.16
3+30 60	1743.68	1743.33	1721.58
3+30 70	1736.46	1736.05	1721.00
3+30 80	1728.55	1728.85	1720.42
3+30 90	1722.58	1723.06	1720.00
3+40 -50	1767.68	1766.28	1755.23
3+40 -40	1767.17	1766.15	1734.41
3+40 -30	1767.25	1766.15	1729.99
3+40 -20	1767.13	1766.85	1729.06
3+40 -10	1767.17	1766.90	1728.58
3+40 0	1767.40	1767.28	1728.08
3+40 10	1768.50	1768.40	1725.95
3+40 20	1768.03	1768.40	1724.01
3+40 30	1761.47	1761.63	1723.24
3+40 40	1755.07	1754.98	1722.66
3+40 50	1748.04	1748.02	1722.08
3+40 60	1741.39	1740.87	1721.50
3+40 70	1734.11	1733.58	1720.92
3+40 80	1726.67	1726.31	1720.34
3+50 -50	1768.21	1767.26	1758.24
3+50 -40	1767.90	1767.36	1735.07
3+50 -30	1768.43	1768.283	1731.97
3+50 -20	1767.96	1767.79	1731.20

3+50 -10	1768.55	1768.26	1730.71
3+50 0	1769.88	1769.87	1730.07
3+50 10	1770.97	1771.46	1727.81
3+50 20	1765.29	1766.60	1724.51
3+50 30	1758.37	1759.41	1723.29
3+50 40	1751.77	1752.26	1722.33
3+50 50	1745.16	1745.14	1721.89
3+50 60	1738.68	1737.97	1721.41
3+50 70	1731.48	1730.98	1720.83
3+50 80	1723.64	1723.92	1720.25
3+60 -50	1766.98	1767.05	1758.61
3+60 -40	1768.66	1768.38	1736.67
3+60 -30	1770.34	1770.34	1733.92
3+60 -20	1771.95	1772.19	1732.76
3+60 -10	1772.00	1773.64	1731.58
3+60 0	1772.00	1774.04	1730.41
3+60 10	1769.63	1768.32	1728.28
3+60 20	1762.23	1763.09	1725.12
3+60 30	1755.44	1756.69	1723.35
3+60 40	1748.71	1749.72	1721.95
3+60 50	1741.93	1742.52	1721.22
3+60 60	1735.39	1735.40	1720.99
3+60 70	1728.35	1728.22	1720.70
3+60 80	1720.78	1721.02	1720.16
3+70 -50	1762.83	1761.59	1757.84
3+70 -40	1762.23	1761.73	1736.66
3+70 -30	1765.40	1766.20	1732.43
3+70 -20	1768.00	1768.54	1730.83
3+70 -10	1767.92	1768.89	1729.82
3+70 0	1767.29	1767.51	1728.77
3+70 10	1764.11	1762.47	1727.44
3+70 20	1757.95	1757.21	1725.57
3+70 30	1751.10	1751.92	1723.26
3+70 40	1745.40	1746.38	1721.56
3+70 50	1738.85	1739.42	1720.01
3+70 60	1731.99	1732.33	1720.00
3+70 70	1724.47	1725.16	1720.00
3+80 -40	1755.34	1756.13	1735.46
3+80 -30	1758.44	1758.63	1731.04
3+80 -20	1759.84	1760.90	1729.50
3+80 -10	1759.96	1761.38	1728.89
3+80 0	1759.72	1760.02	1728.17
3+80 10	1757.42	1756.63	1727.30

3+80 20	1752.24	1751.39	1725.87
3+80 30	1745.87	1746.22	1723.18
3+80 40	1739.96	1741.10	1720.43
3+80 50	1735.06	1735.47	1720.00
3+80 60	1728.47	1729.00	1720.00
3+80 70	1721.45	1721.75	1720.00
3+90 -40	1748.75	1748.63	1735.44
3+90 -30	1750.96	1751.01	1729.81
3+90 -20	1752.00	1753.18	1729.04
3+90 -10	1752.46	1753.73	1728.21
3+90 0	1752.13	1752.41	1727.43
3+90 10	1750.23	1750.20	1726.80
3+90 20	1746.85	1745.68	1725.76
3+90 30	1742.48	1740.49	1722.43
3+90 40	1736.64	1735.20	1720.00
3+90 50	1731.83	1730.05	1720.00
3+90 60	1724.93	1724.47	1720.00
4+00 -40	1741.80	1741.07	1734.98
4+00 -30	1743.84	1743.24	1729.64
4+00 -20	1744.81	1745.35	1728.80
4+00 -10	1745.49	1745.78	1727.96
4+00 0	1745.36	1744.84	1727.13
4+00 10	1743.80	1742.82	1726.32
4+00 20	1740.62	1739.86	1725.45
4+00 30	1736.46	1734.66	1721.86
4+00 40	1731.34	1729.46	1720.00
4+00 50	1726.18	1724.29	1720.00
4+00 60	1720.62	1719.42	
4+10 -30	1736.04	1735.55	1729.52
4+10 -20	1737.05	1737.63	1728.70
4+10 -10	1737.94	1737.91	1727.88
4+10 0	1738.010	1737.31	1727.06
4+10 10	1736.28	1735.50	1726.24
4+10 20	1733.21	1732.90	1725.42
4+10 30	1729.29	1728.65	1721.52
4+10 40	1726.35	1723.94	1720.00
4+10 50	1720.59	1720.09	1720.00
4+20 -10	1730.27	1729.92	
4+20 0	1729.68	1729.80	
4+20 10	1728.02	1728.06	
4+20 40	1721.59	1720.43	

## BIBLIOGRAPHY

Abeid, J., Allouche, E., Arditi, D., & Hayman, M. (2003). PHOTO-NET II: a computer-based monitoring system applied to project management. *Automation in construction*, 12(5), 603-616.

Agüera-Vega, F., Carvajal-Ramírez, F., & Martínez-Carricondo, P. (2016). Accuracy of digital surface models and orthophotos derived from unmanned aerial vehicle photogrammetry. *Journal of Surveying Engineering*, 143(2), 04016025.

Armstrong, J. S., & Collopy, F. (1992). Error measures for generalizing about forecasting methods: Empirical comparisons. *International journal of forecasting*, 8(1), 69-80.

Balasubramanian, K. (1997). *Relativistic Effects in Chemistry, Applications*. Wiley-Interscience.

Balasubramanian, V. (1997). Statistical inference, Occam's razor, and statistical mechanics on the space of probability distributions. *Neural computation*, 9(2), 349-368.

Beale, C. M., Lennon, J. J., Yearsley, J. M., Brewer, M. J., & Elston, D. A. (2010). Regression analysis of spatial data. *Ecology letters*, 13(2), 246-264.

Beauchamp, J. J., & Olson, J. S. (1973). Corrections for bias in regression estimates after logarithmic transformation. *Ecology*, 54(6), 1403-1407.

Bendea, H., Chiabrandò, F., Tonolo, F. G., & Marenchino, D. (2007, October). Mapping of archaeological areas using a low-cost UAV. The Augusta Bagiennorum test site. In XXI International CIPA Symposium (Vol. 1).

Cardenal, J., Mata, E., Perez-Garcia, J. L., Delgado, J., Andez, M., Gonzalez, A., & Diaz-de-Teran, J. R. (2008). Close range digital photogrammetry techniques applied to landslide monitoring. *International Archives of Photogrammetry, Remote Sensing and Spatial Information Sciences*, 37(Part B8).

Carr, E. B. (2013). Unmanned aerial vehicles: Examining the safety, security, privacy and regulatory issues of integration into US airspace. *National Centre for Policy Analysis (NCPA)*. Retrieved on September, 23, 2014.

Chiabrandò, F., Nex, F., Piatti, D., & Rinaudo, F. (2011). UAV and RPV systems for photogrammetric surveys in archaeological areas: two tests in the Piedmont region (Italy). *Journal of Archaeological Science*, 38(3), 697-710.

Chou, T. Y., Yeh, M. L., Chen, Y. C., & Chen, Y. H. (2010). Disaster monitoring and management by the unmanned aerial vehicle technology.

- Christiansen, M. P., Laursen, M. S., Jørgensen, R. N., Skovsen, S., & Gislum, R. (2017). Designing and Testing a UAV Mapping System for Agricultural Field Surveying. *Sensors*, 17(12), 2703.
- Coifman, B., McCord, M., Mishalani, R. G., Iswalt, M., & Ji, Y. (2006, March). Roadway traffic monitoring from an unmanned aerial vehicle. In *IEE Proceedings-Intelligent Transport Systems* (Vol. 153, No. 1, pp. 11-20). IET Digital Library.
- Colomina, I., & Molina, P. (2014). Unmanned aerial systems for photogrammetry and remote sensing: A review. *ISPRS Journal of Photogrammetry and Remote Sensing*, 92, 79-97.
- Contreras, M., Aracena, P., & Chung, W. (2012). Improving accuracy in earthwork volume estimation for proposed forest roads using a high-resolution digital elevation model. *Croatian Journal of Forest Engineering: Journal for Theory and Application of Forestry Engineering*, 33(1), 125-142.
- Cope, M. E. *Digital Surface Modeling and Volumetric Analysis Techniques Applied to the Measurement of Plan-View Earthwork Quantities*, 1993.
- Costa, D. B., & Mendes, A. T. (2016). Lessons Learned from Unmanned Aerial System-Based 3D Mapping Experiments.
- Dadi, G.B., Sturgill Jr, R.E. and Wang, X., 2016. Uses of Mobile Information Technology Devices in the Field for Design, Construction, and Asset Management (No. Project 20-05 (Topic 46-06)).
- Dielman, T. E. (2005). Least absolute value regression: recent contributions. *Journal of Statistical Computation and Simulation*, 75(4), 263-286.
- d'Oleire-Oltmanns, S., Marzloff, I., Peter, K. D., & Ries, J. B. (2012). Unmanned aerial vehicle (UAV) for monitoring soil erosion in Morocco. *Remote Sensing*, 4(11), 3390-3416.
- Epps, J. W., & Corey, M. W. (1990). Cut and fill calculations by modified average-end-area method. *Journal of Transportation Engineering*, 116(5), 683-689.
- Ezequiel, C. A. F., Cua, M., Libatique, N. C., Tangonan, G. L., Alampay, R., Labuguen, R. T., ... & Loreto, A. B. (2014, May). UAV aerial imaging applications for post-disaster assessment, environmental management and infrastructure development. In *Unmanned Aircraft Systems (ICUAS), 2014 International Conference on* (pp. 274-283). IEEE.
- Feifei, X., Zongjian, L., Dezhu, G., & Hua, L. (2012). Study on construction of 3D building based on UAV images. *The International Archives of the Photogrammetry, Remote Sensing and Spatial Information Sciences*, 469-473.

Fernández-Hernandez, J., González-Aguilera, D., Rodríguez-Gonzálvez, P., & Mancera-Taboada, J. (2015). Image-Based Modelling from Unmanned Aerial Vehicle (UAV) Photogrammetry: An Effective, Low-Cost Tool for Archaeological Applications. *Archaeometry*, 57(1), 128-145.

Furukawa, Y., & Ponce, J. (2010). Accurate, dense, and robust multiview stereopsis. *IEEE transactions on pattern analysis and machine intelligence*, 32(8), 1362-1376.

Gates, M., & Scarpa, A. (2004). Earthwork quantities by random sampling. *Journal of the Construction Division*, 95, 65-83.

Gómez-Candón, D., De Castro, A. I., & López-Granados, F. (2014). Assessing the accuracy of mosaics from unmanned aerial vehicle (UAV) imagery for precision agriculture purposes in wheat. *Precision Agriculture*, 15(1), 44-56.

Grenzdörffer, G. J., Engel, A., & Teichert, B. (2008). The photogrammetric potential of low-cost UAVs in forestry and agriculture. *The International Archives of the Photogrammetry, Remote Sensing and Spatial Information Sciences*, 31(B3), 1207-1214.

Haas, C. T., Borcharding, J., Allmon, E., & Goodrum, P. (1999). US construction labor productivity trends. Center for Construction Industry Studies, Univ. of Texas at Austin, Austin, TX.

Hallermann, N., & Morgenthal, G. (2014, July). Visual inspection strategies for large bridges using Unmanned Aerial Vehicles (UAV). *In Proc. of 7th IABMAS, International Conference on Bridge Maintenance, Safety and Management* (pp. 661-667).

Hintz, C., & Vonderohe, A. (2011). Comparison of earthwork computation methods. *Transportation Research Record: Journal of the Transportation Research Board*, (2215), 100-104.

Hirt, C., Filmer, M. S., & Featherstone, W. E. (2010). Comparison and validation of the recent freely available ASTER-GDEM ver1, SRTM ver4. 1 and GEODATA DEM-9S ver3 digital elevation models over Australia. *Australian Journal of Earth Sciences*, 57(3), 337-347.

Hudzietz, B. P., & Saripalli, S. (2011). An experimental evaluation of 3D terrain mapping with an autonomous helicopter. *Proc. Int. Archives of the Photogrammetry, Remote Sensing and Spatial Information Sciences*, XXXVIII-1/C22, 137-142.

Hugenholtz, C. H., Whitehead, K., Brown, O. W., Barchyn, T. E., Moorman, B. J., LeClair, A., ... & Hamilton, T. (2013). Geomorphological mapping with a small unmanned aircraft system (sUAS): Feature detection and accuracy assessment of a photogrammetrically-derived digital terrain model. *Geomorphology*, 194, 16-24.

Hyndman, R. J., & Koehler, A. B. (2006). Another look at measures of forecast accuracy. *International journal of forecasting*, 22(4), 679-688.

Irizarry, J., & Costa, D. B. (2016). Exploratory study of potential applications of unmanned aerial systems for construction management tasks. *Journal of Management in Engineering*, 32(3), 05016001.

Irizarry, J., Gheisari, M., & Walker, B. N. (2012). Usability assessment of drone technology as safety inspection tools. *Journal of Information Technology in Construction (ITcon)*, 17(12), 194-212.

## KENTUCKY 2012. STANDARD SPECIFICATIONS FOR ROAD AND BRIDGE CONSTRUCTION

Kespry (2018), <https://kespry.com/>

Kim, H., & Kano, N. (2008). Comparison of construction photograph and VR image in construction progress. *Automation in Construction*, 17(2), 137-143.

Küng, O., Strecha, C., Beyeler, A., Zufferey, J. C., Floreano, D., Fua, P., & Gervais, F. (2011). The accuracy of automatic photogrammetric techniques on ultra-light UAV imagery. In *UAV-g 2011-Unmanned Aerial Vehicle in Geomatics* (No. EPFL-CONF-168806).

Lee, S., & Choi, Y. (2015). On-site demonstration of topographic surveying techniques at open-pit mines using a fixed-wing unmanned aerial vehicle (drone). *Tunnel and Underground Space*, 25(6), 527-533.

Luhmann, T., Robson, S., Kyle, S., & Boehm, J. (2013). Close-range photogrammetry and 3D imaging. Walter de Gruyter.

Metni, N., & Hamel, T. (2007). A UAV for bridge inspection: Visual servoing control law with orientation limits. *Automation in construction*, 17(1), 3-10.

Memon, Z. A., Majid, M. Z. A., & Mustaffar, M. (2005). An automatic project progress monitoring model by integrating auto CAD and digital photos. In *Computing in Civil Engineering* (2005) (pp. 1-13).

Mesas-Carrascosa, F. J., Notario García, M. D., Meroño de Larriva, J. E., & García-Ferrer, A. (2016). An analysis of the influence of flight parameters in the generation of unmanned aerial vehicle (UAV) orthomosaics to survey archaeological areas. *Sensors*, 16(11), 1838.

Michael E. C. (1993). Digital Surface Modeling and Volumetric Analysis Techniques Applied to the Measurement of Plan-View Earthwork Quantities



- Micheletti, N., Chandler, J. H., & Lane, S. N. (2015). Structure from motion (SFM) photogrammetry.
- Molina, P., Colomina, I., Victoria, T., Skaloud, J., Kornus, W., Prades, R., & Aguilera, C. (2012). Searching lost people with UAVS: The system and results of the CLOSE-SEARCH project. *In International Archives of the Photogrammetry, Remote Sensing and Spatial Information Sciences* (Vol. 39, No. EPFL-CONF-182482, pp. 441-446).
- Morgenthal, G., & Hallermann, N. (2014). Quality assessment of unmanned aerial vehicle (UAV) based visual inspection of structures. *Advances in Structural Engineering*, 17(3), 289-302.
- Nassar, K., & Jung, Y. H. (2012). Structure-From-Motion Approach to the Reconstruction of Surfaces for Earthwork Planning. *Journal of Construction Engineering and Project Management*, 2(3), 1-7.
- Nassar, K., Aly, E. A., & Jung, Y. (2011). Structure-from-motion for earthwork planning. *Proc. 28th ISARC*, 310-316.
- Natarajan, G. (2001). Ground control stations for unmanned air vehicles. *Defence Science Journal*, 51(3), 229.
- Nunnally, S. W. (2010). Construction methods and management. Prentice Hall Inc., NJ.
- Nex, F., & Remondino, F. (2014). UAV for 3D mapping applications: a review. *Applied geomatics*, 6(1), 1-15.
- Oglesby, C. H., & Hicks, R. G. (1982). Highway engineering (No. Monograph).
- Oglesby, C. H., Parker, H. W., & Howell, G. A. (1989). Productivity improvement in construction. McGraw-Hill College.
- OSHA (2018) <https://www.osha.gov/Publications/OSHA2226/2226.html>
- Peurifoy, R. L., & Ledbetter, W. B. (1985). Construction planning, equipment, and methods (No. 8th ed.).
- Photogrammetric Engineering & Remote Sensing (2015). ASPRS Positional Accuracy Standards for Digital Geospatial Data. America Society for Photogrammetry and Remote Sensing (ASPRS): Bethesda, MD, USA, 81(A1-A26).
- Pix4D (2016). <https://support.pix4d.com/hc/en-us/articles/202557459#label>
- Pontius, R. G., Thontteh, O., & Chen, H. (2008). Components of information for multiple resolution comparison between maps that share a real variable. *Environmental and Ecological Statistics*, 15(2), 111-142.

Puri, A., Valavanis, K. P., & Kontitsis, M. (2007, June). Statistical profile generation for traffic monitoring using real-time UAV based video data. In *Control & Automation, 2007. MED'07. Mediterranean Conference on* (pp. 1-6). IEEE.

Puri, A., Valavanis, K., & Kontitsis, M. (2007, April). Generating traffic statistical profiles using unmanned helicopter-based video data. In *Robotics and Automation, 2007 IEEE International Conference on* (pp. 870-876). IEEE.

Ragheba, A. E., & Ragabb, A. F. (2011). GPS Enabled Digital Photogrammetry for 3D Earth Modeling. In *Gi4DM (Geoinformation for Disaster Management) Conference*, Antalya, Turkey.

Rango, A., Laliberte, A., Steele, C., Herrick, J. E., Bestelmeyer, B., Schmutge, T., ... & Jenkins, V. (2006). Using unmanned aerial vehicles for rangelands: current applications and future potentials. *Environmental Practice*, 8(3), 159-168.

Rathinam, S., Kim, Z. W., & Sengupta, R. (2008). Vision-based monitoring of locally linear structures using an unmanned aerial vehicle. *Journal of Infrastructure Systems*, 14(1), 52-63.

Saari, H., Pellikka, I., Pesonen, L., Tuominen, S., Heikkilä, J., Holmlund, C., ... & Antila, T. (2011, October). Unmanned Aerial Vehicle (UAV) operated spectral camera system for forest and agriculture applications. In *Remote Sensing for Agriculture, Ecosystems, and Hydrology XIII* (Vol. 8174, p. 81740H). International Society for Optics and Photonics.

Schenk, T. (1997). Towards automatic aerial triangulation. *ISPRS Journal of Photogrammetry and remote Sensing*, 52(3), 110-121.

Shahbazi, M., Sohn, G., Théau, J., & Menard, P. (2015). Development and evaluation of a UAV-photogrammetry system for precise 3D environmental modeling. *Sensors*, 15(11), 27493-27524.

Siebert, S., & Teizer, J. (2014). Mobile 3D mapping for surveying earthwork projects using an Unmanned Aerial Vehicle (UAV) system. *Automation in Construction*, 41, 1-14.

Snavely, N., Seitz, S. M., & Szeliski, R. (2006, July). Photo tourism: exploring photo collections in 3D. In *ACM transactions on graphics (TOG)* (Vol. 25, No. 3, pp. 835-846). ACM.

Tang, L., Braun, J. and Debitsch, R.(1997). Automatic aerotriangulation—concept, realization and results. *ISPRS journal of photogrammetry and remote sensing*, 52(3), pp.122-131.

Tavakoli, A. (1985). Productivity analysis of construction operations. *Journal of construction engineering and management*, 111(1), 31-39.

Thomas, H. R., Maloney, W. F., Horner, R. M. W., Smith, G. R., Handa, V. K., & Sanders, S. R. (1990). Modeling construction labor productivity. *Journal of Construction Engineering and Management*, 116(4), 705-726.

Thomas, H. R., Sanders, S. R., & Bilal, S. (1992). Comparison of labor productivity. *Journal of construction engineering and management*, 118(4), 635-650.

Turner, D., Lucieer, A., & Wallace, L. (2014). Direct georeferencing of ultrahigh-resolution UAV imagery. *IEEE Transactions on Geoscience and Remote Sensing*, 52(5), 2738-2745.

Utts, J. M., & Heckard, R. F. (2011). *Mind on statistics*. Cengage Learning.

Vincent, R. A., & Ecker, M. (2010). Light detection and ranging (LiDAR) technology evaluation (No. OR11-007). Missouri. Dept. of Transportation.

Virginia Department of Transportation (2018). <http://www.virginiadot.org/>

Wang, J., Ge, Y., Heuvelink, G. B., Zhou, C., & Brus, D. (2012). Effect of the sampling design of ground control points on the geometric correction of remotely sensed imagery. *International Journal of Applied Earth Observation and Geoinformation*, 18, 91-100.

Wang, X., Al-Shabbani, Z., Sturgill, R., Kirk, A., & Dadi, G. B. (2017). Estimating Earthwork Volumes Through Use of Unmanned Aerial Systems. *Transportation Research Record: Journal of the Transportation Research Board*, (2630), 1-8.

Waugh, L. (2006, May). Construction site photography: Virtual reality vs. the focus+ context problem. In *Proceeding of 2006 Annual CSCE Conference of the Canadian Society for Civil Engineering* (pp. 1-8).

Westoby, M. J., Brasington, J., Glasser, N. F., Hambrey, M. J., & Reynolds, J. M. (2012). 'Structure-from-Motion' photogrammetry: A low-cost, effective tool for geoscience applications. *Geomorphology*, 179, 300-314.

Yakar, M., Yilmaz, H. M., & Mutluoglu, O. (2008). Data Collecting to Volume Computing Using Digital Close Range Photogrammetry and Laser Technics. *Integrating Generations FIG Working Week*.

Yanalak, M. (2005). Computing pit excavation volume. *Journal of surveying engineering*, 131(1), 15-19.

Y.Furukawa, J. Ponce, "Accurate, Dense, and Robust Multiview Stereopsis", *IEEE Transactions on Pattern Analysis and Machine Intelligence*, vol. 32, no.8,pp. 1362-1376, 2010.

Yuan, C., Zhang, Y., & Liu, Z. (2015). A survey on technologies for automatic forest fire monitoring, detection, and fighting using unmanned aerial vehicles and remote sensing techniques. *Canadian journal of forest research*, 45(7), 783-792.

Yuan, X., Fu, J., Sun, H., & Toth, C. (2009). The application of GPS precise point positioning technology in aerial triangulation. *ISPRS Journal of Photogrammetry and Remote Sensing*, 64(6), 541-550.

Zhu, Z., & Brilakis, I. (2009). Comparison of optical sensor-based spatial data collection techniques for civil infrastructure modeling. *Journal of Computing in Civil Engineering*, 23(3), 170-177.

## VITA

### Name

Xi Wang

### Education

January, 2015 --- Present

Doctoral Student in Construction Engineering and Project Management

Department of Civil Engineering

University of Kentucky

August, 2012 --- 2014

Master of Civil Engineering

Department of Civil Engineering

Auburn University

September 2008 --- July, 2012

B.S. in Management

Department of Civil Engineering

Sanjiang University, Nanjing, China

### Publications

#### **Peer-reviewed journal articles**

- Wang, X., Al-Shabbani, Z., Sturgill, R., Kirk, A., and Dadi, G. B. (2017). Estimating Earthwork Volumes through Use of Unmanned Aerial Systems. *Transportation Research Record: Journal of the Transportation Research Board*, (2630), 1-8.
- Wang, X., Deshpande, S. A., and Dadi, G. B. (2017). Application of Parameters-Free Adaptive Clonal Selection in Optimization of Construction Site Utilization Planning. *Journal of Construction Engineering and Project Management*, 7(2), 1-11.
- Wang, X., Dadi, G. B., Taylor, T. R., and Saladin, T. M (2018). The Influence of Potential Factors on Measurement Accuracy of Applying the Unmanned Aerial System (UAS) and Photogrammetry in Construction Earthwork. *Journal of Construction Engineering and Management*, **under review**.

- Wang, X., Dadi, G. B., and Taylor, T. R. (2018). Assessing the Performance of Using the Unmanned Aerial Systems (UAS) in Earthwork Volume Estimations. *Transportation Research Record: Journal of the Transportation Research Board*, **under review**.
- Wang, X., Rister, B., and Dadi, G. B. (2018). Evaluating Performance of Ground Penetrating Radar (GPR) and Pachometer for Bridge Deck Reinforcing Steel Cover Height Verification. *Transportation Research Record: Journal of the Transportation Research Board*, **under review**.

### **Technical/Research Reports**

- Dadi, G.B., Sturgill Jr., R.E., and Wang, X. (2016). “Uses of Mobile Information Technology Devices in the Field for Design, Construction, and Asset Management.” National Cooperative Highway Research Program. NCHRP Synthesis 491, Transportation Research Board. Washington, D.C. ISBN: 978-0-309-27212-4.

### **Conference Proceedings and Presentation**

\* - presenter

- Wang, X., Dadi, G.B., and Taylor, T.R.B.\* (2017) “A Case Study Application of Unmanned Aerial Systems (UAS) on Highway Construction Projects.” 24th International Workshop on Intelligent Computing in Engineering. University of Nottingham, United Kingdom. July 10-12, 2017.
- Wang, X.\* and Dadi, G.B. (2017). “Strategies to Model Complex Architectural Objects Using Unmanned Aerial Systems and Photogrammetry.” International Construction Specialty Conference. Vancouver, B.C., May 31-June 3, 2017.
- Wang, X.\*, Sturgill, Jr., R.E., and Dadi, G.B. (2016). “Analyzing Use and Policies for Mobile Information Technology Devices within State Departments of Transportation”. *Proceedings from the 2016 Construction Research Congress (CRC)*. San Juan, Puerto Rico
- Wang, X.\*, Deshpande, A., Dadi, G.B., and Salman, B. (2016). “Application of Artificial Immune Systems in Construction Engineering.” *Proceedings from the 2016 International Conference on Sustainable Design, Engineering and Construction*. Elsevier, Procedia Engineering. Tempe, AZ, 145(2016), 267-273. doi: 10.1016/j.proeng.2016.04.073.
- Sturgill, Jr., R.E.\*, Wang, X., and Dadi, G.B.\* (2017). “Mobile Information Technology Device Strategies, Uses, and Needs across State Transportation Agencies.” *Proceedings from the Transportation Research Board 96th Annual Meeting*, Washington, D.C. January 8-12, 2017.